SIRAMESINE AND LAPATINIB INDUCE SYNERGIC CELL DEATH VIA A FERROPTOTIC MECHANISM IN LUNG ADENOCARCINOMA AND GLIOBLASTOMA CELLS

by

Anna R. Blankstein

A Thesis submitted to the Faculty of Graduate Studies of
The University of Manitoba
in partial fulfillment of the requirements of the degree of

MASTER OF SCIENCE

Department of Biochemistry and Medical Genetics
University of Manitoba
Winnipeg, Manitoba

ABSTRACT

In cancer cells, the most common forms of cell death are often actively inhibited, contributing to the development of drug resistance. Identifying and exploiting alternative cell death pathways are essential to overcoming or bypassing drug resistance. Ferroptosis, a newly described, morphologically and biochemically distinct, cell death mechanism is characterized by iron-dependent cellular accumulation of reactive oxygen species. The combination of siramesine, a lysosome disruptor, and lapatinib, a dual tyrosine kinase inhibitor (TKI), synergistically induced death in breast cancer cells. This cell death had characteristics of ferroptosis: it was blocked by the ferroptosis inhibitor ferrostatin-1 and the iron chelator deferoxamine. The objective of the present study was to determine whether lysosome disruptors and TKIs, in combination, would induce synergic cell death via a ferroptotic mechanism in lung adenocarcinoma and glioblastoma cells. Inducing ferroptosis could be a potential therapeutic strategy for these cancers that have limited available treatment options.

"The central therapeutic challenge of the newest cancer medicine, then, was to find, among the vast numbers of similarities in normal cells and cancer cells, subtle differences in genes, pathways, and acquired capabilities—and to drive a poisoned stake into that new [Achilles'] heel."

Siddhartha Mukherjee

The Emperor of All Maladies

ACKNOWLEDGEMENTS

I would like to thank my supervisor, Dr. Spencer Gibson, for giving me the opportunity to pursue first my Honour's project, and then this Master's research project in his lab, and for providing me with mentorship at every stage. I would also like to express my gratitude to my committee members, Dr. Mark Nachtigal and Dr. Afshin Raouf, who have given their time, and expert guidance as I progressed through my program.

I acknowledge the Terry Fox Research Institute and CIHR for their financial support of my research through graduate studentships.

I would like to thank Elizabeth Henson for her time in teaching me the required techniques, for her encouragement, guidance, and humour. I would like to acknowledge all the past and present members of the Gibson lab for giving me experimental advice and creating a welcoming and stimulating work environment. Particularly I want to acknowledge Dr. Shumei Ma who set the groundwork for my project. Also, I would like to thank Sara Kost for her help with the isobolograms and combination analyses.

I must also thank Dr. Donna Wall for offering me a summer student position when I was an undergraduate student, and giving me my first experience of laboratory-based research. I learned flow cytometry techniques in her laboratory, and have been able to put that knowledge to good use during the present project.

Finally, I am grateful to my friends and family for ongoing nutritional and grammatical support.

TABLE OF CONTENTS

LIST OF TABLES

LIST OF FIGURES

LIST OF ABBREVIATIONS

3-MA	3-methyladenine
ALK	Anaplastic lymphoma kinase
AML	Acute myeloid leukemia
ASM	Acid sphingomyelinase
β-ME	β-mercaptoethanol
BCA	Bicinchoninic acid
BSA	Bovine serum albumin
CAD	Cationic amphiphilic drug
CI	Combination index
CLL	Chronic lymphocytic leukemia
Dcytb	Duodenal cytochrome *b*
DFO	Deferoxamine
DHE	Dihydroethidium
DMEM	Dulbecco's modified Eagle's medium
DMSO	Dimethyl sulfoxide
DMT1	Divalent metal transporter 1
ECL	Enhanced chemiluminescence
EDTA	Ethylenediaminetetraacetic acid
EGFR	Epidermal growth factor receptor
EML4	Echinoderm microtubule-associated protein-like 4
FBS	Fetal bovine serum
FDA	Food and Drug Administration
Fer-1	Ferrostatin-1
FIN	Ferroptosis-inducing compound
FTH1	Ferritin heavy chain 1
FTL	Ferritin light chain
FIASMA	Functional inhibitor of acid sphingomyelinase
GBM	Glioblastoma
GPX4	Glutathione peroxidase 4
GSH	Glutathione
HCP1	Heme-carrier protein 1
HEPH	Hephaestin
HER2	Human epidermal growth factor receptor 2
HH	Hereditary hemochromatosis
HO-1	Heme oxygenase 1
IRE	Iron-response element
IRP	Iron-regulatory protein
LIP	Labile iron pool
MGMT	O^6-methylguanine–DNA methyltransferase
MLKL	Mixed lineage kinase domain like pseudokinase
NSCLC	Non-small cell lung cancer
PAGE	Polyacrylamide gel electrophoresis
PBS	Phosphate buffered saline
PCBP1	Poly(rC)-binding protein 1

PCDI	Programmed cell death type I
PCDII	Programmed cell death type II
PD-1	Programmed cell death protein 1
PD-L1	Programmed death ligand 1
PMSF	Phenylmethanesulfonyl fluoride
RIPK1/3	Receptor-interacting serine/threonine-protein kinase 1/3
ROS	Reactive oxygen species
RSL3	RAS Selective Lethal 3
SAS	Sulfasalazine
SDS	Sodium dodecyl sulfate
TCGA	The Cancer Genome Atlas
Tf	Transferrin
TfR1	Transferrin receptor 1
TfR2	Transferrin receptor 2
TKI	Tyrosine kinase inhibitor
TMZ	Temozolomide
TNFα	Tumour necrosis factor alpha
TNFR	Tumour necrosis factor receptor
TRADD	Tumour necrosis factor receptor type 1-associated death domain protein
UTR	Untranslated region
VDAC2/3	Voltage dependent anion channel 2/3
VEGF	Vascular endothelial growth factor
WHO	World Health Organization

CHAPTER 1: INTRODUCTION

1.1 CANCER IN CANADA

In 2016 more than 202,400 Canadians were diagnosed with cancer and 78,800 died of cancer (1-3). It is expected that almost half of all Canadians will develop cancer in their lifetime and a quarter of Canadians will die as a result of a cancer diagnosis (1-3). In 2012, 30% of all deaths in Canada were the result of cancer, more than deaths due to cardiovascular disease (21%) and cerebrovascular disease (6%), combined (1-3). The economic costs are equally profound, with billions of dollars spent to treat and care for individuals with cancer and 10s of billions of dollars lost in decreased productivity and early death. As the Canadian population ages, cancer rates are increasing and the burden of cancer, personal and economic, will increase unless prevention and treatment improve. That is why scientists, physicians, health agencies and government are all engaged in improving our understanding of the biological basis, the prevention and the treatment of cancer. This thesis will investigate the synergistic killing effects of several combinations of lysosome targeting agents and tyrosine kinase inhibitors, and determine whether the mechanism of cell death is consistent with ferroptosis.

1.2 HALLMARKS OF CANCER

In maintaining integrity and homeostasis in multicellular organisms, the balance between cell death and survival is fundamental. Damaged cells, cells in inappropriate microenvironments or potentially harmful cells, undergo cell death, while healthy cells are able to survive and thrive even when exposed to physiological stresses. When the homeostatic balance between cell death

and cell survival is altered, diseases such as cancer can occur. Cancer development, or tumourigenesis, is a multistep process that involves the acquisition of successive genetic, epigenetic or somatic alterations as a result of increasing genomic instability (4). Carcinogenesis frequently involves over-activation of oncogenes through dominant gain-of-function mutations, and/or inhibition of tumour suppressor genes through recessive loss-of-function mutations (5). Together, these alterations enable cancer cells to acquire atypical characteristics including: self-sufficiency in growth signals, insensitivity to anti-growth signals, evasion of cell death, limitless replication potential, abnormal angiogenesis, evasion of the immune system, deregulated cellular metabolism, tissue invasion and metastasis (4, 6).

1.3 GLIOBLASTOMA

Gliomas encompass a wide range of tumours that arise from the glial cells of the central nervous system or their precursors. Gliomas are divided into three main types of tumours: astrocytomas, oligodendrogliomas, and ependymomas. Astrocytomas are categorized by their degree of aggressiveness, based on the World Health Organization (WHO) grading system. Glioblastoma (formerly known as glioblastoma multiforme, GBM), with a WHO astrocytoma grade of IV (highly aggressive), represents both the most common and most malignant primary brain tumour in adults (7, 8), while only three percent of childhood brain tumours are glioblastomas (9). In North America, the estimated incidence is 5 per 100,000, typically occurring more frequently in males (1). It arises by two pathogenically distinct routes, either emerging from a pre-existing low-grade astrocytoma (secondary GBM) or more commonly, emerging *de novo* in a fully malignant and aggressive state (primary GBM) (8).

The Cancer Genome Atlas (TCGA) identifies four GBM subtypes, based on differing patterns of gene expression: Proneural, Neural, Classical and Mesenchymal (10).

Classical GBM tumours are characterized by increased expression of epidermal growth factor receptor (EGFR), which is less common in the other GBM subtypes. However, *TP53* mutations, frequently identified in the other subtypes, are not found in Classical GBM. Clinically, patients with Classical GBM survive longer than patients with other GBM subtypes.

TP53 is frequently mutated in Proneural tumours. Proneural tumours are also characterized by mutations in the *IDH1* gene, which encodes an isocitrate dehydrogenase. *PDGFRA* (encoding platelet derived growth factor receptor alpha), is also mutated and overexpressed in the Proneural tumours. Patients with the Proneural subtype are significantly younger than patients with other subtypes, and tend to survive longer (10).

The Mesenchymal GBM subtype is characterized by mutations in the *NF1* tumour suppressor gene, and by increased expression of tumour necrosis factor (TNF) family and NF-kB signaling pathways. Frequent mutations in the *PTEN* and *TP53* tumour suppressor genes are also seen in this subtype. Patients with the Mesenchymal subtype have improved survival after treatment compared to patients with other subtypes (10).

The Neural subtype is defined by increased neuronal gene expression, and oligodendrocytic and astrocytic differentiation. Patients with the Neural subtype are older and have a poorer response to therapy than patients with Classical and Mesenchymal subtypes (10).

Presently, treatment for GBM is inadequate to provide cure to the majority of patients. Tumours are often resistant to available chemotherapy, the blood brain barrier blocks effective drugs from reaching the tumour site in the central nervous system, and treatment toxicity can

include permanent damage to normal brain tissue. Due to its infiltrative growth (which makes complete surgical resection difficult) and its aggressive behavior, GBM usually has a poor clinical outcome. Despite treatment options that include surgery, radiation and chemotherapy, the median overall survival is only 15 months, highlighting the urgent need for more effective targeted therapeutics (7, 8).

Currently, the surgical goal is complete resection, although the diffuse nature of GBM often makes this impossible (11). The extent of GBM resection correlates with survival. A study from 2001 showed that patients lived approximately 5 months longer when tumour resection was greater than 98% (12). A more recent study demonstrated that a survival advantage was conferred with more than 78% resection, although median overall survival continued to improve as the extent of resection increased (13).

Radiotherapy is the main non-surgical therapeutic modality, usually used in combination with temozolomide (TMZ), which sensitizes the tumour cells to radiation. TMZ is an alkylating agent that methylates purine bases, leading to DNA base mismatch, resulting in DNA strand breaks and apoptosis (14, 15).

Poor long-term outcomes in treatment of GBM are due to high rates of recurrence and the development of chemotherapy resistance. It has been estimated that more than 80% of GBMs recur, typically at the site of the original tumour (16). Acquired resistance to TMZ is a major limitation, as more than 90% of recurrent gliomas show no response to retreatment with TMZ. The primary mechanism for resistance involves O^6-methylguanine–DNA methyltransferase (MGMT), a small enzymatic protein acting to directly reverse the DNA alkylation. It has been

demonstrated that MGMT repairs the principle alkylation site of TMZ, limiting its effectiveness. High levels of MGMT are reported in many cases of glioblastoma, and correlate with resistance to TMZ (14, 17).

Hypoxia potentially increases GBM resistance to treatment through several mechanisms. Limited blood flow to hypoxic regions of tumours prevents the distribution of chemotherapeutic agents administered via the blood stream (18, 19). Additionally, radiation and some chemotherapeutic agents produce cytotoxic effects by generating reactive oxygen species (ROS), but in the setting of hypoxia, the production of ROS is limited (19, 20).

1.4 LUNG ADENOCARCINOMA

Lung cancer is the leading cause of cancer death for males in both developed and developing countries, and the first and second most prevalent cause of cancer death for females in developed and developing countries, respectively (21). Approximately 1.8 million new lung cancer diagnoses, and 1.6 million deaths are estimated to have occurred worldwide in 2012 (21). Lung cancer is typically diagnosed at advanced stages because many patients are asymptomatic in the early stages of the disease, and because symptoms are non-specific, resulting in a delay in diagnosis (22).

While lung cancer is singularly deadly, it is not a single disease. Historically it has been divided into two main categories: small cell lung cancer comprises 13-15% of all lung cancer diagnoses, while non-small cell lung cancer (NSCLC) makes up the majority of cases, 85%. The most prevalent type of NSCLC is adenocarcinoma, which currently comprises 55% of NSCLC. Lung adenocarcinoma arises in glandular cells at the periphery of the lung (23). It can be slower growing than other subtypes of lung cancer, and affects smokers and non-smokers, alike.

NSCLC is divided into four stages based on the degree of spread to the lymph nodes and other tissues; prognosis is greatly dependent on stage at diagnosis. The system used most often to stage NSCLC is the American Joint Committee on Cancer TNM system, which stages tumours based on the size of the primary tumour (T), spread to regional lymph nodes (N), and metastases (M). Once the T, N, and M categories are assigned, this information is combined to assign an overall stage of 0 to IV (with some stages subdivided into A and B). Staging identifies cancers with similar prognosis, requiring similar therapeutic approaches (24, 25).

Stage 0 NSCLC is found only in the top layers of cells lining the air passages; Stage I NSCLC is located only in lung tissue; Stage II NSCLC has spread to local lymph nodes; Stage III has spread to mediastinal lymph nodes (with substages A and B defining the extent of mediastinal lymph node involvement. Stage IV disease has spread beyond the lung and regional lymph nodes to the pleura, distant lymph nodes or other organs (24, 25). Stage at diagnosis is predictive for survival at five years: Stage IA patients having a five-year survival of 50-80% and Stage IV patients having a five-year survival of only 2% (26).

Treatment is also determined by the stage of the disease. Complete surgical resection is the preferred treatment for early stage disease (Stage 0-II) (27, 28). Patients with a high risk of post-operative morbidity may opt for incomplete resection with radiotherapy. After a complete surgical resection, Stage II patients usually receive adjuvant chemotherapy (27, 28). Stage III disease is a large, heterogeneous category, with some patients being candidates for surgery while others are not. Stage IIIA patients with potentially resectable disease are treated with either induction chemotherapy or induction chemo-radiotherapy, followed by surgery, while patients

with unresectable Stage IIIA or IIIB disease typically receive concurrent chemo-radiotherapy (29). Treatment of Stage IV disease is individualized and depends on tumour histology and molecular profile, and on the patient's age and comorbidities (30).

Cisplatin/carboplatin are the most frequently used agents, platinum containing complexes that crosslink DNA, leading to cell death. Most patients receive systemic treatment with platinum agents combined with additional agents such as paclitaxel, vinorelbine, gemcitabine, or docetaxel (27, 30). Bevacizumab, a monoclonal antibody that inhibits angiogenesis by targeting vascular endothelial growth factor (VEGF), is also commonly used in combination with carboplatin and paclitaxel as first-line therapy (31).

In the last ten years, significant advances in the treatment of lung adenocarcinoma have resulted from the identification of specific genetic changes. A driver mutation can be detected in 64% of lung adenocarcinomas (32). The American Society of Clinical Oncology recently published guidelines on molecular testing for *EGFR* and anaplastic lymphoma kinase (*ALK)* mutations (31).

EGFR tyrosine kinase inhibitors (TKIs) erlotinib, gefitinib and afatinib, which preferentially bind the EGFR ATP-binding pocket with greater affinity than ATP, improve median survival by 17-37 months (33, 34). However, despite initial responses to EGFR TKIs, the majority of patients will progress within the first two years of starting therapy. In approximately 50–60% of these patients, the loss of tumour sensitivity to TKIs is due to the acquisition of an additional *EGFR* mutation, T790M (34).

ALK gene fusions with echinoderm microtubule-associated protein-like 4 (*EML4*) occur

in about 2-7% of advanced lung adenocarcinoma patients, resulting in oncogenic gain-of-function due to constitutive oligomerization and activation (35). Patients with tumours that harbor the *ALK* mutation do not benefit from *EGFR* TKIs because these mutations are mutually exclusive, with rare exception (tumours either have *EGFR* or *ALK* mutations, but not both) (36). The ALK small molecule inhibitor crizotinib was developed for the treatment of locally advanced or metastatic NSCLC harboring the *EML4-ALK* fusion. Resistance to crizotinib eventually develops, but the mechanism of this resistance is currently unknown. The second generation TKIs, ceritinib and alectinib, are now a treatment option for patients with disease that has progressed on crizotinib, and seem to have the ability to limit disease metastasis to the central nervous system (31).

NSCLC has recently been identified as susceptible to immunotherapy involving immune checkpoint inhibitors. Expression of the programmed death ligand 1 (PD-L1) on tumour cells interacts with programmed death protein 1 (PD-1) on the surface of T cells, promoting immune tolerance by inhibition of function and proliferation of cytotoxic T cells (37). In 2015, the United States Food and Drug Administration (FDA) approved nivolumab and pembrolizumab for the treatment of metastatic lung cancer. Both agents are anti-PD-1 monoclonal antibodies and work by restoring the immune response against the cancer cells. Nivolumab and pembrolizumab have now become recognized second-line treatments for NSCLC (31).

1.5 IRON HOMEOSTASIS IN HEALTH AND DISEASE

The relationship between iron and carcinogenesis has long been observed, but not fully understood. Iron is an essential element for cellular homeostasis. However, iron can contribute to

tumourigenesis through the generation of ROS via the reaction of peroxides and iron (38). Excess iron supports tumour progression, as rapidly proliferating malignant cells require larger labile iron pools to support their increased energy requirements (39). To understand the role of iron in cancer growth and progression, it is necessary to understand the role of iron in normal cellular processes.

Almost all cells in the body use iron as a cofactor for fundamental biochemical activities including oxygen transport, energy metabolism and DNA synthesis. This is due to iron's flexible coordination chemistry and redox reactivity, which allow it to associate with proteins, bind to oxygen, transfer electrons or mediate catalytic reactions. However, iron is also potentially toxic, because, under aerobic conditions, it can catalyze the propagation of ROS and the generation of reactive radicals through Fenton chemistry (40). As a result, iron levels in the body are, under normal circumstances, tightly regulated.

The majority of iron in the body is found in hemoglobin in red blood cells and in myoglobin in muscle cells, where it plays an important role in oxygen transport. A much smaller proportion of body iron (either as a component of heme or iron-sulfur clusters) acts as a cofactor for proteins that are essential for respiration and energy metabolism, and as a component of enzymes involved in the synthesis of collagen and neurotransmitters. Iron is also required for optimal function of the immune system (39, 40).

Dietary sources of iron consist of heme and non-heme iron. Non-heme iron is derived from plant-based dietary sources and makes up about 90% of humans' dietary iron: cereals, legumes, fruits and vegetables are the main sources. Heme iron is derived from meat, fish and poultry sources where it is found in hemoglobin, myoglobin and cytochromes.

Humans lose iron through blood loss (men and post-menopausal women have a higher risk of iron overload than pre-menopausal women), sweat, and sloughing of epithelial cells, but do not possess a regulated mechanism for iron excretion. As a result, the absorption and transportation of iron is tightly controlled (41, 42).

1.5.1 Iron Regulation

Dietary iron (in the Fe^{3+} form) is initially reduced in the intestinal lumen by ferric reductases, such as duodenal cytochrome b (Dcytb), and Fe^{2+} is transported across the apical membrane of enterocytes by divalent metal transporter 1 (DMT1). Dietary heme iron is transported across the membrane by heme-carrier protein 1 (HCP1) and is metabolized to Fe^{2+} by heme oxygenase 1 (HO-1) (40). The Fe^{2+} is then processed and transferred to the blood stream via the cellular iron export protein, ferroportin. During this process, the iron is re-oxidized to Fe^{3+} by the ferroxidase hephaestin (HEPH) (Figure 1.1) (40, 43, 44).

The exported iron is picked up by the plasma protein transferrin (Tf), which transports iron through the plasma and delivers it to the tissues. The iron bound to Tf represents a small portion of the total iron in the body, but is very dynamic in order to sustain erythropoiesis. This iron is replenished by iron recycled from red blood cells and by newly absorbed dietary iron (40).

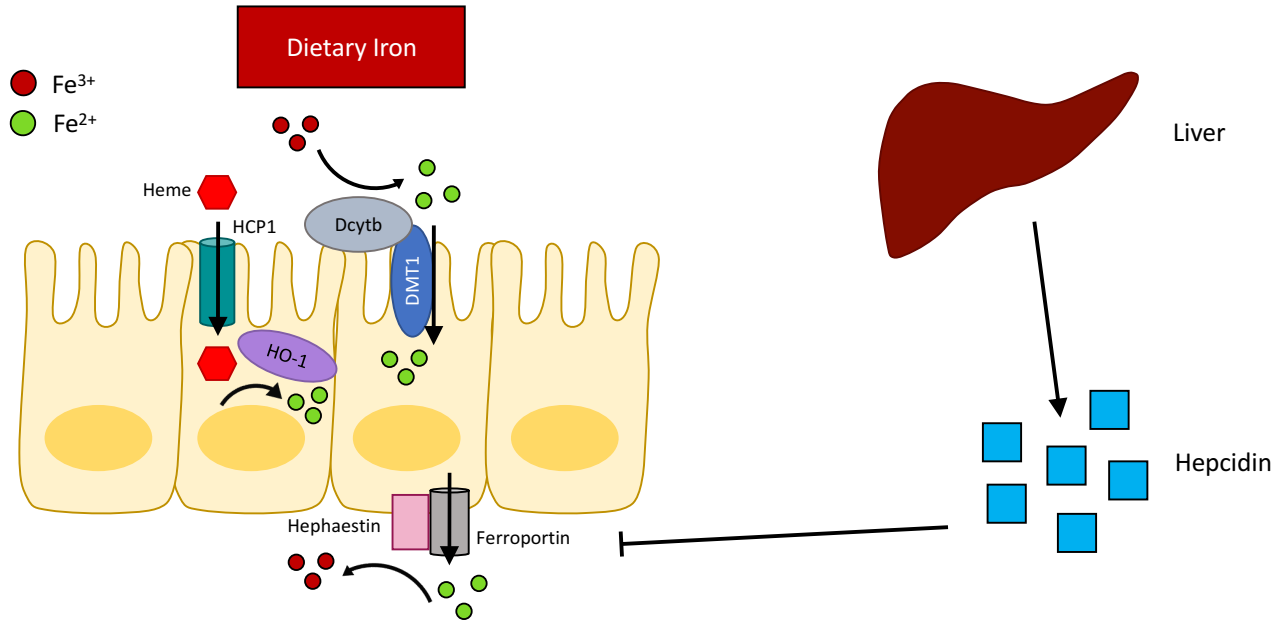

Figure 1.1: Systemic iron homeostasis in humans.
Dietary iron (predominantly in the form of ferric iron) is absorbed in the duodenum through the action of a reductase, such as duodenal cytochrome b (Dcytb) (which reduces it to ferrous iron) and divalent metal transporter 1 (DMT1). Iron can also be absorbed into the enterocytes in the form of heme through the heme-carrier protein 1 (HCP1). Heme is then broken down to ferrous iron by heme oxygenase 1 (HO-1). Iron exits the enterocyte through the iron efflux pump ferroportin, functioning together with the oxidase hephaestin to re-oxidize ferrous iron to ferric iron, which is bound to, and carried by, transferrin (Tf). The iron-Tf complex circulates through the bloodstream to deliver iron to body tissues. There is no excretory pathway for iron; iron levels are primarily regulated at the absorption step. Excess iron induces hepatic synthesis of the peptide hormone hepcidin, the master regulator of systemic iron homeostasis. Hepcidin binds to ferroportin and triggers its degradation, inhibiting absorption of dietary iron through the enterocytes. Hepcidin levels also increase in response to inflammatory cytokines resulting in anemia of chronic inflammation and cancer.

Each Tf molecule can carry two molecules of iron (referred to as holo-Tf). Iron loaded holo-Tf binds to the cell surface transferrin receptor 1 (TfR1) and undergoes endocytosis via clathrin-coated pits (45). A proton pump promotes acidification of the endosome, which triggers the release of Fe^{3+} from Tf. The metalloreductase STEAP3 reduces Fe^{3+} to Fe^{2+} (46), which is then transported out of the endosome by DMT1 (44, 47). Once the iron is released from Tf, the affinity of Tf to TfR1 decreases, resulting in dissociation. The apo-Tf is secreted back into the bloodstream where it can pick up more iron (Figure 1.2) (40).

A second transferrin receptor, transferrin receptor 2 (TfR2), is also involved in the uptake of transferrin-bound iron into cells, although its role is minor compared to TfR1 (48). There are a number of differences between TfR1 (encoded by the *TFRC* gene) and TfR2 (encoded by the *TFR2* gene): TfR2 has a 30-fold lower affinity for iron bound Tf than TfR1 and, while TfR1 is ubiquitously expressed, TfR2 is predominantly expressed in liver cells, suggesting a tissue-specific function (48). TfR2 levels show a dose-dependent response to transferrin saturation, with increasing concentrations of iron bound Tf leading to increased levels of TfR2 by directly stabilizing the TfR2 protein. Unlike TfR1, TfR2 is not regulated by cellular iron levels. TfR2 cannot compensate for the loss of TfR1; the *Tfrc* knockout mouse is embryonic lethal, and *Tfrc* heterozygote knockout mice display iron deficiency and reduced hepatic iron content compared with wild-type mice. Conversely, *TFR2* mutations in humans and murine models produce an iron overload phenotype with increased hepatic iron loading (48).

Cells can store excess intracellular iron within the storage protein ferritin (49). Iron can enter ferritin using poly(rC)-binding protein 1 (PCBP1), which is an iron chaperone, and the stored iron is considered to be bioavailable (50). Ferritin is composed of heavy (FTH1) and light (FTL) subunits, the levels of each subunit being tissue dependent. The storage and import/export

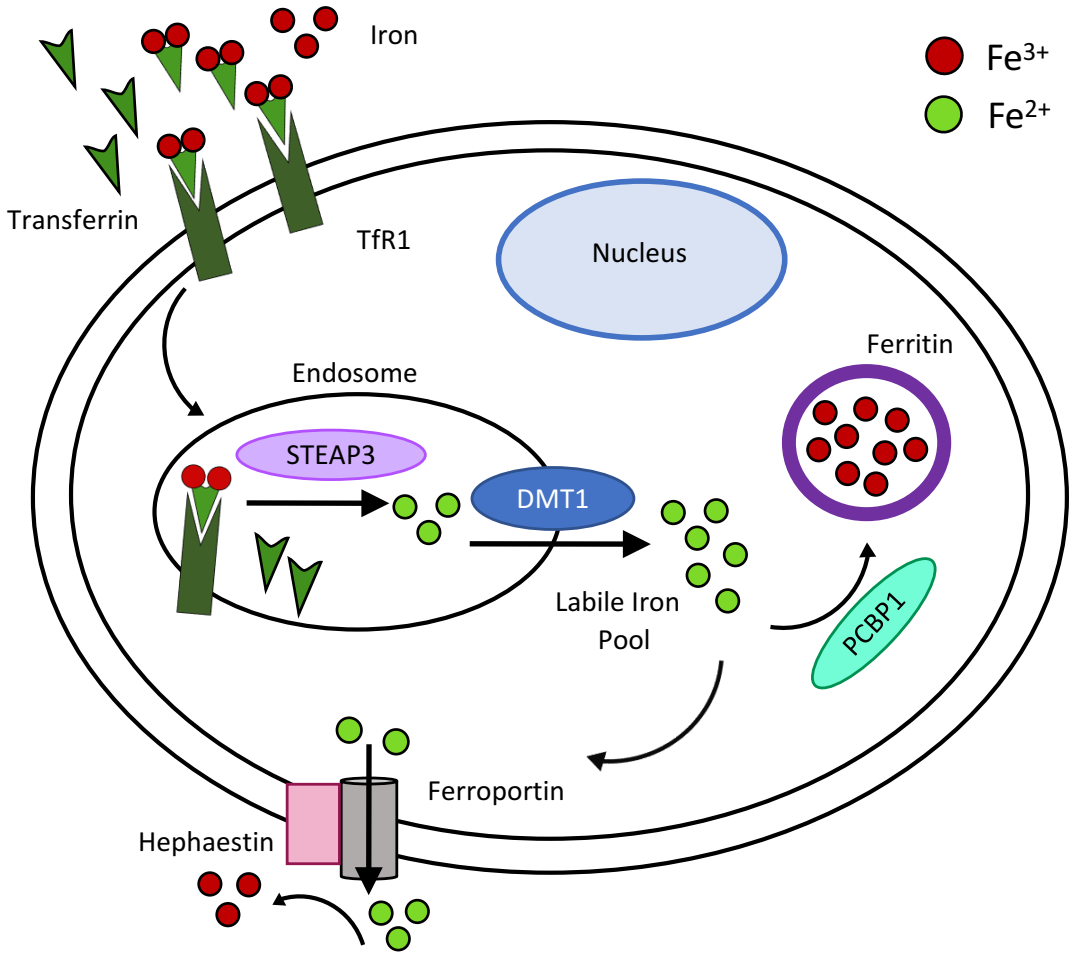

Figure 1.2: Mammalian cellular iron metabolism.
Iron circulates in blood plasma bound to transferrin. Iron-bound transferrin binds to transferrin receptor 1 (TfR1) on the plasma membrane of most cells, and is endocytosed. In the acidic environment of the endosome, ferric iron (Fe^{3+}) is released from transferrin and is reduced to ferrous iron (Fe^{2+}) through the ferrireductase activity of STEAP3. Ferrous iron is transported out of the endosome into the cytosol by divalent metal transporter 1 (DMT1), and enters the metabolically active pool of iron (the labile iron pool). Excess iron is stored in the iron storage protein ferritin. Iron can enter ferritin using the iron chaperone poly(rC)-binding protein 1 (PCBP1). Iron leaves the cell through the efflux pump ferroportin, and is re-oxidized to ferric iron by hephaestin.

of iron controls the size of the intracellular labile iron pool (LIP). The LIP is defined as the transient cytosolic pool of iron, which is presumably bound to low molecular mass chelates, such as organic anions and polypeptides (51). Cells can also remove excess iron via ferroportin, the cellular iron exporter (Figure 1.2) (40, 44).

Iron metabolism is balanced by two regulatory systems, one that functions systemically and relies on the hormone hepcidin and the iron exporter ferroportin, and another that predominantly controls cellular iron metabolism through iron-regulatory proteins that bind iron-response elements in specific regulated messenger RNAs (43).

Ferroportin-mediated efflux of Fe^{2+} is crucial for systemic iron homeostasis and is negatively regulated by hepcidin, a liver derived peptide hormone that binds to ferroportin and promotes its phosphorylation, internalization and lysosomal degradation (39, 41). Hepcidin accumulates following iron intake and under inflammatory conditions, resulting in iron retention and decreased dietary absorption. Hepcidin levels fall during iron deficiency and hypoxia, promoting intestinal iron absorption and iron release. Disruption of hepcidin regulation is associated with iron overload, while pathological elevation contributes to chronic anemia (Figure 1.1) (52).

Iron homeostasis and cellular iron balance are regulated post-transcriptionally by the iron-response element (IRE) / iron-regulatory protein (IRP) system. These proteins bind to iron-response elements (IREs) present in either the 5′ or the 3′ untranslated region (UTR) of mRNAs (38, 43, 53). IREs are found in the 5′ UTR of mRNAs encoding ferroportin and both subunits of ferritin, and in the 3′ UTR of mRNAs encoding TfR1 and IRE-containing isoforms of DMT1 (38, 54, 55). Binding of IRPs to 5′ IREs inhibits translation, whereas binding to 3′ IREs stabilizes mRNA and promotes translation (38). IRPs bind to IREs under conditions of low iron

availability. Thus, under conditions of low iron levels, the IRE-IRP system functions to increase iron uptake (by stabilizing mRNAs that encode TFR1 and IRE-containing isoforms of DMT1) and decreases iron storage and efflux (by inhibiting the translation of ferritin and ferroportin) (38). Conversely, in cells that are iron replete, the IRPs are unavailable for IRE binding as IRP1 is sequestered by binding to iron-sulfur clusters and IRP2 undergoes proteosomal degradation (40). Therefore, iron storage and efflux is increased (by translation of ferritin and ferroportin) and iron uptake is decreased (by the degradation of mRNAs encoding TfR1 and DMT1) (Figure 1.3) (38).

1.5.2 Iron and Disease

Despite the existence of a highly organized and regulated network that maintains iron homeostasis, genetic, physiological or environmental factors may drive the development of either iron overload or iron deficiency states.

Iron deficiency is the most common nutritional deficiency in the world. Iron is present in all cells in the human body serving vital functions that include carrying oxygen as a key component of hemoglobin, acting as a transport medium for electrons in the form of cytochromes, facilitating oxygen use and storage in muscle as a component of myoglobin, and serving as a cofactor for many enzyme reactions.

Total body iron averages approximately 3.8 g in men and 2.3 g in women. There are several mechanisms (as mentioned above) that control human iron regulation and safeguard against iron deficiency. When loss of iron is not sufficiently compensated by adequate intake of iron from the diet or by mobilization of iron stores, iron deficiency develops over time.

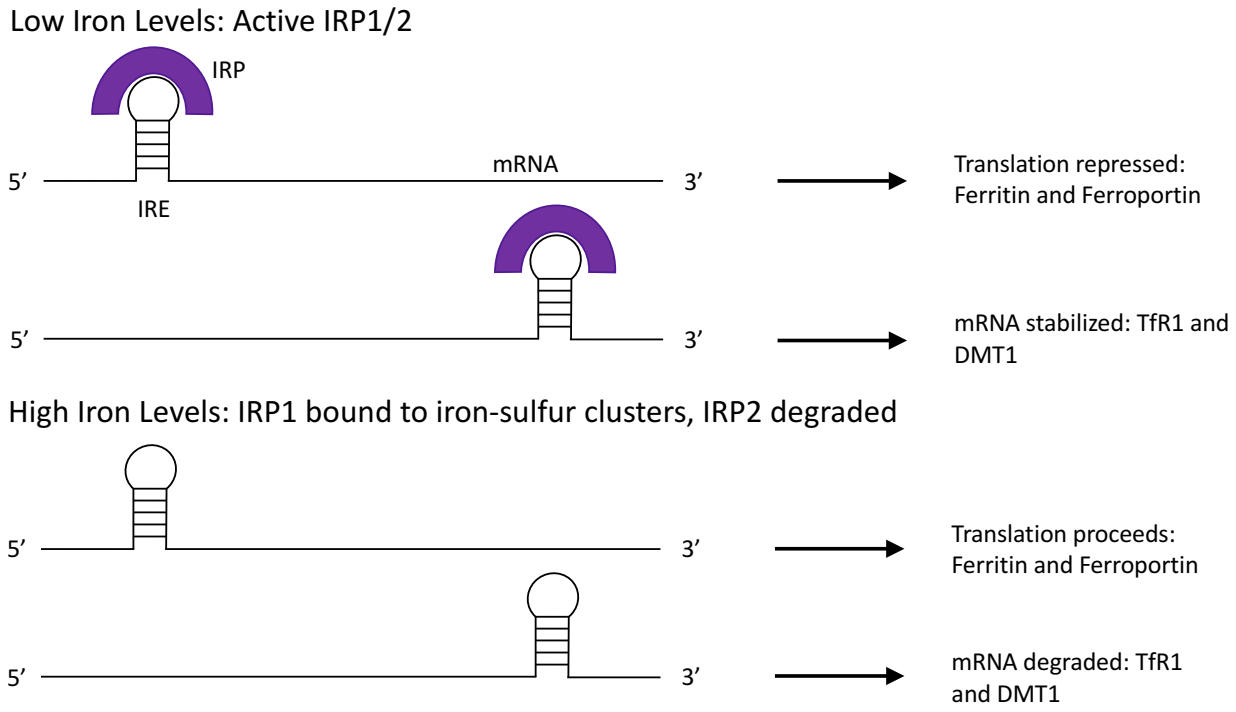

Figure 1.3: Control of cellular iron metabolism by the IRE-IRP regulatory axis.
Iron-regulatory protein (IRP) 1 and IRP2 are crucial proteins in the maintenance of cellular iron homeostasis. These proteins bind to iron-response elements (IREs) present in either the 5′ or the 3′ untranslated region (UTR) of mRNAs. IREs are found in the 5′ UTR of mRNAs encoding ferroportin and both subunits of ferritin, and in the 3′ UTR of mRNAs encoding transferrin receptor 1 (TfR1) and IRE-containing isoforms of divalent metal transporter 1 (DMT1). Binding of IRPs to 5′ IREs inhibits translation; binding to 3′ IREs stabilizes mRNA and promotes translation. IRPs bind to IREs under conditions of low iron levels; under conditions of high iron levels, IRP1 is sequestered and bound in iron-sulfur clusters and IRP2 is degraded.

Untreated iron deficiency can lead to iron deficiency anemia. Anemia is characterized by inadequate numbers of red blood cells or low levels of hemoglobin. Iron deficiency anemia occurs when the body lacks sufficient iron to maintain hemoglobin production. Hemoglobin is the iron containing protein in red blood cells that binds oxygen for transport from lungs to body tissues. Children, pre-menopausal women, and individuals with an iron-poor diet are most susceptible to iron deficiency anemia (56). At its worst, iron deficiency anemia is characterized by fatigue, impairment of thermoregulation, immune dysfunction and neurocognitive impairment (42, 57).

Anemia of chronic inflammation is the result of inadequate red blood cell production that accompanies a persistent state of inflammation, occurring as a consequence of chronic disease or infection (58). Inflammation causes macrophages to produce high levels of IL-6, a pro-inflammatory cytokine that triggers the expression of hepcidin, promoting degradation of ferroportin (52, 59). This in turn, lowers both dietary iron absorption and stored iron release (52, 59), resulting in decreased iron availability for hemoglobin synthesis and the development of anemia (Figure 1.1).

Excess iron intake can lead to iron overload, which if undiagnosed and untreated increases the risk for organ injury and dysfunction with the risk of hepatopathy, hypothyroidism, gonadal dysfunction, diabetes, arthritis, cardiomyopathy, and the progression of neurodegenerative diseases. Iron overload can be inherited or acquired from repeated blood transfusions or excessive intake of iron supplements. Accumulating the amount of iron required to produce symptoms can take decades, and as women are protected by menstruation and child bearing, iron overload is more common in older men (60).

Hereditary Hemochromatosis (HH) is one of the most common genetic disorders, affecting an estimated 1 in 300 Canadians, and is characterized by excessive intestinal absorption of dietary iron resulting in a pathological increase in total body iron stores (60). The molecular defect in HH is in the iron sensing-hepcidin axis. In HH, hepcidin levels are inappropriately low for the levels of iron present in the body, resulting in increased iron being transferred from the gut to other tissues. HH is divided into four subtypes defined by clinical presentation and genetic basis: (i) HFE-related HH (mutated *HFE*), (ii) juvenile hemochromatosis, (iii) TFR2-associated hemochromatosis (mutated *TFR2*) and (iv) ferroportin disease (mutated *SLC40A1*) (41).

HFE-related HH, also known as classic HH or Type 1 HH (representing 90% of cases), is the mildest form of the disease, characterized by a gradual accumulation of iron in organs over a period of decades, with most diagnoses in males older than 50 years and post-menopausal women (41, 60). In people of European descent, the condition is usually associated with homozygosity for a mutation in the *HFE* gene. The two most common mutations, C282Y and H63D, account for 85% of all cases of hemochromatosis (61).

1.5.3 Iron and Cancer

Excess iron can contribute to tumour initiation and growth. In the setting of pathological conditions such as hemochromatosis, hepatitis B and C virus infection, asbestosis, and endometriosis, iron overload may increase the risk of cancer. However, the precise relationship between iron overload and carcinogenesis is still unclear (39). At a macro level, although the results of studies are not always consistent, the evidence supports a model in which increased iron burden is associated with increased cancer risk (38).

At a micro level, iron loading may lead to an increased risk of malignancy, the result of generation of ROS via the Fenton reaction (Figure 1.4). The Fenton reaction describes the reaction of peroxides and iron yielding hydroxyl or lipid alkoxy radicals that can damage lipids, proteins and DNA. Oxidative damage to DNA, resulting in DNA base modifications and DNA strand breaks, can be mutagenic (38, 39). ROS are also believed to induce a wide range of effects through modulation of signals that regulate cell transformation. Although the molecular mechanisms responsible for these effects are not completely understood, an increase in ROS has the potential to influence malignant transformation at several levels: inducing mutations in DNA, modulating gene expression, increasing cell proliferation, or inhibiting apoptosis. Angiogenesis and metastasis may also be influenced by ROS (39).

Excess iron has been shown to contribute to tumour initiation and growth (62), and epidemiological evidence has established links between changes in iron metabolism and clinical outcomes in cancer patients (63). Malignant cells have demonstrated higher levels of intracellular labile iron than non-malignant cells, the result of increased expression of TfR1 and hepcidin, and down regulated expression of ferroportin (Figure 1.5) (38, 44, 64). Although hepcidin is primarily produced by hepatocytes, the presence of hepcidin has been confirmed in some breast cancer cell lines. Its presence in other cancer cell types is still unknown (38). Iron acquisition and export pathways are altered in cancer cells in ways that predict the increased labile iron pool (63). Rapidly proliferating malignant cells possess larger labile iron pools to support their increased requirements for DNA synthesis, repair, and mitochondrial respiration. Iron plays an essential role as a cofactor for enzymes that participate in this proliferation process. For example, ribonucleotide reductase, an iron-containing enzyme, catalyzes the limiting step for DNA synthesis (38).

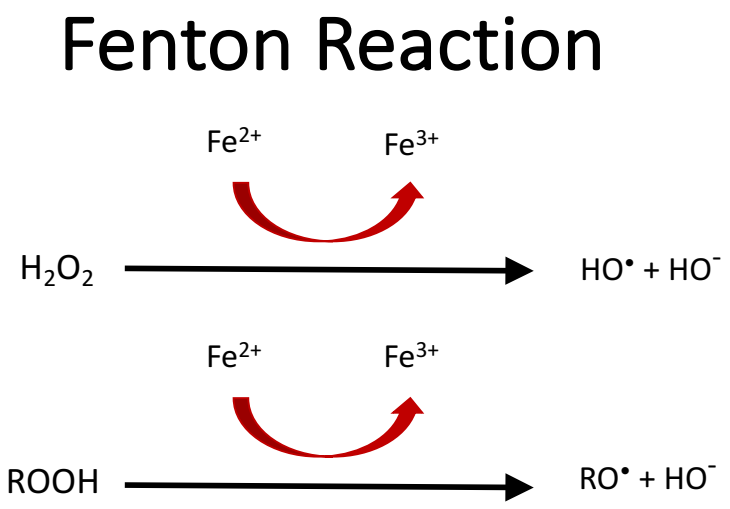

Figure 1.4: Iron as a catalyst for ROS production via the Fenton reaction.
Free iron can be toxic under aerobic conditions by catalyzing the formation of reactive oxygen species (ROS) via the Fenton reaction. In the Fenton reaction, ferrous iron reacts with peroxides to produce hydroxyl or lipid alkoxy radicals, which can damage intracellular lipids, proteins, and DNA. H_2O_2, hydrogen peroxide; ROOH, hydroperoxide.

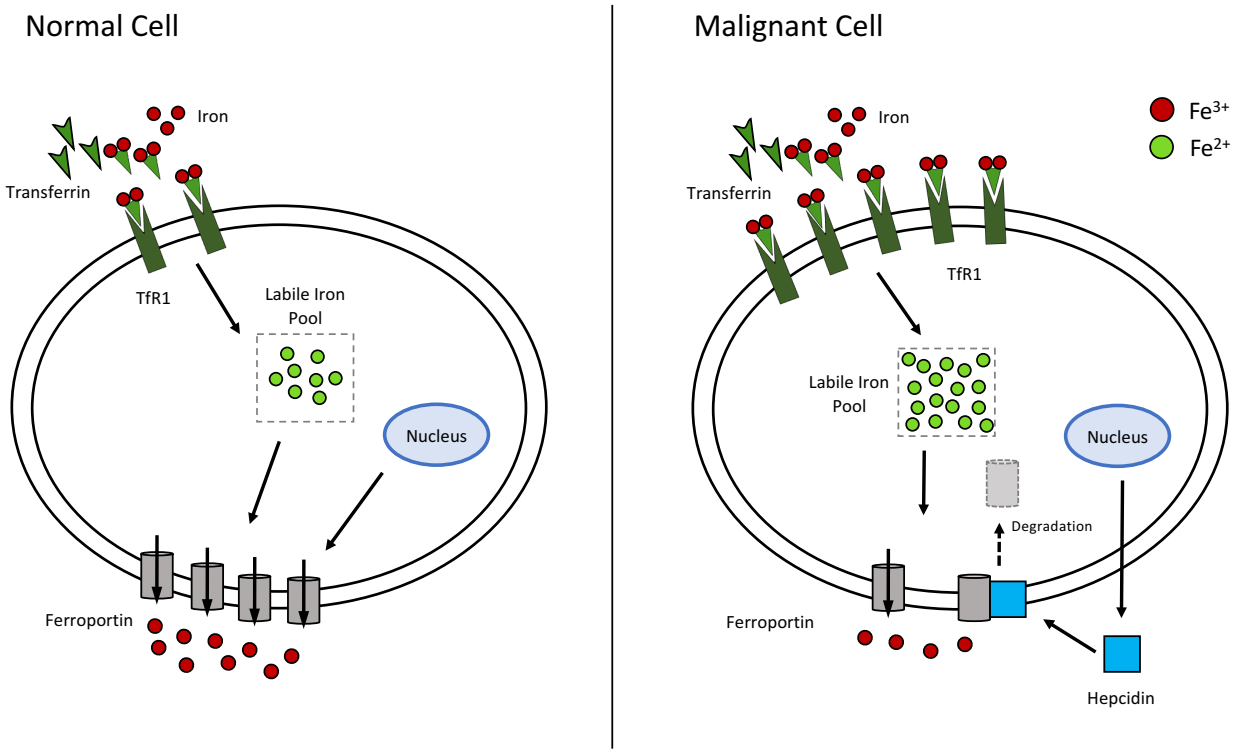

Figure 1.5: Iron uptake and efflux in malignant and non-malignant cells.
Malignant cells have upregulated expression of transferrin receptor 1 (TfR1) and hepcidin, and down regulated expression of ferroportin compared to non-malignant cells. These alterations result in an increased intracellular labile iron pool that supports the increased metabolic activity of the malignant phenotype. The contribution of cellular hepcidin has not been confirmed in all cell types.

1.6 CELL DEATH

Cell death is a physiological process that is essential to both the development and homeostasis of multicellular organisms (65). Some cell death is necessary in biological processes such as embryogenesis, and is needed in order to dispose of damaged cells, which may present a risk to the organism's health. Physiological cell death is tightly regulated, as either too much (e.g., myocardial infarction) or too little (e.g., cancer) can lead to disease.

The most recognized forms of cell death are necrosis, necroptosis, apoptosis, and autophagy, which are distinguished by morphologic and molecular features (66). More recently identified forms of cell death include ferroptosis, pyroptosis, parthanatosis, and methuosis (67, 68). Several of these cell death mechanisms are variants of the already well-understood forms of cell death. Ferroptosis, however, represents a unique death pathway and is the focus of this thesis.

1.6.1 Necrosis

Whereas necroptosis, apoptosis, and autophagy are forms of "programmed" cell death (see below), necrosis is generally regarded as a more "accidental" or uncontrolled form (65). Necrosis is caused by factors external to the cell, such as trauma or infection. This type of cell death is characterized by mitochondrial swelling, loss of membrane potential, and ROS production, all leading to cellular rupture and release of intracellular contents into the extracellular space (66).

1.6.2 Necroptosis

There is also a tightly regulated version of necrosis, which is called necroptosis. Necroptosis is stimulated through the tumour necrosis factor receptor (TNFR) by tumour necrosis factor alpha (TNFα), leading to the recruitment of tumour necrosis factor receptor type 1-associated death domain protein (TRADD), which in turn recruits receptor-interacting serine/threonine-protein kinase 1 (RIPK1). In the absence of caspase 8, RIPK1 and RIPK3 form the necrosome. The necrosome activates mixed lineage kinase domain-like pseudokinase (MLKL), which inserts into the cellular membrane and eventually leads to rupture of the plasma membrane. If caspase 8 is active, then formation of the necrosome is inhibited and apoptosis is initiated (see below) (69). Necroptosis has often been defined as a viral defense mechanism, allowing cell death to occur in a caspase-independent manner; a program of defensive cellular suicide that can be engaged to limit pathogen spread and promote inflammatory and immune responses (70).

1.6.3 Apoptosis

Apoptosis, often referred to as programmed cell death type I (PCDI), is a tightly regulated process that leads to elimination of cells without activating an inflammatory response. It is characterized by chromatin condensation, membrane blebbing, and formation of vesicles referred to as apoptotic bodies, which are then phagocytosed (66). Apoptosis can also be identified by the release of cytochrome c from mitochondria and the activation of caspases. Apoptosis can be initiated through two different pathways: the extrinsic pathway (caused by signals from other cells) and the intrinsic pathway (caused by intracellular stress).

The extrinsic pathway is triggered by the activation of death receptors on the cell surface that recruit intracellular adaptor proteins that bind procaspase 8. This allows dimerization, proteolytic cleavage, and activation of caspase 8. Activated caspase 8 can then, in turn, cleave and activate numerous substrates, such as caspase 3 (activating the caspase cascade), and initiate loss of mitochondrial membrane potential (71, 72).

The intrinsic pathway begins with loss of mitochondrial membrane potential induced by ROS, growth factor withdrawal, irradiation, or chemotherapeutic agents. Pro-apoptotic proteins such as Bad, Bax, and Bid oligomerize in the outer mitochondrial membrane and form pores. As mitochondrial membrane potential is lost, cytochrome c is released into the cytoplasm. Cytochrome c, Apaf-1 and procaspase 9 form the apoptosome, leading to cleavage of procaspase 9 to active caspase 9, activation of caspase 3 and the caspase cascade (71, 72).

1.6.4 Autophagy

Autophagy is the cellular process of self-digestion. The cellular components are isolated in autophagosomes, which fuse with lysosomes; their cargo is then degraded and recycled (73). Primarily an adaptive survival response, autophagy helps the cell to recycle and reuse components. However, severe or sustained autophagy can destroy vital cellular resources and result in cell death.

Conserved from yeast to humans, autophagy occurs at basal levels in all cells to ensure homeostatic function, such as protein and organelle turnover, and removal of intracellular pathogens. Rates of autophagy can be greatly increased during periods of stress, such as nutrient deprivation, leading initially to recycling of cellular components to provide energy for survival, but eventually to cell death (73). It is often referred to as programmed cell death type II (PCDII).

Autophagy shares some common upstream signals with apoptosis, which can initiate combined autophagy and apoptosis. On a molecular level, this means that the apoptotic and autophagic response machineries share common pathways that sometimes link cellular responses (74). However, autophagic cell death can occur through apoptosis-independent pathways.

1.6.5 Ferroptosis

Ferroptosis, or iron-mediated cell death, is a recently identified form of regulated cell death that is morphologically, biochemically, and genetically distinct from previously described types of cell death. It is characterized by the iron-dependent accumulation of ROS within the cell, which, in contrast to other forms of cell death, appears to depend on lipid peroxidation (75, 76). In brief, ferroptosis is an iron-dependent oxidative process.

Ferroptosis was first recognized as a unique cell death pathway by the Stockwell and Dixon laboratories through studies designed to identify small molecules that were selectively lethal to cells expressing oncogenic mutant Ras proteins (77, 78). The Stockwell laboratory isolated two novel oncogenic Ras Selective Lethal (RSL) small molecules named eradicator of Ras and ST (erastin) and Ras Selective Lethal 3 (RSL3). Both compounds were selectively lethal to cells expressing oncogenic mutant Ras, in comparison to cells expressing wild-type Ras (77, 78).

Characterization of the mechanism of action of erastin and RSL3 led to the recognition of ferroptosis as a unique form of cell death (79). It was observed that erastin and RSL3 did not trigger morphological changes or biochemical processes that were typical of apoptosis (77, 78). Moreover, erastin- and RSL3-induced cell death was not attenuated by caspase inhibition, by deletion of the intrinsic apoptotic effectors, by inhibitors of necroptosis, or by inhibition of

autophagy (75, 77, 78, 80). Crucially, erastin- and RSL3-induced cell death was inhibited by iron chelators, such as deferoxamine (DFO) and by lipophilic antioxidants, such as the specific ferroptosis inhibitor ferrostatin-1 (Fer-1) (75, 78, 81). These results indicated that iron-dependent lipid ROS accumulation was essential for erastin- and RSL3-induced cell death (75).

Analysis of the mechanism of action of erastin provided the first insights into proteins and pathways necessary to induce ferroptosis. Early studies identified the mitochondrial voltage dependent anion channels 2 and 3 (VDAC2 and VDAC3) as direct erastin targets (82). However, more recent studies suggest that the ability of erastin to trigger ferroptosis is determined primarily by its inhibition of a different target, the cystine/glutamate antiporter, which is often referred to as System X_C- (75, 83). System X_C- is a heterodimeric cell surface amino acid antiporter composed of the twelve-pass transmembrane transporter protein SLC7A11 (xCT) linked by a disulfide bridge to the single-pass transmembrane regulatory protein SLC3A2 (4F2hc) (84). The SLC7A11 subunit is credited with the transporter activity of the dimer, while SLC3A2 acts in the trafficking of the SLC7A11 subunit and is required for cell surface expression (85). System X_C- imports extracellular cystine, while exporting intracellular glutamate (Figure 1.6).

It was also noted that cell death induced by erastin had similarities to cell death induced by sulfasalazine (SAS) (75), a known System X_C- inhibitor (86). The lethal effects of both SAS and erastin were reversed by treatment with β-mercaptoethanol (β-ME) (75, 83), which bypasses the need for System X_C- by forming mixed disulfides with cystine that can be imported into the cell by a different transporter. Most convincingly, erastin and SAS block the uptake of radiolabelled cystine in cultured cancer cells (75, 83). Thus, erastin appears to act as a direct inhibitor of System X_C- function. This links the effect of erastin to a process that normally

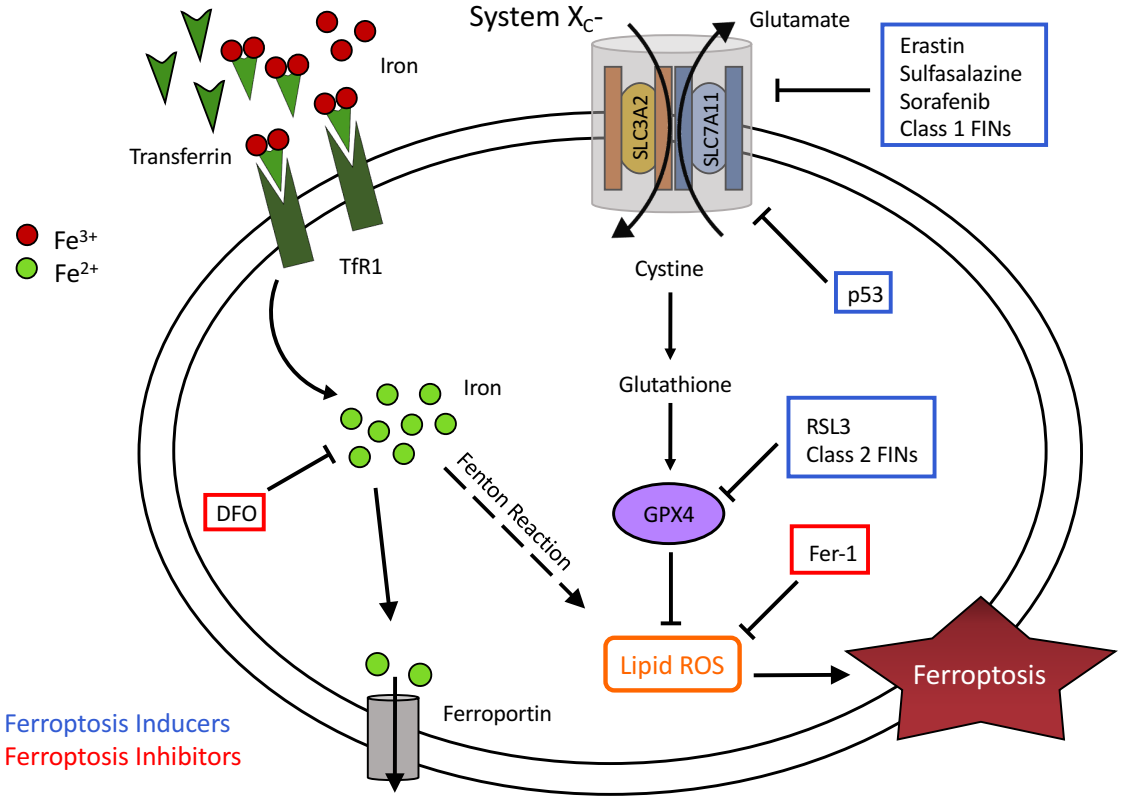

Figure 1.6: Overview of the ferroptosis pathway.
In many cells, cystine import via System X_C- (cystine/glutamate antiporter) is required for glutathione synthesis, and the function of glutathione peroxidase 4 (GPX4). GPX4 activity prevents the accumulation of lipid reactive oxygen species (ROS) that are lethal to the cell. Ferroptosis inducers block cystine uptake, depleting the cell of glutathione and inhibiting GPX4. Inducers of ferroptosis are indicated in the blue boxes, while suppressors of ferroptosis are in the red boxes. Transferrin, a plasma iron transport protein, is also an inducer of ferroptosis, leading to increased intracellular iron, which drives generation of lipid ROS via the Fenton reaction (see Figure 1.4). DFO, deferoxamine; Fer-1, ferrostatin-1; FIN, ferroptosis inducing agent; TfR1, transferrin receptor 1.

opposes the accumulation of lipid ROS. The imported cystine is required for synthesis of glutathione (GSH), which is essential for the activity of glutathione peroxidase 4 (GPX4). GPX4 down regulates the production of lipid ROS by converting peroxides to water. Indeed, erastin treatment leads to significant depletion of intracellular GSH (80). Therefore, both the antiporter and GPX4 are negative regulators of ferroptosis (Figure 1.6) (75, 80).

It is not known precisely how erastin or SAS inhibit System X_C- -mediated cystine import. It was initially proposed that erastin bound to a related transport protein, SLC7A5, and inhibited the SLC7A11 subunit, indirectly (75, 83). However, more recent data suggest that erastin most likely inhibits SLC7A11 directly (83).

In addition to erastin and SAS, the FDA- and Health Canada-approved kinase inhibitor sorafenib can block System X_C- function, deplete GSH and trigger ferroptosis in cancer cell lines (83, 87, 88). Related kinase inhibitors, such as nilotinib and imatinib, have no ability to block System X_C- function or cause ferroptosis (83, 87), suggesting that the effects of sorafenib may be due either to modulation of a very specific kinase (that in turn modulates System X_C- activity) or to a direct effect on System X_C-, unrelated to sorafenib's kinase inhibition. This may explain the ability of sorafenib to trigger caspase-independent cell death and enhance ROS accumulation in certain cell types (89, 90). However, the effects of sorafenib are varied and context specific. In some cell lines sorafenib triggers apoptosis (91), and even in cell lines where ferroptosis is observed at low doses of sorafenib, apoptosis or some other form of cell death is observed at higher doses (83).

The elucidation of the RSL3 mechanism of action provided the next major insight into the regulation of ferroptosis. Studies using RSL3 identified GPX4 as a candidate target for this compound (80, 92). GPX4 is a GSH-dependent enzyme that reduces lipid hydroperoxides to

lipid alcohols. GPX4, therefore, normally limits the iron-dependent formation of highly reactive lipid alkoxy radicals (93). Cells appear to be continually exposed to the threat of lipid peroxidation-mediated destruction, as inhibition of GPX4 activity leads to the rapid accumulation of lipid ROS and cell death in culture, and deletion of *Gpx4* in mice is embryonic lethal (80). Several other synthetic small molecules (including ML162 and ML210), in addition to RSL3, can directly inhibit GPX4 activity (80, 94). Thus, RSL3 and functionally related compounds are classified as class 2 ferroptosis-inducing compounds (FINs), to distinguish them from erastin and other System X_C- inhibitors that block GPX4 function indirectly by inhibiting the antiporter (class 1 FINs) (80, 95).

Ferroptosis was originally characterized through the study of compounds that had selective lethality for oncogenic Ras mutant cancer cells. Additional RSL compounds have been identified on the basis of this cellular phenotype, and subsequently confirmed to trigger ferroptosis (80, 94). These results suggest a relationship between ferroptosis and oncogenic Ras activity. Constitutive Ras pathway activity can promote the expression of TfR1 and suppress the expression of iron storage proteins in BJ fibroblast cell lines engineered to express the catalytic subunit of human telomerase (hTERT), the large T and small T SV40 antigens, and an oncogenic allele of Ras, providing one explanation for how oncogenic Ras activity could promote sensitivity to ferroptosis (78). However, this model has not yet been tested in additional cell lines.

The link between Ras pathway activity and ferroptosis is complicated by two observations. First, when comparing profiles of erastin sensitivity across a panel of 117 cancer cell lines, Ras-mutant cancer cell lines are on average no more sensitive to ferroptosis-inducing compounds than cancer cells expressing wild-type Ras (80). In fact, for unknown reasons,

diffuse large B cell lymphoma and renal cell carcinoma cancer cell lines, which do not typically contain Ras pathway mutations, have demonstrated the greatest sensitivity to ferroptosis-inducing agents (95). Second, RMS13 rhabdomyosarcoma cells overexpressing oncogenic Ras are resistant to erastin and RSL3 (96). A possible explanation for this observation is that the effects of the Ras pathway on ferroptosis differ depending on cell lineage or mutant Ras protein expression levels (79).

In some instances, the activation of p53 is required for ferroptosis. p53 up-regulation has been shown to repress expression of *SLC7A11* (the transporter subunit of the cystine/glutamate antiporter), sensitizing cells to ferroptosis in the presence of ROS stress. In fact, $p53^{3KR}$, an acetylation-defective mutant that has lost the ability to induce cell-cycle arrest, senescence and apoptosis, fully retains the ability to regulate expression of *SLC7A11* and induce ferroptosis (97). Therefore, in the context of cancer, ferroptosis may act as an endogenous tumour suppressive mechanism downstream of p53.

Iron is essential for the execution of ferroptosis. Both membrane permeable and membrane impermeable iron chelators prevent cells from undergoing ferroptosis, whether induced by erastin, RSL3 or a physiological stimulus such as high concentrations of extracellular glutamate (75, 80). Likewise, ferroptosis induced by erastin or cystine deprivation is prevented by silencing of the transferrin receptor (78, 98). Conversely, supplementing the growth medium with iron-bound transferrin or another bioavailable form of iron, but not with other divalent metals, accelerates erastin-induced ferroptosis (98).

Although ferroptosis is dependent on intracellular iron, iron's exact role in the process within the cell has not specifically been elucidated (79). Intracellular iron can generate ROS via the Fenton reaction, where the reaction of iron and peroxides yields hydroxyl or lipid alkoxy

radicals (83). It is also possible that iron-containing enzymes associated with lipid redox regulation (e.g., lipoxygenases), are activated during ferroptosis (76). Although a redox-independent role for iron cannot be ruled out, the most obvious explanation for the ability of iron chelators to block ferroptosis is that they prevent iron from participating in the Fenton reaction and generating lipid ROS (Figure 1.4) (83).

1.6.5.1 Ferroptosis and Development

Recent *in vivo* and clinical studies of components of the ferroptotic pathway are beginning to reveal a role for this cell death process in development. Knockout of *Gpx4* in mice caused embryonic lethality between E7.5 and E8.5, indicating an essential role of *Gpx4* in mouse development (99). A recent study found that conditional ablation of *Gpx4* in mouse neurons caused selective and rapid motor neuron degeneration via ferroptosis, and ultimately onset of paralysis (100), suggesting that ferroptosis may drive some types of motor neuron disease and its suppression may be critical in motor neuron development and homeostasis. Renal tubular cells are also susceptible to ferroptosis induction by *Gpx4* deletion in mice (101), relevant to the enhanced erastin sensitivity of renal cell carcinoma cell lines in culture (80). In addition, conditional deletion of *Gpx4* in mouse T cells resulted in T cell ferroptosis and a deficient immune response to infection (102), suggesting that *Gpx4* is essential for a functional T cell-mediated immune response.

Apart from the embryonic lethality of loss of *Gpx4* in mice, ferroptosis may be involved in the normal development of mammalian limbs. During development in mammals, inter-digital webbing is removed by activation of programmed cell death processes. In addition to the presence of apoptotic markers in these inter-digital dying tissues, ROS levels are elevated and

Gpx4 expression levels are reduced, suggesting possible involvement of ferroptotic pathways (103).

1.6.5.2 Ferroptosis and Disease

There is limited information about the role of ferroptosis in disease, especially in humans. However, there are studies in cell culture and animal models demonstrating a potential role for ferroptosis in several diseases. Inhibition of ferroptosis by ferrostatin-1 protected organisms from glutamate-induced neurotoxicity in a rat hippocampal slice culture model (75), and prevented neuronal cell death in a Huntington disease model (104, 105). Ferrostatins were also shown to have a protective role in a primary renal tubule damage model, implicating ferroptosis-mediated cell death in acute kidney failure (104). Ferroptosis has also been implicated in hepatic ischemic damage in mice: ischemia/reperfusion-induced liver injury can be improved in mice by the use of ferrostatins (101). Inhibition of ferroptosis by DFO or Fer-1 was also shown to limit ischemia/reperfusion-induced heart injury in an *ex vivo* mouse model (98).

1.6.5.3 Ferroptosis and Cancer

An increasing number of studies have revealed the close relationship of ferroptosis with various human diseases, including Huntington's disease, kidney failure, and liver and heart injury. However, the role of ferroptosis in tumour occurrence, progression and cancer treatment remains to be clarified. A number of cancer cell lines derived from diffuse large B-cell lymphoma, hepatocellular carcinoma, cervical carcinoma, osteosarcoma and prostate adenocarcinoma cells, have been shown to be susceptible to ferroptosis induced by erastin (80). *In vivo*, erastin and RSL3 were able to prevent tumour growth in a xenograft mouse model (80).

In addition to erastin's single agent effects, erastin also enhances the effect of chemotherapy drugs including temozolomide, cisplatin, cytarabine, and doxorubicin *in vitro* (92, 106, 107).

Previous work done by members of our laboratory demonstrated that the combination of siramesine, a lysosome disruptor, and lapatinib, a dual tyrosine kinase inhibitor of EGFR and human epidermal growth factor receptor 2 (HER2), synergistically induced cell death in breast cancer cell lines. This effect was blocked by the ferroptosis inhibitor Fer-1 and the iron chelator DFO, suggesting that death was occurring via ferroptosis. It was also observed that iron transport was altered in the treated cells: transferrin levels were elevated, ferroportin expression was reduced, and intracellular levels of iron were increased (108).

It has been noted that ferroptosis is best described as a form of cellular *sabotage*, where the inactivation of an essential metabolic process leads to cell death (109). It is an iron-catalyzed, lipid peroxidation-mediated cellular collapse, which has the potential for therapeutic targeting.

CHAPTER 2: RATIONALE, HYPOTHESIS AND RESEARCH AIMS

2.1 RATIONALE

Targeting the recently discovered ferroptotic cell death pathway holds the potential for novel therapies directed at cancers that presently have limited therapeutic options. Malignant cells often demonstrate defects in pathways that initiate or affect apoptosis, making them resistant to currently available chemotherapeutic agents that target apoptosis. Therefore, it is essential to identify alternative cell death pathways that could be exploited to bypass known resistance and enhance cancer cell killing. Because ferroptosis exploits a ubiquitous cellular metabolic pathway to induce death, it may be a therapeutic strategy applicable to a variety of tumour types.

As previous work done in our laboratory demonstrated that the combination of siramesine and lapatinib synergistically induced cell death in breast cancer cell lines that could be blocked by Fer-1 and DFO, this thesis focuses on studies to determine whether siramesine and lapatinib could produce synergic cell death in cell lines other than breast cancer, and whether the mechanism of death was consistent with ferroptosis. As the initial observations were made in breast cancer cell lines (MDA MB 231, SKBr3, MCF-7, and ZR-75), the lung adenocarcinoma cell line A549 and the glioblastoma cell line U87 were chosen to determine whether the synergic effects of siramesine and lapatinib were reproducible in tumour types other than breast cancer. Additionally, these cell lines were chosen because they represent fatal cancers with few available effective therapeutic options. Novel approaches to treatment are urgently required for both of these diseases.

2.2 HYPOTHESIS

We hypothesize that the combination of lysosome targeting agents and tyrosine kinase inhibitors will induce synergic cell death in glioblastoma and lung adenocarcinoma cells. We further propose that the specific combination of siramesine and lapatinib will induce synergic cell death via a ferroptotic mechanism in these cancer types.

2.3 RESEARCH AIMS

The aims of this study were to:

1. Determine whether lysosome targeting agents and tyrosine kinase inhibitors induce synergic cell death in glioblastoma and lung adenocarcinoma cells.
2. Determine whether this synergic cell death is occurring via a ferroptotic mechanism.
3. Determine the specific mechanism of action of the combination of siramesine and lapatinib.

CHAPTER 3: MATERIALS AND METHODS

3.1 REAGENTS

Appendix A contains a list of the solutions and the reagents used in this study. In general, all reagents were obtained from one of the following sources: Life Technologies, Thermo Scientific, Sarstedt, Invitrogen, and Sigma.

3.2 CELL CULTURE

Adherent human cancer cell lines were utilized in the experiments described in this thesis. The two cell lines employed in this study were A549 and U87 (Table 3.1). Both cell lines were maintained in a humidified 5% CO_2 environment (normoxia = 21% O_2) at 37°C, and cultured in Dulbecco's modified Eagle's medium (DMEM; Hyclone, Life Technologies) with 5% (v/v) fetal bovine serum (FBS; Life Technologies) and 1% Pen Strep (Gibco, Life Technologies). Cells were grown in 100 x 20 mm tissue culture plates (Sarstedt). Generally, cells were passaged upon reaching ~80% confluency (see below).

Table 3.1. Common Properties of the Cell Lines Employed in this Study

	A549	**U87**
Organism	Human	Human
Tissue/Cell Type	Lung/Epithelial	Brain/Epithelial
Disease	Lung Adenocarcinoma	Glioblastoma
Culture Properties	Adherent	Adherent
Gender	Male	Male
Culture Medium	DMEM + 5% FBS + 1% Pen Strep	DMEM + 5% FBS + 1% Pen Strep
Approximate Doubling Time	22 h	34 h
Karyotype	Hypotriploid 66, XY	Hypodiploid 44, XY
Source	ATCC	ATCC

3.2.1 Passaging of Cells

Typically, cells were passaged at a 1/5, 1/10, or 1/20 dilution after reaching 80% confluency. The cells were detached from their culture plates by incubating with 2 mL of trypsin (Sigma) for 5 minutes at room temperature. Trypsin is a proteolytic enzyme that helps adherent cells to detach from the culture dish and from each other, so that they can easily be transferred to another plate. The reaction was neutralized by the addition of 3 mL of media. The cells were then pelleted at 290 x g and re-suspended in 10 mL of the appropriate growth media before being seeded into new culture plates.

3.2.2 Preservation of Cells

Cells were preserved for future use by freezing once cells reached ~80% confluency. Cells were harvested by trypsinization as described above, and then pelleted by centrifugation at 290 x g for 5 minutes. The supernatant was removed and the cell pellet was re-suspended in 10 mL of media before being added to a cryovial (Sarstedt) in a 1:1 ratio with freezing media containing 50% complete media, 30% FBS and 20% dimethyl sulfoxide (DMSO; Sigma). The cryovials were then placed in a room temperature Nalgene Mr. Frosty Freezing Container (Thermo Scientific), which lowers the temperature at a rate of approximately 1°C/minute, and frozen at -80°C. Once frozen, cryovials were transferred to liquid nitrogen tanks for long-term storage.

3.2.3 Thawing of Cells

Frozen cells were transported from liquid nitrogen tanks on ice and warmed briefly by hand. Thawed cells were then mixed with 10 mL of room temperature complete media in a 50

mL tube, and then pelleted by centrifugation at 290 x g for 5 minutes. The supernatant was removed, cell pellets were re-suspended in 10 mL of fresh media, and the solution was transferred into a T25 culture flask (Corning). After incubation for 24 hours at 37°C, the media was changed and the cells were allowed to reach ~80% confluency before passaging. Cells were passaged at least once before being used for experiments.

3.2.4 Cell Counting

After harvesting by trypsinization, as described above, cells were counted using the TC20 Automated Cell Counter (Bio-Rad). 20 µL of re-suspended cells were mixed with 20 µL of 0.4% trypan blue (Sigma) and 10 µL of this solution was pipetted into each side of a dual chamber counter slide (Bio-Rad). The TC20 Cell Counter automatically calculated cell counts and viability once the counter slide was inserted.

3.3 Drugs, Inducers and Inhibitors

Table 3.2. Drugs, Inducers and Inhibitors Used in this Study

	Class	Concentrations Tested	Solvent/Storage Temperature	Source
Siramesine	Antidepressant	5-75 µM	DMSO/Room Temperature	Gift from Lundbeck
Lapatinib	TKI*	0.5-40 µM	DMSO/-20°C	LC Labs
Desipramine	Antidepressant	1-175 µM	Water/-20°C	Sigma
Sorafenib	TKI	2-20 µM	DMSO/-20°C	LC Labs
Tafenoquine	Antimalarial	3-20 µM	DMSO/-20°C	Sigma
Gefitinib	TKI	10-80 µM	DMSO/-20°C	Cederlane Labs
Clemastine	Antihistamine	5-80 µM	DMSO/-20°C	Sigma
Loratadine	Antihistamine	5-150 µM	DMSO/-20°C	Sigma
Desloratadine	Antihistamine	5-90 µM	DMSO/-20°C	Sigma
Erastin	Ferroptosis Inducer	1-50 µM	DMSO/-20°C	Sigma
Ferrostatin-1 (Fer-1)	Ferroptosis Inhibitor	10 µM	DMSO/-20°C	Sigma

Deferoxamine (DFO)	Iron Chelator	200 μM	DMSO/-20°C	Sigma
Iron Chloride ($FeCl_3$)	Chemical Compound	50 μM	Water/-20°C	Sigma

*TKI - tyrosine kinase inhibitor

Dose-response curves were generated for siramesine, lapatinib, desipramine, sorafenib, tafenoquine, gefitinib, clemastine, loratadine, desloratadine, and erastin (Table 3.2 and Sections 4.1.1 and 4.1.4) in order to identify the optimal concentrations to be used in the combination studies and in the construction of isobolograms to test for synergy (as described below). The optimal concentration of each drug used for combination studies are listed in Table 3.3. When selecting the doses to be used in the combination experiments, doses were selected that induced limited cell death to allow for clearer identification of synergy. The optimal concentration for each drug was the highest concentration that produced less than 20% cell death.

Table 3.3. Specific Concentrations of Drugs Used in this Study

	Class	**Concentration Used**
Siramesine	Antidepressant (Lysosomotropic Agent)	10 μM
Lapatinib	Tyrosine Kinase Inhibitor	0.5 μM
Desipramine	Antidepressant (Lysosomotropic Agent)	10 μM
Sorafenib	Tyrosine Kinase Inhibitor	2 μM
Tafenoquine	Antimalarial (Lysosomotropic Agent)	3 μM
Gefitinib	Tyrosine Kinase Inhibitor	10 μM
Clemastine	Antihistamine (Lysosomotropic Agent)	20 μM
Loratadine	Antihistamine (Lysosomotropic Agent)	20 μM
Desloratadine	Antihistamine (Lysosomotropic Agent)	40 μM
Erastin	Ferroptosis Inducer	15 μM

3.4 MEMBRANE PERMEABILITY ASSAY FOR TOTAL CELL DEATH

U87 and A549 cells were plated in 12 well dishes and allowed to grow for 24 hours, before treatment. Cells were treated with DMSO (as vehicle control), individual agents, or with combinations of agents, for 24 hours. In some experiments, cells were pretreated with Fer-1, DFO, or $FeCl_3$ for one hour before the addition of drugs. Cells were harvested, re-suspended in phosphate buffered saline (PBS) and stained with 0.04% trypan blue (entry into the cell indicates plasma membrane permeability) for 5-10 minutes at room temperature. Stained cells were analyzed by flow cytometry using a FACSCalibur flow cytometer and CellQuest software (Becton Dickinson). A potential problem with using trypan blue is that even cells with non-permeable membranes can take up dye if exposed for extended periods of time. This was avoided by analyzing the cells within five minutes of staining.

3.5 PRUSSIAN BLUE STAINING AND BRIGHTFIELD MICROSCOPY

U87 and A549 cells were plated on coverslips and allowed to grow for 24 hours before drug treatment. Cells were treated with DMSO (as vehicle control), siramesine, lapatinib, or with the combination of siramesine and lapatinib, for 12 hours. Cells on coverslips were fixed in 3.7% formaldehyde (Sigma) in PBS for 30 minutes at room temperature. Following three washes with PBS, coverslips were incubated with Prussian Blue (Sigma) for 30 minutes at room temperature. Following two more washes, coverslips were dipped in distilled water to remove excess PBS and mounted on glass slides with glycerol. Stained cells were examined using an Olympus BX51 microscope (objective lens magnification 10X) and captured with a CoolSNAP Camera and Image-Pro Plus 5.0 software.

To quantify Prussian Blue staining, the images were analyzed using ImageJ software (v2.0) (developed at the National Institutes of Health) to determine the integrated density, which takes into account the area being analyzed. The following formula was used to reverse the image, so that the signal being quantified is absorbance instead of transmission: – log (Transmission / 255). ImageJ quantifies the mean intensity of the stain, which, when multiplied by the area, provides the integrated density, representative of the amount of Prussian Blue staining.

3.6 MEASUREMENT OF INTRACELLULAR LABILE IRON USING CALCEIN-AM

U87 and A549 cells were plated in 12 well dishes and allowed to grow for 24 hours before drug treatment, as described above. Cells were harvested by trypsinization after 12 hours of drug treatment, and centrifuged at 290 x g for 5 minutes. Cell pellets were re-suspended and incubated with 1 μM Calcein-AM (Thermo Scientific) in the dark for 30 min at 37°C. Then, the cells were washed twice with PBS and treated with deferiprone (100 μM; Sigma), an iron chelator, or left untreated, for one hour at 37°C in the dark. Stained cells were analyzed by flow cytometry using the FACSCalibur flow cytometer and CellQuest software (Becton Dickinson). When Calcein enters the cell, it binds iron, which quenches its fluorescent signal. Upon addition of deferiprone, the iron becomes preferentially bound to deferiprone, and the fluorescent signal of Calcein is no longer quenched. The difference in fluorescent signal between the deferiprone-treated and untreated cells was used as an indirect measure of the labile iron pool.

3.7 DHE STAINING FOR REACTIVE OXYGEN SPECIES

U87 and A549 cells were plated in 12 well dishes and allowed to grow for 24 hours before drug treatment, as described above. Cells were harvested by trypsinization after 24 hours,

and centrifuged at 290 x g for 5 minutes. Cell pellets were re-suspended in PBS with 10 μM of dihydroethidium (DHE; Life Technologies) and incubated in the dark at 37°C for 30 minutes. When DHE is oxidized by ROS, it emits a red fluorescent signal, which can be quantified by flow cytometry and is proportional to the production of ROS. DHE-stained cells were analyzed by flow cytometry using the FACSCalibur flow cytometer and CellQuest software (Becton Dickinson).

3.8 C11-BODIPY STAINING FOR LIPID PEROXIDATION

U87 and A549 cells were plated in 12 well dishes and allowed to grow for 24 hours before drug treatment, as described above. Cells were harvested by trypsinization after 24 hours, and centrifuged at 290 x g for 5 minutes. Cell pellets were re-suspended in PBS with 1 μM of C11-BODIPY 581/591 (Invitrogen) and incubated in the dark at 37°C for 30 minutes. Stained cells were analyzed by flow cytometry using the FACSCalibur flow cytometer and CellQuest software (Becton Dickinson). Oxidation of a component of the C11-BODIPY fluorophore shifts the fluorescence emission from red to green. C11-BODIPY fluorescence was measured simultaneously by both the red filter and the green filter, and a change in the ratio of green to red fluorescence was used as an indicator of an increase in lipid peroxidation.

3.9 PREPARATION OF CELL LYSATES

Cells were cultured as above, however 6 well culture dishes were used for Western blot experiments. Cells were pelleted and washed with 1X PBS before adding 1% NP40 lysis buffer to each pellet. Before use, the following inhibitors were added to the lysis buffer: Complete Protease Inhibitor tablet (Roche), sodium orthovanadate (New England Biolabs),

phenylmethanesulfonyl fluoride (PMSF; Sigma), Phosphatase Inhibitor Cocktail 2 (Sigma) and Phosphatase Inhibitor Cocktail 3 (Sigma).

Lysates were vortexed for 30 seconds, incubated on ice for 5 minutes, vortexed again, and incubated for another 5 minutes on ice. Samples were then centrifuged at 16060 x g at 4°C for 10 minutes. The supernatant was transferred to a new tube and stored at -20°C (short term) or -80°C (long term), until evaluated by Western blotting.

3.10 PROTEIN ELECTROPHORESIS AND WESTERN BLOTTING

Protein concentrations were quantified using the Pierce BCA (bicinchoninic acid) Protein Assay Kit (Thermo Scientific) according to manufacturer's instructions. Briefly, the concentration of each sample was determined by comparing its absorbance to that of a standard curve generated from a series of nine protein standards using bovine serum albumin (BSA) as the standard control. Samples were tested in triplicate with a 1/5 dilution in ddH_2O and absorbance measurements were read at 562 nm using an Epoch Microplate Spectrophotometer (BioTek Instruments) with Gen5 v2.09 software.

Samples with equal amounts of protein were prepared for Western blot by combining protein, lysis buffer and 6X loading buffer to a final volume of 18 µL. Samples were boiled at 98°C for 10 minutes, cooled on ice, and then centrifuged briefly to collect contents at the bottom of tubes. Samples were loaded into wells and separated on a 10% acrylamide gel by SDS-PAGE at 80V for approximately 1.5 hours. Gels were prepared using a TGX FastCast Acrylamide Kit (Bio-Rad) according to the manufacturer's instructions.

The separated proteins were transferred to 0.2 or 0.45 µm nitrocellulose membranes (Bio-Rad) at 24V for 1 hour. Membranes were blocked in 5% milk dissolved in 1X PBST, and

incubated with primary antibody (Table 3.4) overnight in the cold room. Then, membranes were washed with PBST for 10 minutes, 3 times, and incubated with secondary antibody (Table 3.5) for one hour at room temperature, and then washed 3 more times as above. The Western blots were developed using Enhanced Chemiluminescence (ECL; Thermo Scientific) or Super Signal West Pico Chemiluminescent Substrate (Thermo Scientific), and imaged using either the ImageQuant LAS 500 gel imager (GE Healthcare Life Sciences) or autoradiography film (Fujifilm).

Table 3.4. Primary Antibodies

Antigen	Host Species	Dilution	Source	Product Number
Transferrin	Mouse	1:500	Abcam	ab70826
Transferrin Receptor	Rabbit	1:1000	Cell Signaling	13113S
Ferroportin	Rabbit	1:1000	Novus Biologicals	NBP1-21502
FTH1*	Rabbit	1:1000	Cell Signaling	4393S
DMT1**	Rabbit	1:1000	Cell Signaling	15083S
System X_C- (antiporter)	Rabbit	1:1000	Cell Signaling	12691S
Actin	Mouse	1:5000	Sigma	A3853

* Ferritin heavy chain 1; ** Divalent metal transporter 1

Table 3.5. Secondary Antibodies

Antigen	Host Species	Conjugate	Dilution	Source	Product Number
Rabbit IgG	Goat	Horse radish peroxidase	1:4000	Bio-Rad	170-6515
Mouse IgG	Goat	Horse radish peroxidase	1:2000 1:20000 (Actin)	Bio-Rad	170-6516

To assess comparable protein loading, membranes were re-probed for actin, which was used as a loading control. Membranes were incubated with the appropriate primary and secondary antibodies (diluted in PBST) as detailed in the tables above.

To determine the relative protein expression levels, images were quantified using ImageJ software (v2.0). The band intensity of each lane was quantified for both the protein of interest and the loading control (actin), and each protein of interest band was normalized to the corresponding actin loading control band.

3.11 ASSESSMENT OF DRUG INTERACTION

Drug-drug interactions were assessed according to the Combination Index (CI) Model, which provides an objective measure of the magnitude of the interactions by determining CI values, defined as (110-112):

$$\frac{d_{ax}}{D_{ax}} + \frac{d_{bx}}{D_{bx}} = CI$$

Where d_{ax} and d_{bx} are the doses of drugs "a" and "b", respectively, given in combination that are required to produce a given amount of cell death (x); and D_{ax} and D_{bx} are the doses of drugs "a" and b", respectively, given as single-agent treatments that are required to produce the same effect (x).

Using GraphPad Prism 7 software, sigmoidal single-agent dose response curves were generated. For each dose combination assessed, single-agent dose response curves were used to calculate the doses required to produce the same relative cell viability (D_{ax} and D_{bx}). CI values were then calculated for each drug combination. A CI of less than one indicates synergy, a CI that is equal to one indicates additivity, and a CI that is greater than one indicates antagonism (110-112).

The major limitation of the CI model is that it requires that each individual drug be able (at some concentration) to produce the same effect as the drugs in combination (112). Therefore, as is common in studies assessing drug combinations in biological systems, the maximum effect of each individual agent was assumed to be 100% cell death, for the purpose of single-agent dose response curve fitting. Conversely, this method avoids some of the limitations associated with other combination analysis methods, such as being valid only for drugs whose effects are either mutually exclusive or mutually nonexclusive, or only being valid when the dose response curves of both drugs are hyperbolic (110, 111, 113).

3.12 STATISTICAL ANALYSIS

Data analysis was performed using both Microsoft Excel 2016 and GraphPad Prism 7, while all graphs were generated in GraphPad Prism 7. Statistical calculations were performed using GraphPad Prism 7. Statistical significance was determined using unpaired t-tests comparing the different conditions. A p-value of less than 0.05 was defined as the threshold for significant difference. Statistical significance was noted in the figures as $*p<0.05$, $**p<0.01$, $***p<0.001$, or ****p<0.0001. Error bars on all graphs represent standard error of the mean for each group ($n\geq3$).

CHAPTER 4: RESULTS

4.1 AIM 1: TO DETERMINE WHETHER LYSOSOME TARGETING AGENTS AND TYROSINE KINASE INHIBITORS INDUCE SYNERGIC CELL DEATH IN LUNG ADENOCARCINOMA AND GLIOBLASTOMA CELLS

A549 (lung adenocarcinoma) and U87 (glioblastoma) cells were treated with lysosome targeting agents and tyrosine kinase inhibitors, both alone and in combination, to determine whether these agents were synergistic in inducing cell death in these cell lines. The initial studies were done with the drug combination of siramesine and lapatinib.

4.1.1 Determination of optimal doses of siramesine and lapatinib

A549 and U87 cells were treated with a range of concentrations of siramesine (5-75 μM) or lapatinib (0.5-40 μM), to generate dose-response curves. Total cell death was assessed by trypan blue staining and flow cytometry following 24 hours of incubation with the drugs (Figure 4.1). Dose-response curves were required to determine the concentrations of the selected drugs that had a killing effect on the cells. For the combination studies, we were interested in individual drug doses that induced limited cell death to allow for clearer identification of synergy. For these experiments, the highest concentration of each drug that produced less than 20% cell death was chosen. For all subsequent experiments using siramesine and lapatinib, the optimal concentrations were 10 μM siramesine and 0.5 μM lapatinib.

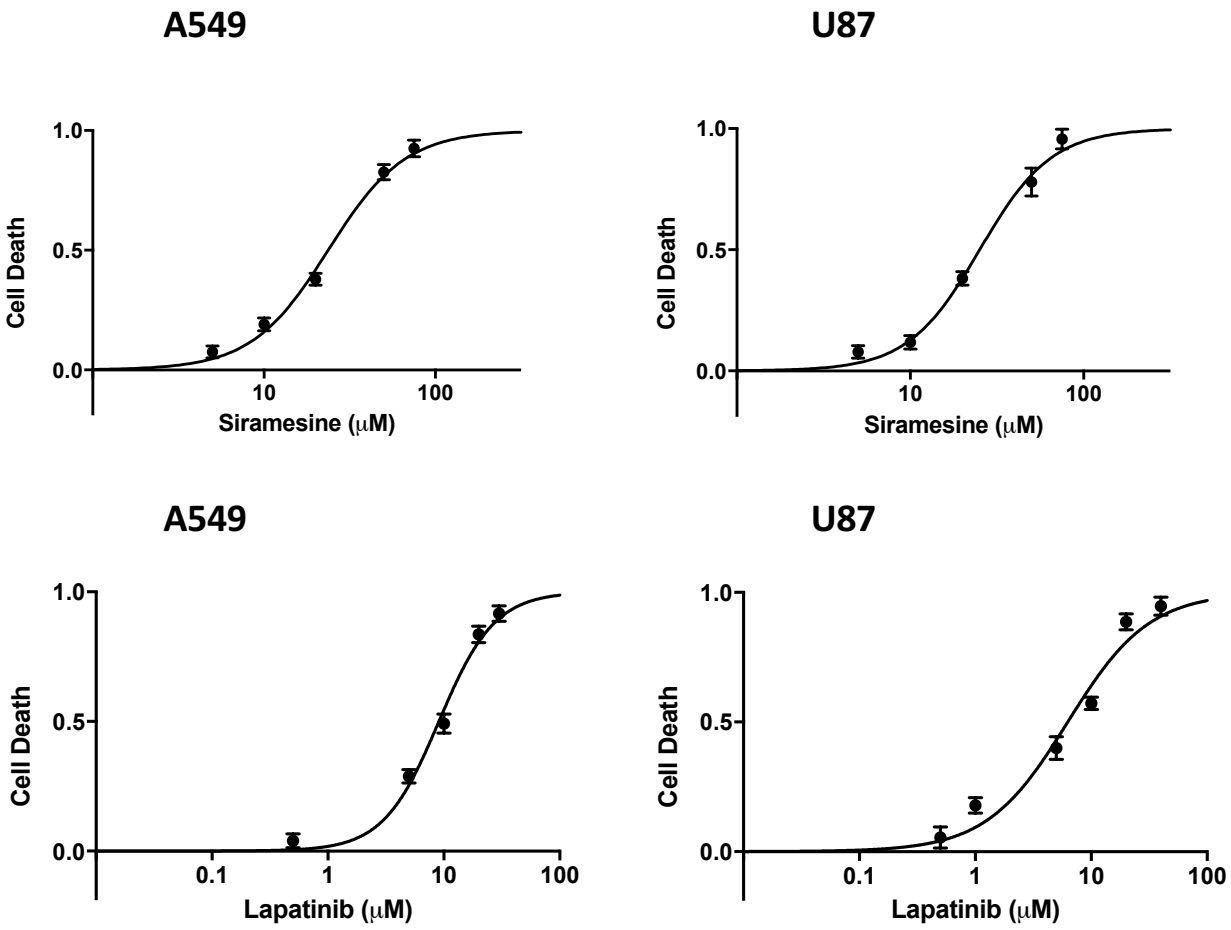

Figure 4.1: Dose-response curves for siramesine and lapatinib.
A549 and U87 cells were treated for 24 hours with a range of concentrations of siramesine or lapatinib, in order to generate dose-response curves. Cell death was measured by trypan blue staining and quantified by flow cytometry (n=3).

4.1.2 Determination of optimal incubation times for cells treated with siramesine and lapatinib

A549 and U87 cells were treated with DMSO (vehicle control), siramesine, lapatinib, or the combination of siramesine and lapatinib for 1, 2, 4, 6, and 24 hours, in order to develop treatment time-response data. While there was minimal synergy at time points ≤ 6 hours, the differences in response between treatment with the drug combination and individual drugs was most significant at 24 hours (Figure 4.2). Therefore, 24-hour incubation times were chosen for most subsequent experiments, to maximize the measurable effects of synergy.

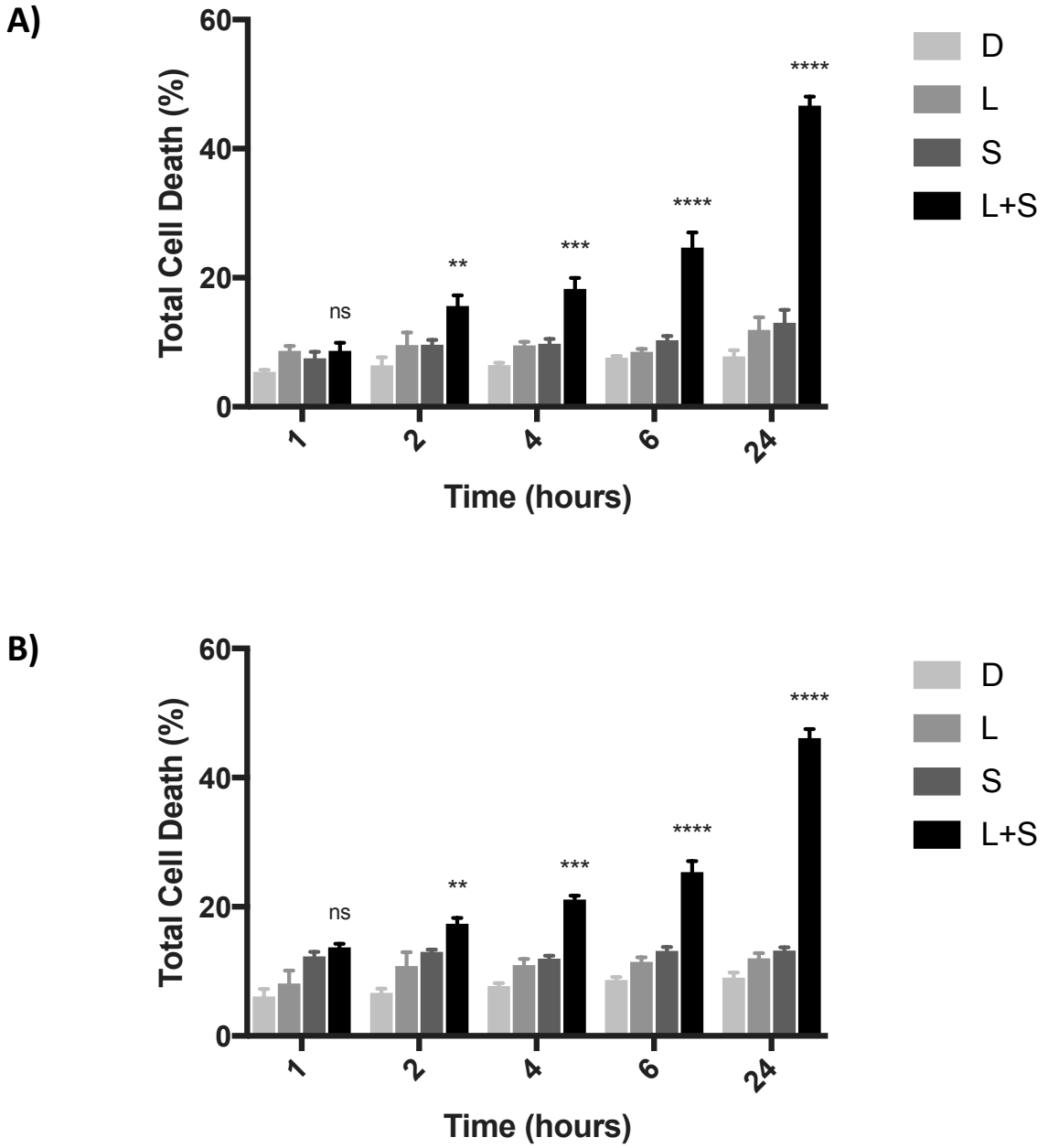

Figure 4.2: Time course of siramesine and lapatinib-induced cell death.
(A) A549 and **(B)** U87 cells were treated with DMSO (D), lapatinib (L) (0.5 μM), siramesine (S) (10 μM), or the combination of lapatinib + siramesine (L+S) for 1, 2, 4, 6, and 24 hours. Cell death was measured by trypan blue staining and quantified by flow cytometry. Each column represents the mean ± 1 SEM (n=3). Statistical significance was determined by unpaired t-tests comparing cells treated with L+S to each of the other conditions (ns, not significant; ** $p<0.01$, *** $p<0.001$, **** $p<0.0001$, n=3).

4.1.3 Siramesine and lapatinib induce synergic cell death in glioblastoma and lung adenocarcinoma cells

To determine whether the combination of siramesine and lapatinib would lead to synergic cell death, A549 and U87 cells were treated for 24 hours with DMSO, siramesine, lapatinib, or the combination of siramesine (10 μM) and lapatinib (0.5 μM). The combination of siramesine and lapatinib led to synergic cell death in both cell lines, with significantly higher rates of death than were seen with either drug alone, and more than if the drug effects were simply additive (Figure 4.3A). For each cell line, < 20% death was observed in the cells treated with DMSO, siramesine or lapatinib, compared to > 45% death in the cells treated with the combination of siramesine and lapatinib ($p<0.0001$).

Isobolograms were generated to confirm that cell death resulting from the combination of siramesine and lapatinib was the result of a synergistic effect of the drug combination. Combination indices (CIs) were calculated to provide a numerical representation of the combinatorial effect. A CI that approaches 1, indicates that a drug combination is additive. A CI > 1 indicates that the combination is antagonistic; and a CI < 1 indicates that the combination is synergistic. The CIs for the combination of siramesine and lapatinib were < 1 in both the A549 (0.454) and U87 (0.436) cell lines at 24 hours, confirming that the combination showed synergism in inducing cell death. (Figure 4.3B).

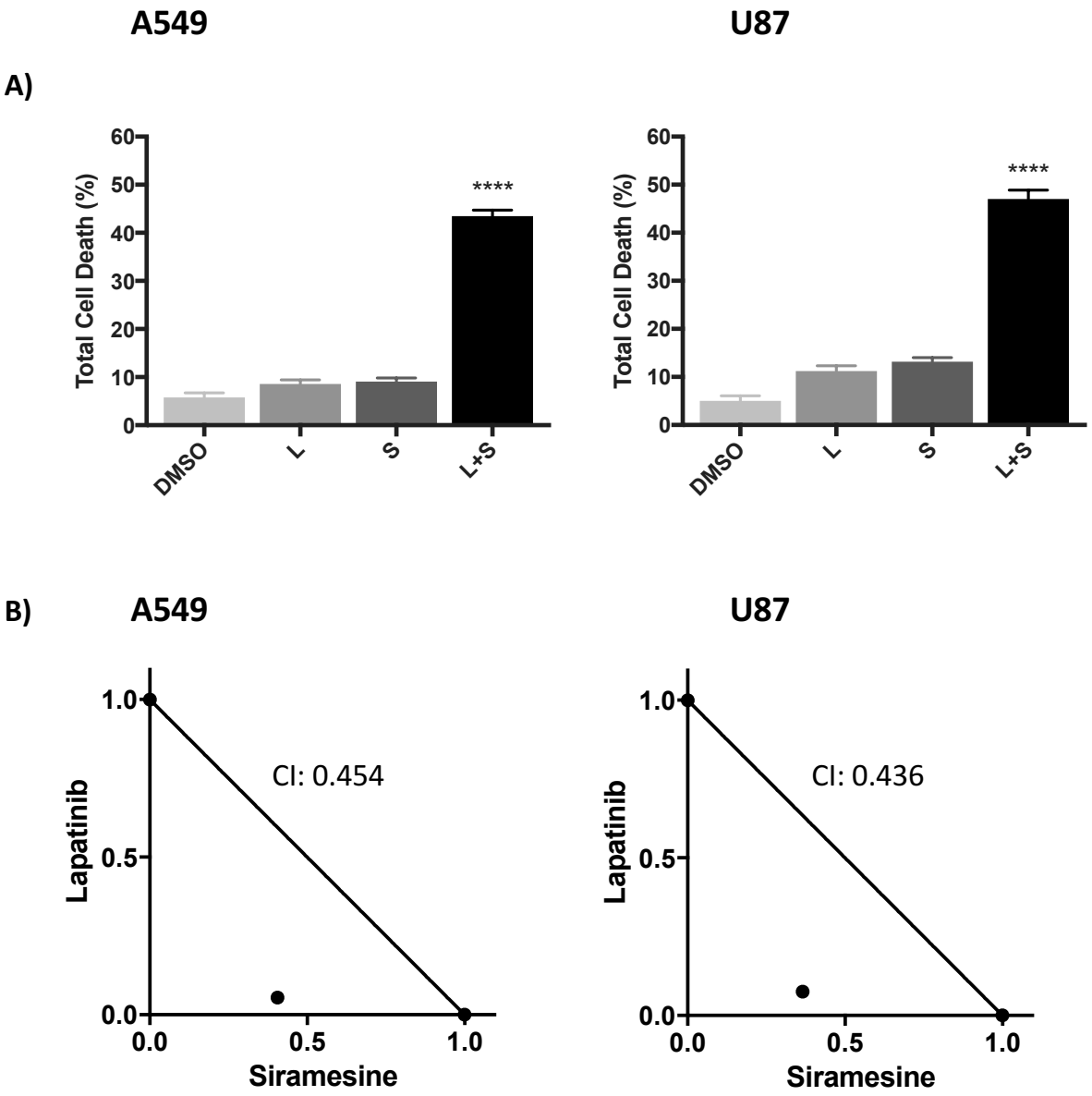

Figure 4.3: Siramesine and lapatinib induce synergic cell death.
(A) A549 and U87 cells were treated for 24 hours with DMSO (D), lapatinib (L) (0.5 μM), siramesine (S) (10 μM), or the combination of lapatinib + siramesine (L+S). Cell death was measured by trypan blue staining and quantified by flow cytometry. Each column represents the mean ± 1 SEM (n=4). Statistical significance was determined by unpaired t-tests comparing cells treated with L+S to each of the other conditions (**** $p<0.0001$ for all comparisons).
(B) Isobolograms demonstrating the effects of the combination of siramesine and lapatinib. Drug-drug interactions were also assessed using the combination index (CI) model. The CI < 1 for siramesine and lapatinib in both the A549 and U87 cell lines at 24 hours indicates synergy.

4.1.4 The synergic effect of siramesine and lapatinib is reproduced by other combinations of lysosome targeting agents and tyrosine kinase inhibitors

To determine whether the synergistic effect on cell death was the result of the specific combination of siramesine and lapatinib, or whether it was the class of drug that was important, the effects of other lysosome targeting agents and tyrosine kinase inhibitors, alone and in combination, were examined.

Before combinations of drugs were studied, preliminary dose-finding studies for each individual drug were required. Dose-response curves were generated for each drug in each cell line (Figure 4.4A and 4.4B). A549 and U87 cells were incubated for 24 hours with a range of concentrations of lysosome targeting agents and TKIs. The lysosomotropic drugs tested were desipramine (1-175 μM), tafenoquine (3-20 μM), clemastine (5-80 μM), loratadine (5-150 μM), and desloratadine (5-90 μM). The TKIs tested were gefitinib (10-80 μM) and sorafenib (2-20 μM). Cell death was measured as described above, and the data were used to generate dose-response curves for each drug.

To optimize the identification of synergy when the drugs were studied in combination, the highest concentration of each drug that produced < 20% cell death was chosen. For the subsequent combination experiments, the specific concentrations of each drug used were: 10 μM desipramine, 3 μM tafenoquine, 20 μM clemastine, 20 μM loratadine, 40 μM desloratadine, 10 μM gefitinib, and 2 μM sorafenib, (with the 10 μM siramesine and 0.5 μM lapatinib, as described above) (See Table 3.3).

Using the drug concentrations that individually produced < 20% death, the drugs were tested in combinations. U87 and A549 cells were treated with DMSO (as a vehicle control), individual agents, or with combinations of agents for 24 hours before measuring cell death.

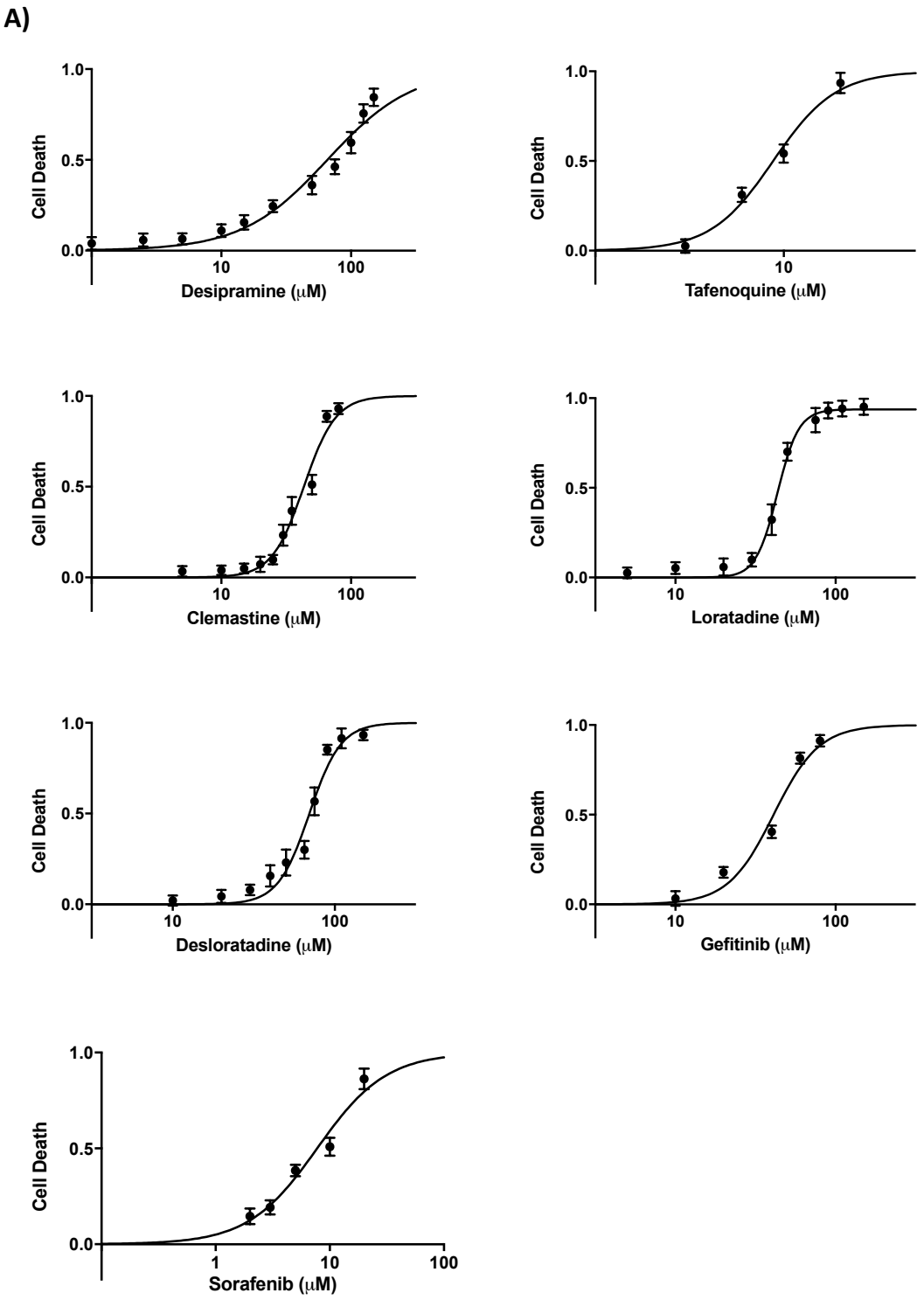

Figure 4.4A: Dose-response curves for other lysosome targeting agents and tyrosine kinase inhibitors investigated. A549 cells were treated for 24 hours with a range of concentrations of desipramine, tafenoquine, clemastine, loratadine, desloratadine, gefitinib and sorafenib to generate dose-response curves. Cell death was measured by trypan blue staining and quantified by flow cytometry (n=3).

B)

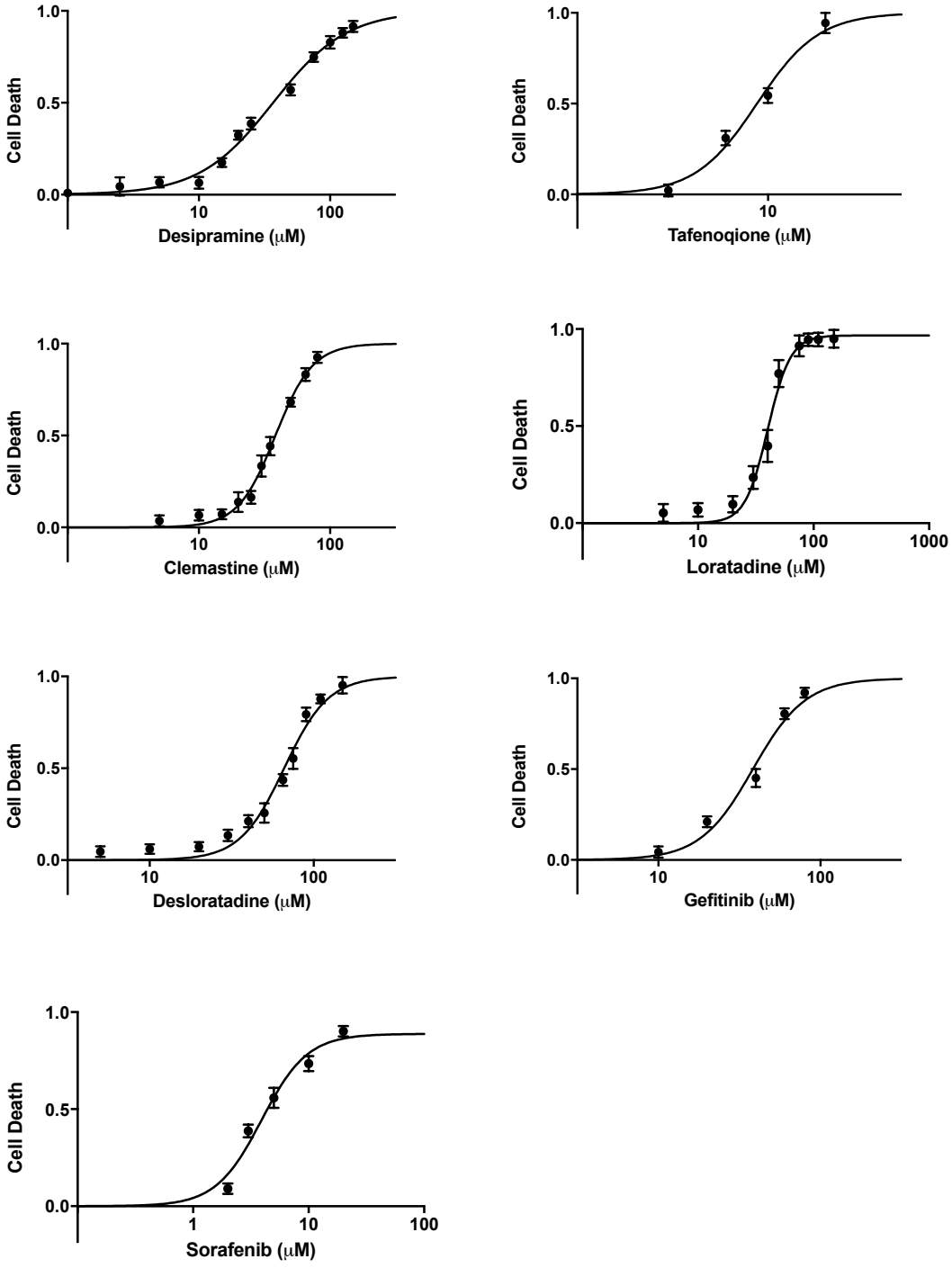

Figure 4.4B: Dose-response curves for other lysosome targeting agents and tyrosine kinase inhibitors investigated. U87 cells were treated for 24 hours with a range of concentrations of desipramine, tafenoquine, clemastine, loratadine, desloratadine, gefitinib and sorafenib to generate dose-response curves. Cell death was measured by trypan blue staining and quantified by flow cytometry (n=3).

Combinations that were synergistic induced > 50% cell death at 24 hours, while the combinations that were not synergistic produced < 30% cell death (Figure 4.5A). Isobolograms were generated to determine whether each drug combination was synergistic, additive, or antagonistic. For all drug combinations, CIs were calculated to confirm that the effects of the drug combinations were synergistic, additive, or antagonistic (Figure 4.5B and 4.5C, and summarized in Table 4.1).

Several drug combinations, in addition to siramesine and lapatinib, produced synergistic effects on cell death (desipramine and lapatinib; siramesine and sorafenib; clemastine and lapatinib; loratadine and lapatinib; desloratadine and lapatinib), while other combinations (tafenoquine and lapatinib; siramesine and gefitinib; tafenoquine and gefitinib) did not (Table 4.1).

Table 4.1. Combination Indices for Combinations of Lysosome Targeting Agents and Tyrosine Kinase Inhibitors

	Combination Index (CI)	
Drug Combinations	**A549 Cells**	**U87 Cells**
Desipramine and Lapatinib	0.484	0.451
Siramesine and Sorafenib	0.503	0.668
Clemastine and Lapatinib	0.486	0.549
Loratadine and Lapatinib	0.493	0.554
Desloratadine and Lapatinib	0.519	0.638
Tafenoquine and Lapatinib	0.922	0.975
Siramesine and Gefitinib	1.251	1.158
Tafenoquine and Gefitinib	1.023	1.177

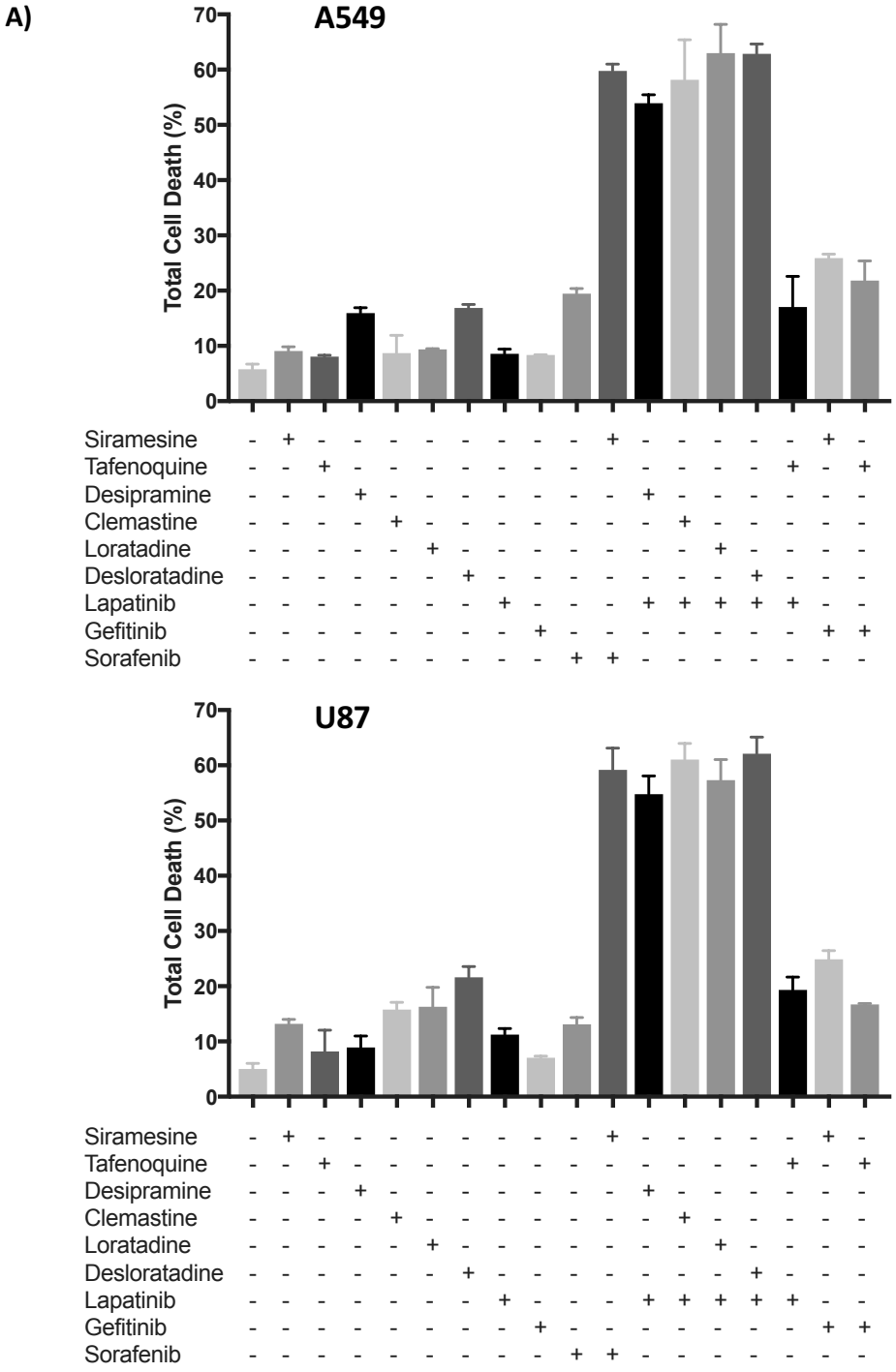

Figure 4.5A: Synergic cell death is induced by other combinations of lysosome targeting agents and tyrosine kinase inhibitors (TKIs). A549 and U87 cells were treated with various combinations of the lysosome targeting agents and TKIs. Cell death was measured by trypan blue staining and quantified by flow cytometry. Each column represents the mean ± 1 SEM (n=3).

B)

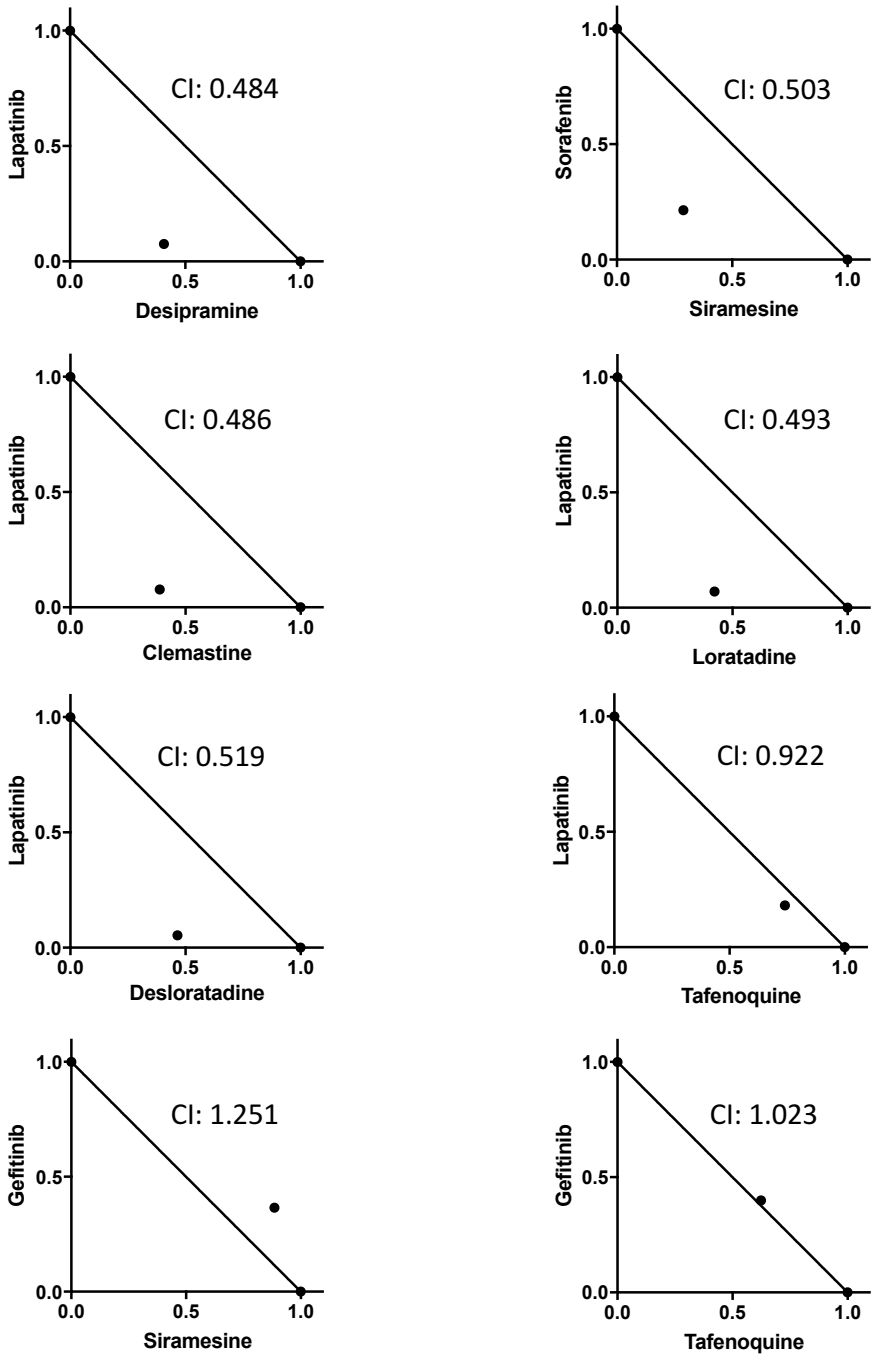

Figure 4.5B: Synergic cell death is induced by other combinations of lysosome targeting agents and tyrosine kinase inhibitors (TKIs). A549 cells were treated with various combinations of the lysosome targeting agents and TKIs. Isobolograms were generated for the A549 cells to determine whether each combination was synergic, additive, or antagonistic. Drug-drug interactions were also assessed using the combination index (CI) model. A combination index (CI) <1 indicates synergy, CI=1 indicates that the drugs are additive, and CI>1 indicates the drugs are antagonistic.

C)

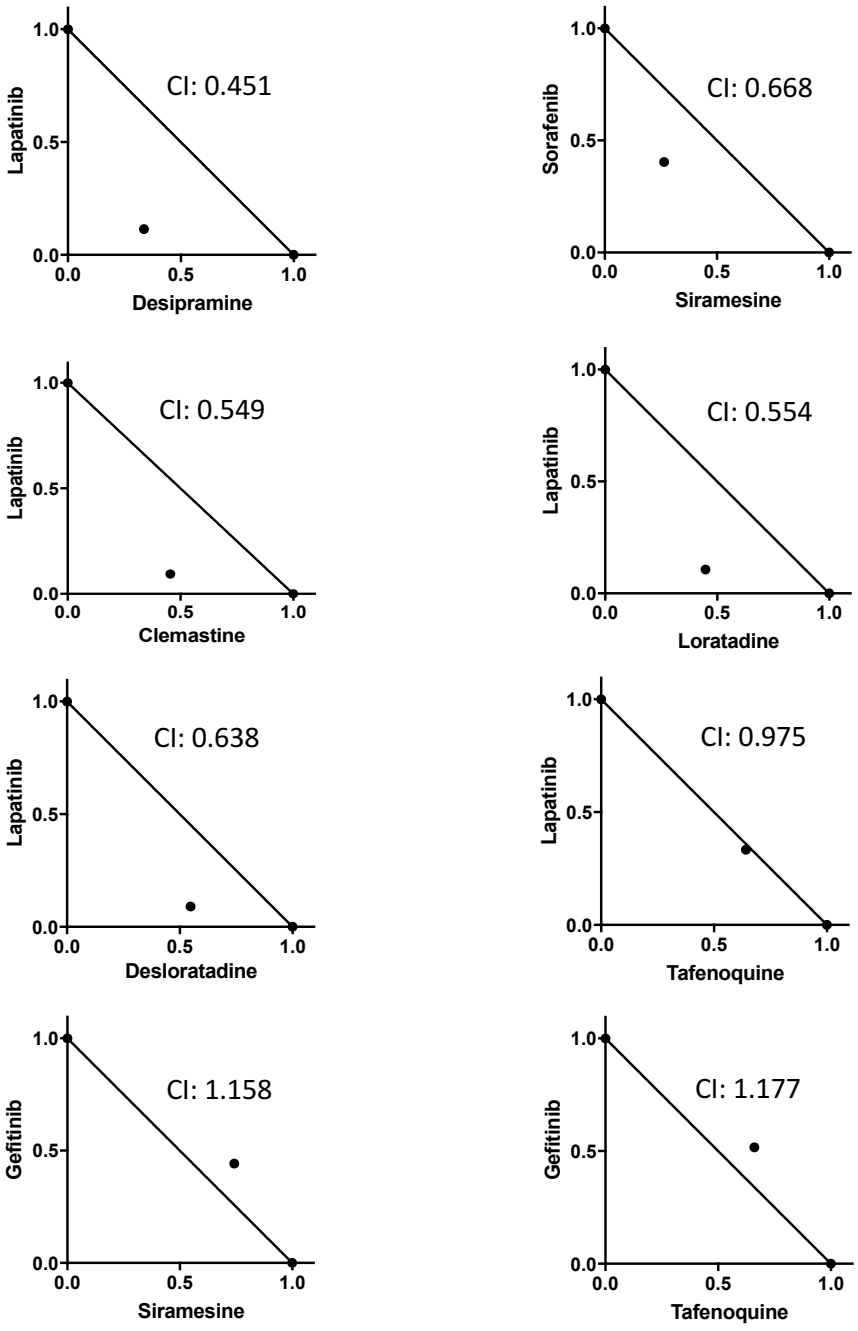

Figure 4.5C: Synergic cell death is induced by other combinations of lysosome targeting agents and tyrosine kinase inhibitors (TKIs). U87 cells were treated with various combinations of the lysosome targeting agents and TKIs. Isobolograms were generated for the U87 cells to determine whether each combination was synergic, additive, or antagonistic. Drug-drug interactions were also assessed using the combination index (CI) model. A combination index (CI) <1 indicates synergy, CI=1 indicates that the drugs are additive, and CI>1 indicates the drugs are antagonistic.

Siramesine, desipramine, tafenoquine, clemastine, loratadine, and desloratadine are all lysosomotropic agents, but only the antidepressant drugs (siramesine and desipramine) and the antihistamines (clemastine, loratadine, and desloratadine) led to synergic cell death when combined with the tyrosine kinase inhibitor lapatinib, as compared to the antimalarial drug (tafenoquine).

4.2 AIM 2: TO DETERMINE WHETHER THE SYNERGIC CELL DEATH INDUCED BY SIRAMESINE AND LAPATINIB IS OCCURRING VIA A FERROPTOTIC MECHANISM

Having determined that some combinations of lysosome targeting agents and tyrosine kinase inhibitors induced synergic cell death, we sought evidence that cell death was occurring via a ferroptotic mechanism. The studies of ferroptosis were performed using the combination of siramesine and lapatinib. In order to determine whether the drug combination-induced cell death was occurring via an iron-dependent mechanism we examined specific aspects of the ferroptosis pathway.

4.2.1 Erastin induces cell death in A549 and U87 cells that can be inhibited by ferrostatin-1 (Fer-1) and deferoxamine (DFO)

Erastin was the original molecule identified to cause the form of cell death that is now recognized as ferroptosis (75). Erastin-induced cell death is considered the model for ferroptosis. Before examining cell death induced by siramesine and lapatinib for characteristics of ferroptosis, we used erastin to confirm that ferroptotic cell death could be induced in A549 cells

and U87 cells, and that this death could be inhibited by Fer-1 and DFO, as previously described (75, 108).

A549 and U87 cells were incubated for 24 and 48 hours with a range of concentrations of erastin (1-50 μM), in order to generate dose-response curves (Figure 4.6A and B). The concentration selected for subsequent experiments was 15 μM because it induced approximately 50% cell death. This was sufficient to demonstrate a cell killing effect and to evaluate the effect of the ferroptosis inhibitors. Cell death was measured as described above. There was significantly more death observed at 48 hours (20-95% cell death) than at 24 hours (5-10% cell death) (Figure 4.6A). Therefore, all subsequent experiments with erastin were performed with 48 hours incubation.

A549 and U87 cells were pretreated with the ferrpoptosis inhibitors Fer-1 (10 μM) or DFO (200 μM) for one hour prior to the addition of erastin (15 μM). In both cell lines, Fer-1 and DFO significantly reduced the amount of cell death induced by erastin (Figure 4.7). The relative reduction in erastin-induced cell death by Fer-1 was 68% in the A549 cells and 81% in the U87 cells ($p<0.0001$). The relative reduction in erastin-induced cell death by DFO was 67% in the A549 cells and 80% in the U87 cells ($p<0.0001$). Therefore, the cell lines in this study were susceptible to death by erastin and could be rescued from erastin-induced cell death by ferroptosis inhibitors.

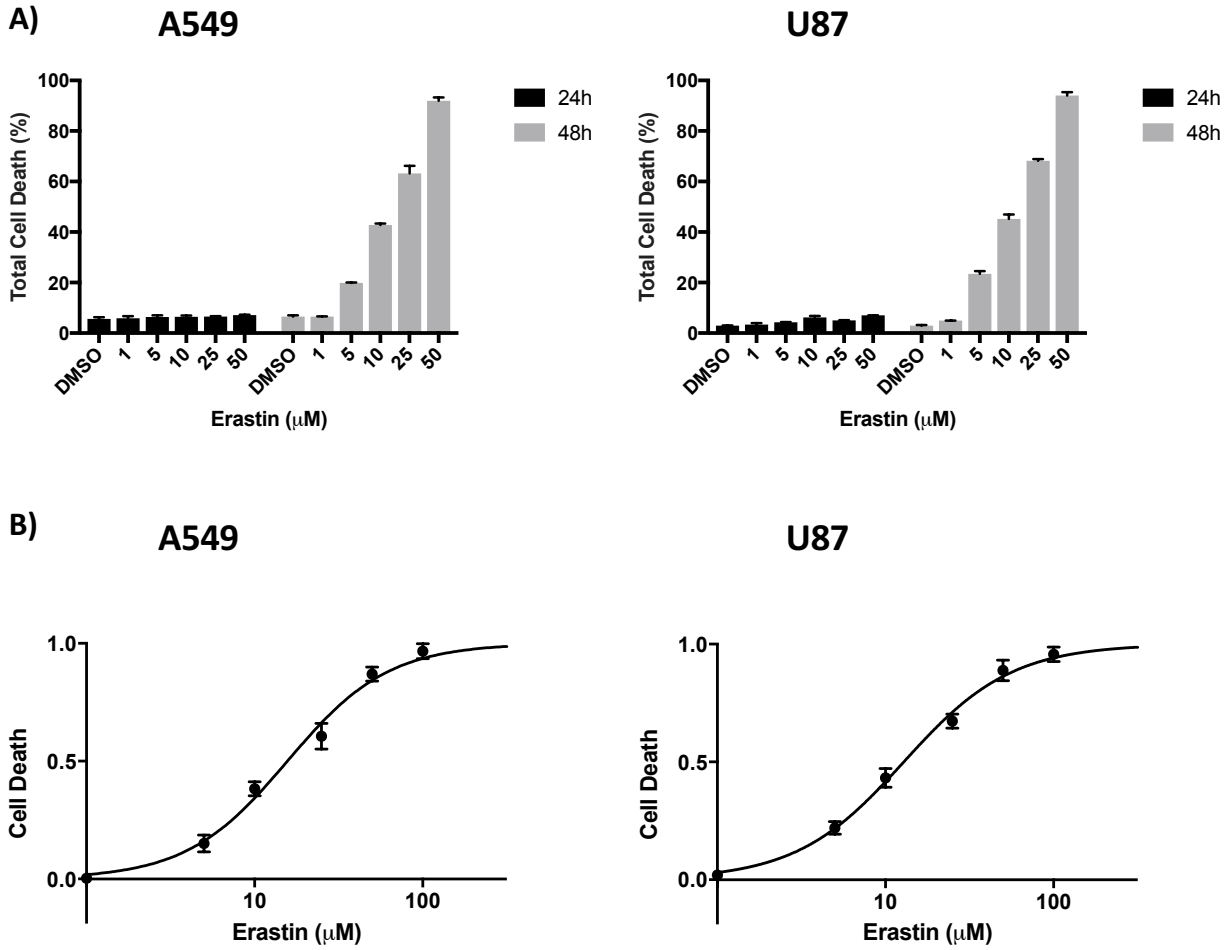

Figure 4.6: Dose-response curves and time course for erastin-induced cell death.
(A) A549 and U87 cells were treated with a range of concentrations of erastin for 24 and 48 hours. Cell death was measured by trypan blue staining and quantified by flow cytometry. Each column represents the mean ± 1 SEM (n=3). **(B)** A549 and U87 cells were treated for 48 hours with a range of concentrations of erastin, in order to generate dose-response curves. Cell death was measured as in (A) (n=3).

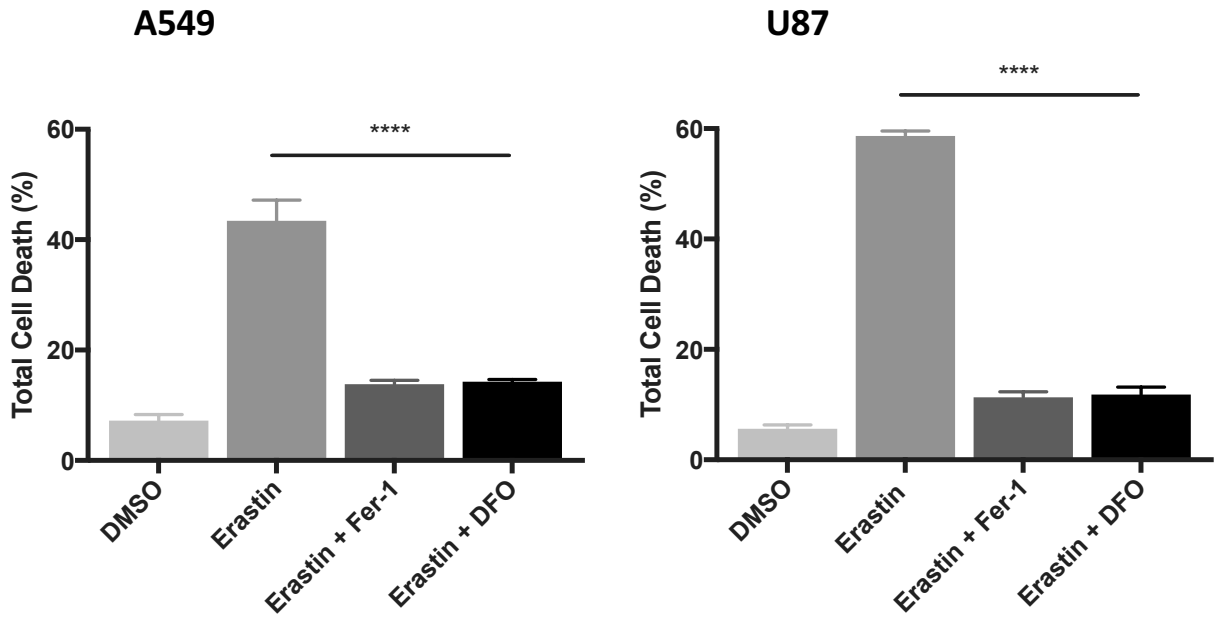

Figure 4.7: Erastin-induced cell death can be inhibited by ferrostatin-1 (Fer-1) and deferoxamine (DFO). A549 and U87 cells were pretreated with Fer-1 (10 μM) or DFO (200 μM) for one hour before incubation with erastin (15 μM) for 48 hours. Cell death was measured by trypan blue exclusion. Each column represents the mean ± 1 SEM (n=3). Statistical significance was determined by unpaired t-tests comparing cells treated with erastin alone to each of the other conditions (**** $p<0.0001$).

4.2.2 Fer-1 protects A549 and U87 cells from siramesine and lapatinib-induced cell death

A549 and U87 cells were pretreated with Fer-1 (10 μM), which inhibits the accumulation of ROS from lipid peroxidation. In both cell lines, Fer-1 had no effect on the cells treated with either DMSO or either drug, individually, but inhibited cell death induced by the combination of siramesine and lapatinib. The relative reduction in siramesine and lapatinib-induced cell death was 38% for the A549 cells and 32% for the U87 cells ($p<0.0001$). The results suggest that a ferroptotic mechanism was contributing to cell death induced by the drug combination (Figure 4.8A).

4.2.3 DFO protects A549 and U87 cells from siramesine and lapatinib-induced cell death

A549 and U87 cells were pretreated with DFO (200 μM), which chelates intracellular free iron. As with the Fer-1, DFO had no effect on the cells treated with DMSO or either drug, individually, but decreased cell death induced by the combination of siramesine and lapatinib. The relative reduction in siramesine and lapatinib-induced cell death was 30% for the A549 cells and 39% for the U87 cells ($p<0.0001$). These results provide evidence that an iron-mediated process contributed to the cell death induced by the drug combination (Figure 4.8B).

4.2.4 Addition of exogenous iron increases siramesine and lapatinib-induced cell death in A549 and U87 cells

An additional approach to investigate the role of iron in siramesine and lapatinib-induced cell death was to pretreat A549 and U87 cells with an excess of exogenous iron in the form of iron chloride ($FeCl_3$). $FeCl_3$ had no effect on the cells treated with DMSO, lapatanib, or siramesine alone, but significantly increased the A549 and U87 cell death following treatment

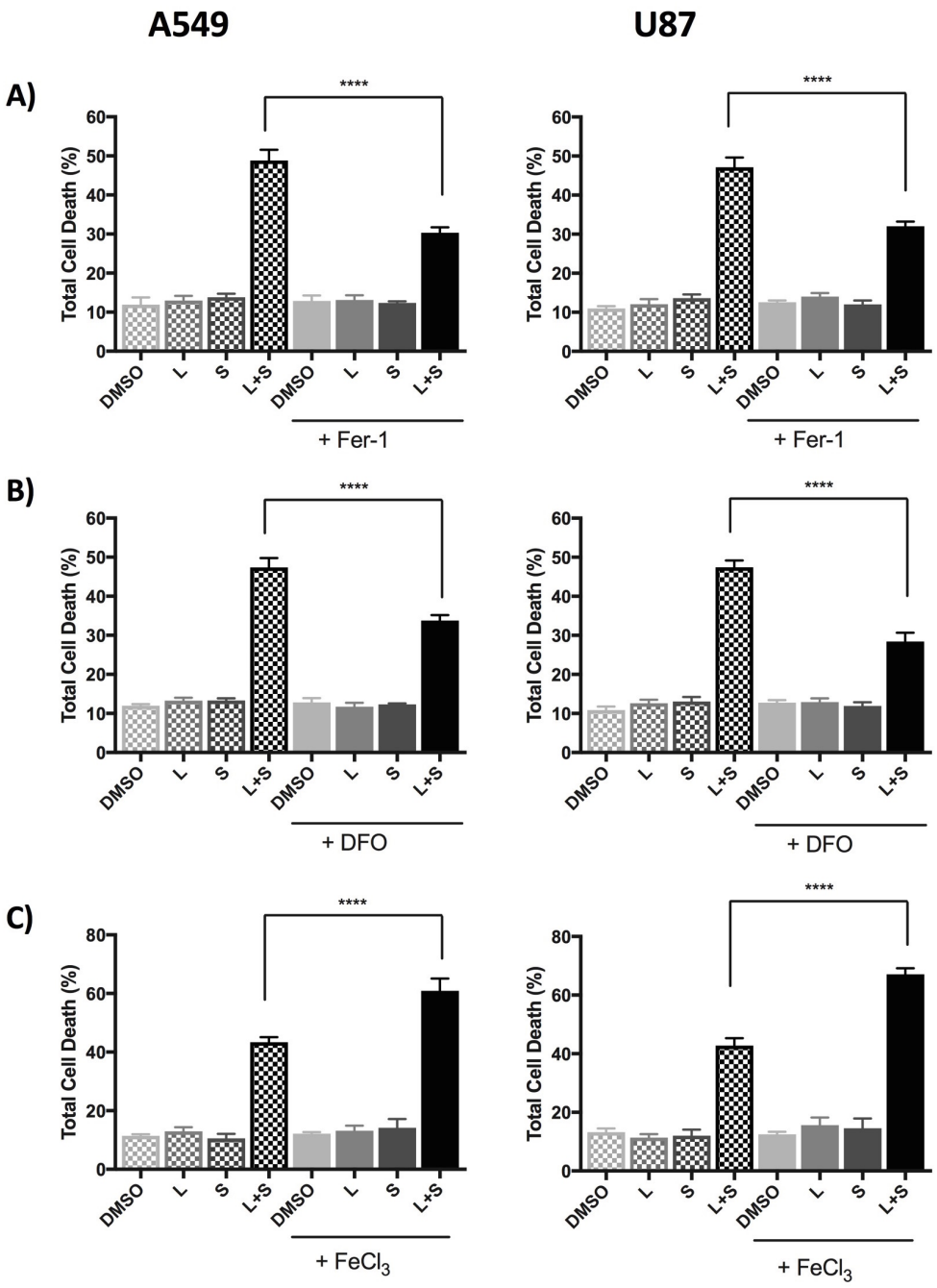

Figure 4.8: Ferrostatin-1 (Fer-1) and deferoxamine (DFO) protect cells from siramesine and lapatinib-induced cell death, and the addition of exogenous iron increased siramesine and lapatinib-induced cell death. A549 and U87 cells were pretreated with (**A)** Fer-1 (10 μM), (**B)** DFO (200 μM) or **(C)** iron chloride ($FeCl_3$; 50 μM) for one hour before treatment with DMSO, lapatinib (L), siramesine (S), or the combination of lapatinib and siramesine (L+S) for 24 hours. Cell death was measured by trypan blue staining and quantified by flow cytometry. Each column represents the mean ± 1 SEM (n=3). Statistical significance was determined by unpaired t-tests comparing cells treated with lapatinib and siramesine in the presence or absence of the inhibitors or $FeCl_3$ (**** $p<0.0001$).

with the combination of siramesine and lapatinib (Figure 4.8C). The relative increase in siramesine and lapatinib-induced cell death was 41% for the A549 cells and 56% for the U87 cells ($p<0.0001$). These results provide additional evidence for the contribution of iron in the cell death induced by the combination of siramesine and lapatinib.

4.3 AIM 3: TO DETERMINE THE SPECIFIC MECHANISM BY WHICH THE COMBINATION OF SIRAMESINE AND LAPATINIB ARE INDUCING CELL DEATH

Having demonstrated that the combination of siramesine and lapatinib was producing iron-dependent cell death consistent with ferroptosis, we proceeded to investigate additional characteristics of cells undergoing ferroptosis, including changes in the levels of intracellular iron and ROS, increased lipid peroxidation and alterations in the expression of iron transport and storage proteins that have been associated with siramesine and lapatinib-induced cell death in other cell types (108).

4.3.1 The combination of siramesine and lapatinib increases the intracellular labile iron pool

Because the combination of siramesine and lapatinib induced cell death via an iron-dependent mechanism, we determined whether the drug combination produced an increase in the intracellular labile iron pool. Prussian Blue staining and light microscopy were used to determine whether the drug combination led to an increase in intracellular iron. Cells were stained and examined 12 hours after treatment with DMSO, siramesine or lapatinib alone, or the drug combination. The 12-hour time point was selected to precede the cell death observed at 24 hours;

it was hypothesized that changes in intracellular iron levels would be best observed before significant death had occurred. Prussian Blue staining was increased at 12 hours in cells treated with the combination of siramesine and lapatinib, compared to cells treated with DMSO or with either drug alone (Figure 4.9A). The Prussian Blue-stained images were subjected to quantitative image analysis using ImageJ software to calculate the integrated density. There was a 2-fold increase in the intracellular iron staining in cells treated with the drug combination, compared to the other conditions ($p<0.0001$) (Figure 4.9B). There was no difference in Prussian Blue staining of cells treated with siramesine or lapatinib compared to the control.

To confirm the findings obtained with the Prussian Blue-stained images, Calcein-AM fluorescence assays were performed after 12 hours of incubation with DMSO, either drug individually, or the drug combination. When Calcein enters the cell, it binds intracellular iron, quenching its fluorescent signal. Upon addition of an iron chelator (deferiprone, in this instance), which binds the iron, the fluorescent signal of Calcein is de-quenched. The difference between the quenched and de-quenched signals is representative of the intracellular labile iron pool. The Calcein assay demonstrated that the combination of siramesine and lapatinib produced a three-fold increase in the intracellular labile iron pool, compared to DMSO or either drug alone ($p<0.0001$) (Figure 4.9C). Collectively, these results indicate that treatment with the combination of siramesine and lapatinib increased the intracellular labile iron pool and provide additional evidence for the involvement of iron in the cell death induced by this drug combination.

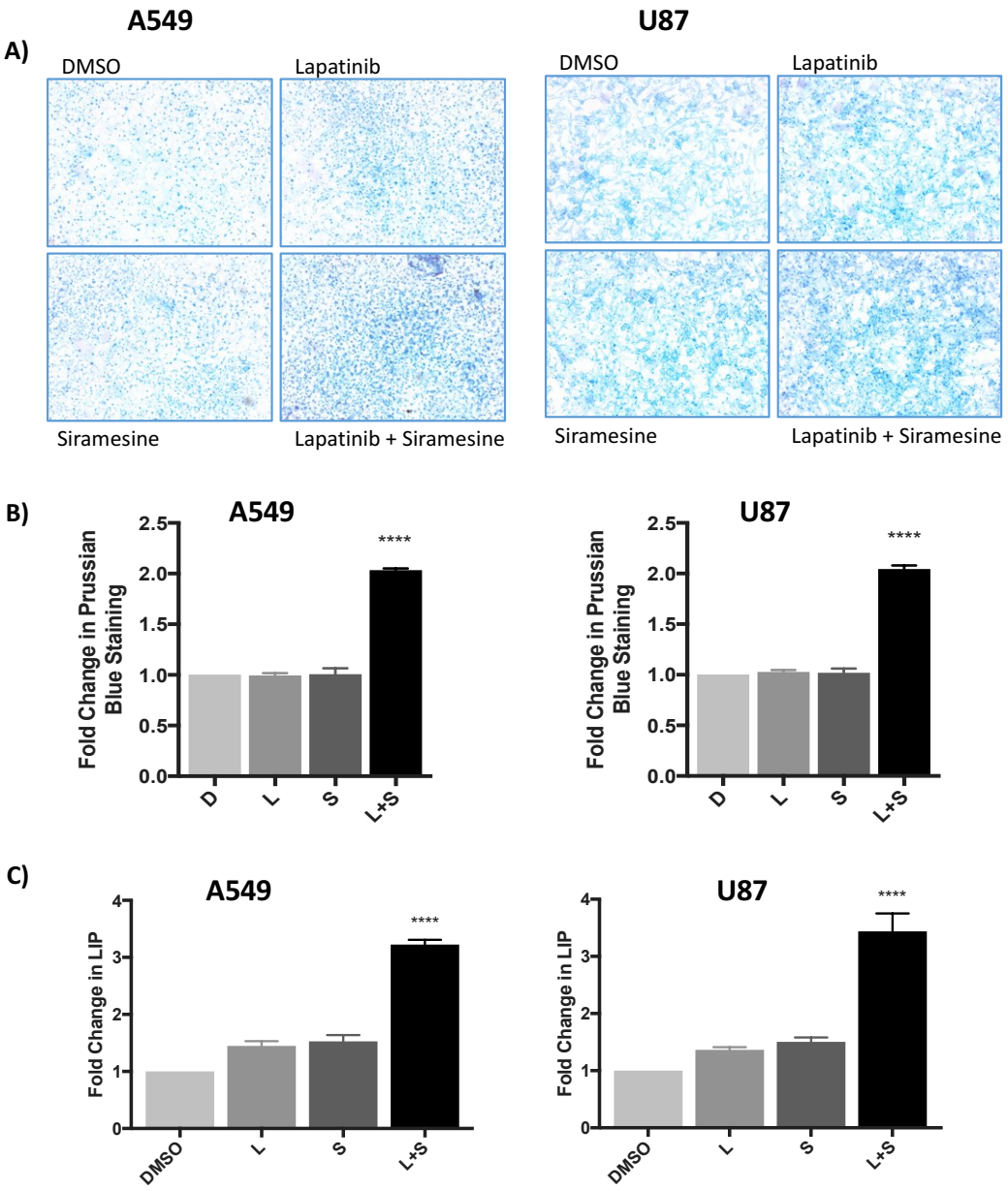

Figure 4.9: Treatment of A549 and U87 cells with the combination of siramesine and lapatinib increases the intracellular labile iron pool (LIP). (A) Prussian blue staining for intracellular iron was performed and evaluated by light microscopy after 12 hours incubation with DMSO, lapatinib (L), siramesine (S), or with the combination of lapatinib + siramesine (L+S). Representative images from 3 separate experiments. **(B)** Quantitative image analysis of Prussian Blue staining. Each column represents the mean ± 1 SEM. Statistical significance was determined by unpaired t-tests comparing cells treated with L+S to each of the other conditions (**** $p<0.0001$ for all comparisons, n=3). **(C)** Calcein fluorescence assays. A549 and U87 cells were stained with Calcein-AM (1 μM) after 12 hours incubation with DMSO, lapatinib (L), siramesine (S), or with the combination of lapatinib + siramesine (L+S). Fluorescence signals were measured by flow cytometry. Each column represents the mean ± 1 SEM. Statistical significance was determined as above (**** $p<0.0001$ for all comparisons, n=3).

4.3.2 The combination of siramesine and lapatinib leads to an increase in total ROS

The mechanism by which erastin-induced ferroptosis results in cell death is the accumulation of damaging intracellular ROS. We determined whether treatment with the combination of siramesine and lapatinib, and its associated increase in intracellular iron, led to an increase in intracellular ROS. A549 and U87 cells were incubated with the drugs, alone or in combination, for 24 hours. Cells were then stained with DHE. When DHE is oxidized by ROS, it emits a red fluorescent signal, which can be quantified by flow cytometry and is proportional to the production of ROS. Cells treated with the combination of siramesine and lapatinib showed a three-fold increase in total ROS, significantly greater than the ROS measured in the cells treated with DMSO or either drug alone ($p<0.0001$) (Figure 4.10). The results show that treatment with the drug combination increases the levels of ROS, providing support that this cell death is occurring via an oxidative process.

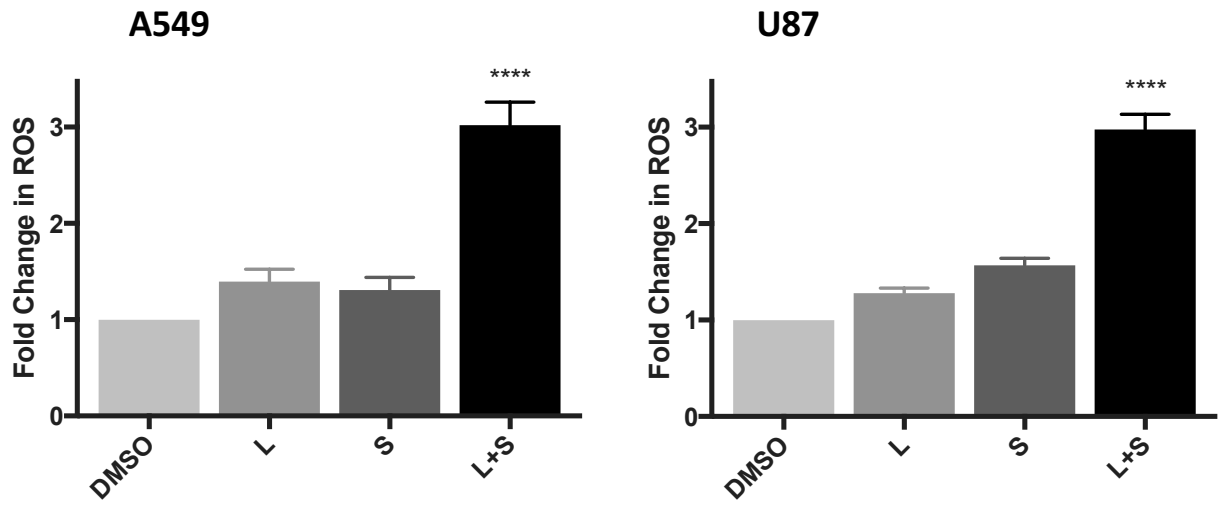

Figure 4.10: Treatment of A549 and U87 cells with the combination of siramesine and lapatinib increases levels of intracellular ROS. A549 and U87 cells were stained with DHE (10 μM) after 24 hours incubation with DMSO, lapatinib (L), siramesine (S), or with the combination of lapatinib + siramesine (L+S). DHE fluorescence was measured by flow cytometry. Each column represents the mean ± 1 SEM. Statistical significance was determined by unpaired t-tests comparing cells treated with L+S to each of the other conditions (**** $p<0.0001$ for all comparisons, n=3).

4.3.3 The combination of siramesine and lapatinib leads to an increase in lipid peroxidation

Ferroptosis is specifically characterized by lipid peroxidation, as opposed to the production of other forms of ROS. We investigated whether the combination of siramesine and lapatinib led to an increase in lipid ROS. A549 and U87 cells were treated with the drugs, alone or in combination, for 24 hours and then stained with C11-BODIPY to identify lipid peroxidation. Oxidation of a component of the C11-BODIPY fluorophore shifts the fluorescence emission from red to green. The ratio of red to green fluorescence is proportional to lipid peroxidation. The cells that were treated with the drug combination showed a two-fold increase in lipid ROS (indicating increased lipid peroxidation) compared to cells treated with DMSO or either drug alone ($p<0.0001$) (Figure 4.11). These results support the hypothesis that treatment with the drug combination increases the levels of lipid peroxidation, and therefore the levels of lipid ROS, supporting the hypothesis that cell death is occurring via a ferroptotic mechanism.

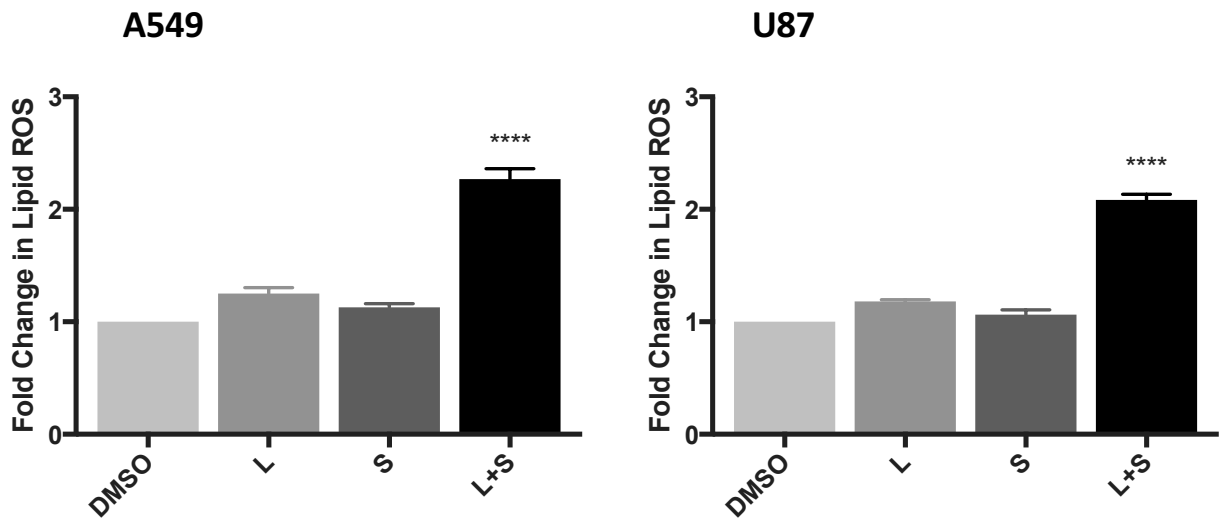

Figure 4.11: Treatment of A549 and U87 cells with the combination of siramesine and lapatinib increases levels of lipid peroxidation. A549 and U87 cells were stained with C11-BODIPY (1 μM) after 24 hours incubation with DMSO, lapatinib (L), siramesine (S), or with the combination of lapatinib + siramesine (L+S). Both red and green C11-BODIPY fluorescence was measured by flow cytometry, and a change in the ratio of green to red fluorescence was used to indicate an increase in lipid peroxidation. Each column represents the mean ± 1 SEM. Statistical significance was determined by unpaired t-tests comparing cells treated with L+S to each of the other conditions (**** $p<0.0001$ for all comparisons, n=3).

4.3.4 The combination of siramesine and lapatinib induces minor increases in expression levels of some iron transport proteins in A549 and U87 cells

To determine whether the drug combination-induced cell death was associated with changes in the expression levels of iron transport or storage proteins, five proteins involved in the regulation of iron were examined. These proteins were transferrin (a plasma iron transport protein), the transferrin receptor (binds transferrin on the cell surface leading to endocytosis), DMT1 (transports iron from the endosome into the cytosol), ferritin (cytosolic iron storage protein), and ferroportin (transports iron out of the cell) (Figure 1.2).

Western blots were performed on lysates of A549 and U87 cells after 12 hours or 24 hours incubation with DMSO, lapatinib, siramesine, or the combination of siramesine and lapatinib (Figure 4.12A). Densitometry analysis of the Western blots was performed using ImageJ software (Figure 4.12B and 4.12C). There were no significant changes in the expression levels of transferrin, ferroportin or ferritin after treatment with the drug combination compared to DMSO or either drug alone. There were small but statistically significant increases in the levels of TfR1 (20-35% at 12 and 24 hours in both the A549 and U87 cells) and DMT1 (20-25% at 24 hours in the A549 cells; 20-25% at 12 and 24 hours in the U87 cells).

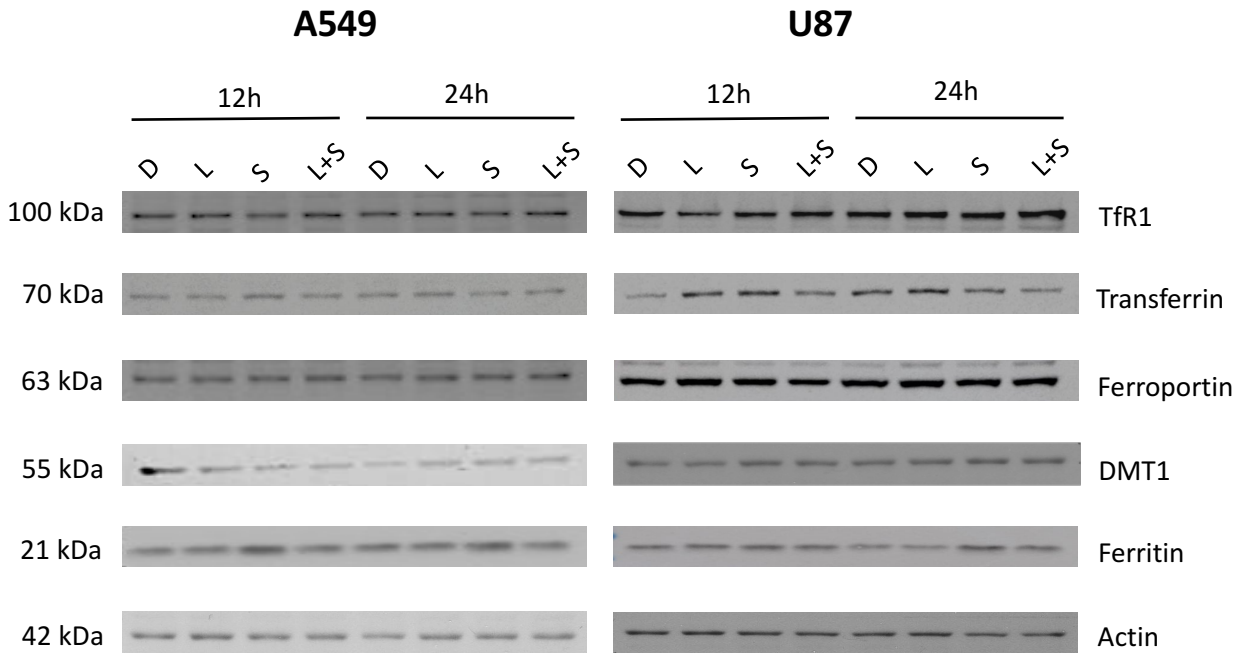

Figure 4.12A: Treatment of A549 and U87 cells with the combination of siramesine and lapatinib does not cause major changes in the levels of iron transport or storage proteins. Western blots were performed on lysates of A549 and U87 cells after 12 hours or 24 hours incubation with DMSO (D), lapatinib (L), siramesine (S), or the combination of lapatinib + siramesine (L+S). Blots were probed for transferrin receptor 1 (TfR1), transferrin, ferroportin, DMT1 and ferritin. Actin was used as the loading control. These are representative images from 3 separate experiments. Quantitative image analysis is shown in Figure 4.12B and 4.12C.

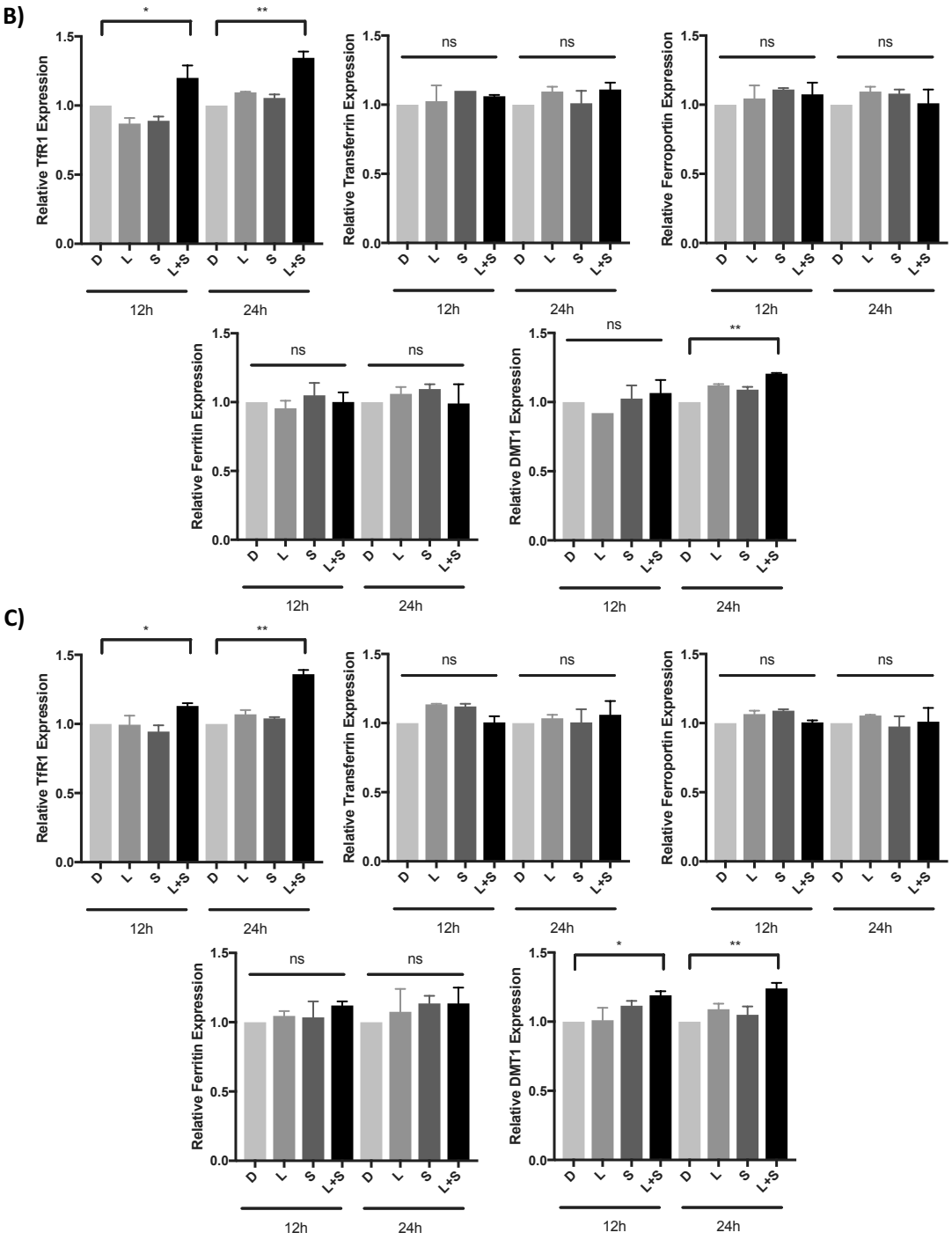

Figure 4.12B and 4.12C: Treatment of A549 and U87 cells with the combination of siramesine and lapatinib does not cause major changes in the levels of iron transport or storage proteins. Quantitative image analysis was performed on the Western blots shown in Figure 4.12A for **(B)** A549 and **(C)** U87 cells. Values obtained for each band of interest were normalized to the loading control (actin), and then normalized to the values obtained for DMSO (vehicle control). Each column represents the mean ± 1 SEM. Statistical significance was determined by unpaired t-tests comparing cells treated with L+S to each of the other conditions (ns, not significant; * $p<0.05$, ** $p<0.01$, n=3).

4.3.5 The combination of siramesine and lapatinib induces increased expression of the SLC7A11 subunit of System X_C^- in A549 and U87 cells

To determine whether siramesine and lapatinib-induced cell death was associated with changes in the expression levels of SLC7A11, a subunit of System X_C^- (the cystine/glutamate antiporter), Western blots were performed on lysates of A549 and U87 cells after 12 hours or 24 hours incubation with DMSO, lapatinib, siramesine, or the combination of siramesine and lapatinib (Figure 4.13A). Quantitative image analysis of the Western blots was performed using ImageJ software (Figure 4.13B). There was a statistically significant increase in the expression levels of SLC7A11 at both 12 and 24 hours following treatment with the combination of siramesine and lapatinib relative to the cells that were treated with DMSO or either drug alone, with the most significant increase occurring at 12 hours. The relative increase in expression at 12 hours was 73% for the A549 cells and 62% for the U87 cells ($p<0.001$). These changes in expression were more substantial than those observed for any of the iron transport or storage proteins evaluated in this study.

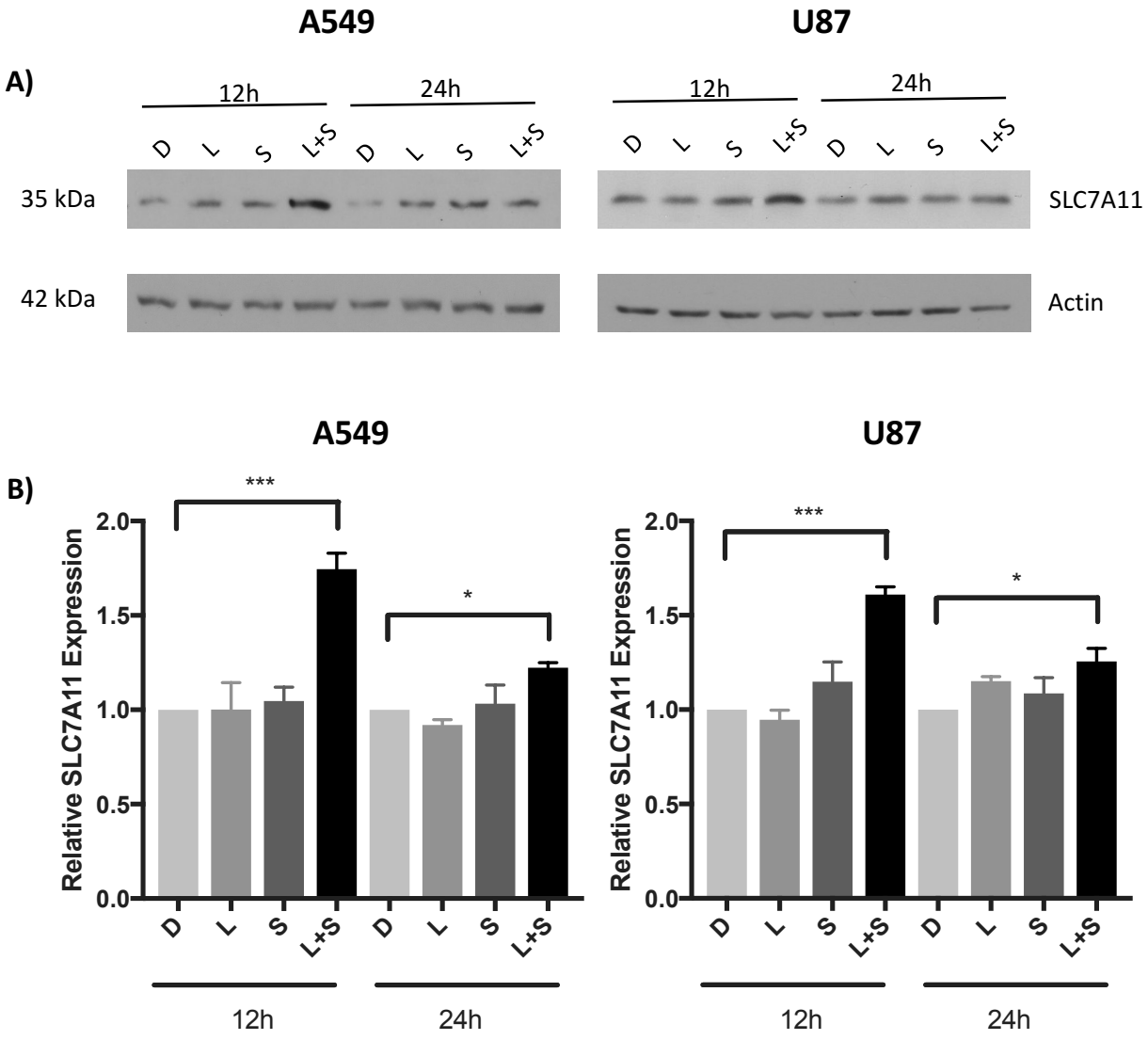

Figure 4.13: Treatment of A549 and U87 cells with the combination of siramesine and lapatinib increased the levels of the SLC7A11 protein, a subunit of System X_C^-. (A) Western blots were performed on lysates of A549 and U87 cells after 12 hours or 24 hours incubation with DMSO (D), lapatinib (L), siramesine (S), or the combination of lapatinib + siramesine (L+S). Actin was used as the loading control. Representative images from 2 separate experiments. **(B)** Quantitative image analysis was performed on the blots in (A). Densitometry values for each protein band were normalized to the loading control (actin), and then compared to the values obtained for DMSO (vehicle control). Each column represents the mean ± 1 SEM. Statistical significance was determined by unpaired t-tests comparing cells treated with L+S to each of the other conditions (* $p<0.05$, *** $p<0.001$ for all comparisons, n=2).

CHAPTER 5: DISCUSSION AND CONCLUSIONS

5.1 DISCUSSION

Drug resistance is a well-known phenomenon that results when diseases become tolerant to pharmaceutical treatments. Some methods of drug resistance are disease-specific, while others, such as drug efflux, which is observed in microbes and human drug-resistant cancers, are evolutionarily conserved. Although many types of cancers are initially susceptible to chemotherapy, over time they develop resistance through mechanisms such as drug inactivation, drug target alteration, drug efflux, DNA damage repair, and cell death inhibition (114, 115).

Malignant cells frequently harbor genetic alterations that allow them to escape spontaneous and therapy-induced apoptosis. Ideally, drug-induced damage should be tightly coupled to the induction of cell death. However, numerous intrinsic adaptive responses can be triggered that promote cancer cell survival. Resistance to apoptosis is often acquired during an early phase of tumour development when genetic changes result in defects in caspase-dependent apoptosis pathways and provide transformed cells with greater growth and survival potential (4).

Accumulating knowledge of natural and acquired drug resistance in cancers is spurring the investigation of alternative cell death pathways. Improving treatment for tumours that have developed resistance to first line therapeutic approaches or to pro-apoptotic agents will mean understanding and exploiting these alternative cell death pathways. Lysosomal cell death programs and ferroptotic cell death are two related alternative pathways that may circumvent resistance. Targeting these death pathways holds the potential for novel therapies directed at cancers that presently have limited therapeutic options.

One approach to identifying novel cancer therapies is the appraisal of existing drugs for new purposes. Previous work done in our laboratory demonstrated that siramesine permeabilized

lysosomes in chronic lymphocytic leukemia (CLL) cells, leading to cell death, and that the combination of siramesine and lapatinib synergistically induced death in breast cancer cell lines. We have extended the evaluation of these drugs by investigating whether siramesine and lapatinib could produce synergic cell death in lung adenocarcinoma and glioblastoma, and whether the mechanism of death was consistent with ferroptosis.

To assess the potential of lysosome targeting agents and tyrosine kinase inhibitors to synergize in inducing cell death, the combined effects of different pairs of lysosome targeting agents and TKIs were tested. Several synergistic combinations were identified that induced death in both A549 and U87 cells. Investigation of the characteristics of cell death triggered by one specific drug combination (siramesine and lapatinib) demonstrated that they were consistent with ferroptosis. Cell death was inhibited by Fer-1 and DFO and enhanced by the addition of exogenous iron, suggesting an iron-dependent process (Figure 4.8). The siramesine and lapatinib combination increased the intracellular labile iron pool, the levels of total ROS, and specifically the levels of lipid ROS (Figures 4.9, 4.10, and 4.11). Collectively these data suggest that the drug combination led to an iron-dependent oxidative cell death process in both lung adenocarcinoma and glioblastoma cells, and are consistent with previous observations from our laboratory on the effects of these drugs in breast cancer cells (108).

In the present study we found no changes in the expression levels of transferrin, ferroportin or ferritin, but we did see small (statistically significant) increases in the levels of TfR1 and DMT1 (Figure 4.12). This is in contrast to the study by Ma and colleagues in breast cancer cells, which showed an increase in the levels of transferrin and a decrease in the levels of ferroportin (108), and to a study by Gao et al. in fibrosarcoma cells, where ferroptosis was shown to be associated with an increase in the endogenous levels of ferritin (116). Changes in protein

expression in response to initiation of ferroptotic pathways may be cell type or condition-specific. These results suggest that the increase in intracellular iron and the corresponding cell death is not associated with a major change in the expression of one or more of these proteins. It is possible that the drug combination altered the activity or the localization of these transport/storage proteins, which would not be detected by Western blot.

The present study demonstrated an increase in the levels of SLC7A11, the subunit of System X_C^- that is responsible for the transport activity of the antiporter, following 12 and 24 hours of treatment of A549 and U87 cells with the combination of siramesine and lapatinib (Figure 4.13). A similar increase has been observed in breast cancer cell lines (108). Increases in *SLC7A11* mRNA have also been observed in HT1080 fibrosarcoma cells after treatment with erastin (75). These observations would appear to be counter to expectations, as ferroptosis-inducing drugs are considered to be inhibitors of System X_C^- at the protein level. However, the increase may be a compensatory response to inhibition; the cells upregulate SLC7A11 expression to overcome the functional inhibition.

As previously demonstrated in other studies of ferroptosis (75, 79, 83, 98), the ferroptosis inhibitor Fer-1 and iron chelator DFO protected both A549 and U87 cells from siramesine and lapatinib-induced cell death, although the protection was not complete. Levels of cell death were not reduced to that seen in control cells or those treated with the individual drugs (Figure 4.8). This raises the possibility of a second death mechanism, in addition to ferroptosis, contributing to the total cell death observed after treatment with siramesine and lapatinib. The second mechanism may represent a form of autophagy, as studies performed in our laboratory, in breast cancer cell lines, have shown that death induced by the combination of siramesine and lapatinib transitioned from ferroptosis to autophagy (117). In that study, at early time points (four hours

after drug treatment), death was consistent with ferroptosis and inhibition of autophagy led to increased cell death, suggesting that autophagy was promoting cell survival. At 24 hours post-treatment, inhibition of autophagy reduced the levels of cell death, suggesting that at this later time point autophagy was contributing to the cell death. It is therefore possible that autophagy was also contributing to the cell death observed 24 hours after treatment of the A549 and U87 cells with siramesine and lapatinib.

Intracellular iron levels are tightly regulated in both normal and malignant cells. Alterations in these iron levels are key to the induction of ferroptosis. Although malignant cells have increased levels of intracellular iron that support their increased metabolic activity, there is a fine line between the levels of intracellular iron that support the malignant phenotype and the levels of intracellular iron that lead to cell death (38, 64). Alterations in iron metabolism, in particular the acquisition and retention of excess iron, contribute to both tumour initiation and tumour growth (38, 53, 64). These observations have led to divergent approaches to target intracellular iron in anti-cancer therapy and have included both the sequestering of available iron using iron chelators, and the increase in intracellular iron levels to initiate cell death (38, 64).

Treating cancer cells with agents that induce iron-dependent cell death represents a potential strategy for turning the excess iron present in cancer cells into a therapeutic advantage. A recent study investigated the iron dependence of ovarian cancer cells both *in vitro* and in a mouse model. *In vitro* studies demonstrated that tumour cells were significantly more dependent on iron than normal cells (64). The iron addiction of the malignant cells could be targeted by either reducing the levels of intracellular iron, or conversely, by using the increased levels of iron to initiate cell death. This was demonstrated by decreased viability of transformed fallopian stem cells in the presence of the iron chelator DFO, and by increased death of these cells by

ferroptosis, induced by erastin (64). Basuli et al. also demonstrated that in a xenograft mouse model (generated by intraperitoneal injection of tumour cells), mice treated with erastin showed a significant reduction in tumour number and mass, indicating that ferroptosis-inducing agents have the potential to target ovarian tumours (64).

As with the ovarian tumour model, inducing ferroptosis via a combination of lysosomal targeting agents and TKIs may be a potential therapeutic strategy for lung adenocarcinoma and glioblastoma, tumours that presently have few successful treatment options. This drug combination has now been tested in our laboratory in three different types of cancer, and ideally, ferroptosis may be a cell death pathway that can be exploited to treat a variety of cancers. As ferroptosis is the inactivation of a metabolic pathway that is shared by many cells, it is possible that this process could be recruited to kill cancer cells regardless of the specific type of cancer.

The ferroptosis pathway has some unique features when compared to other forms of cell death. Apoptosis is triggered by diverse lethal stimuli (e.g. DNA damage, protein misfolding) leading to activation of a pro-death enzymatic process and the ordered disassembly of the cell. Ferroptosis, by contrast, results from the inactivation of an essential metabolic process, leading to an iron-catalyzed, lipid ROS-mediated cellular collapse. It has been suggested that ferroptosis is a form of cellular *sabotage*, where normal metabolic functions of the cell are hijacked to precipitate cell death (109). This distinguishes ferroptosis from apoptosis and other forms of cell death that have been described as cell *suicide* (109). Whether the inactivation of other essential metabolic processes could trigger ferroptosis or other novel cell sabotage programs is unknown but worthy of investigation in the search for novel approaches to overcome cancer's resistance to drug therapies (79).

There is still much to be learned about the mechanism of ferroptotic cell death and its inducers. In our laboratory, investigations of cell death in breast cancer cells induced by the combination of siramesine and lapatinib demonstrated that the mechanism was consistent with ferroptosis (108). Siramesine and lapatinib were initially used for the extension of studies into A549 and U87 cell lines to observe whether the synergic cell death could be reproduced in other tumour types. We subsequently examined additional lysosome targeting agents and TKIs, alone and in combination, to determine whether the cell death effects were specific to siramesine and lapatinib, or whether other drugs in the same classes would also produce the synergic cell death effect. The synergy studies of various lysosomotropic drugs with lapatinib were particularly enlightening.

Despite the ubiquitous nature of lysosomes in all mammalian cells, cancer cells have an altered lysosome biology. Increased lysosome biogenesis has been demonstrated in a variety of cancer types, including acute myeloid leukemia (AML), bladder cancer, melanoma, and pancreatic cancer (118-121). Cancer cell lysosomes are large (122), and may be more fragile than normal-sized lysosomes (123). Cancer cells may also have an increased number of lysosomes compared to healthy cells (118, 124). Because cancer cells have high metabolic rates, there is an increased turnover of iron-containing proteins, and increased lysosomal accumulation of iron. These characteristics may contribute to cancer cells' increased sensitivity to treatment with lysosomotropic agents. For example, it was demonstrated that CLL cells have more lysosomes and were more sensitive to lysosome targeting agents than nonmalignant B cells (124). Using lysosomotropic agents to induce lysosome permeabilization releases lysosomal contents, including iron, into the cytosol, and may contribute to the production of ROS via the Fenton reaction (Figure 1.4).

There are several different classes of lysosomotropic drugs, which include antidepressants, antimalarials and antihistamines (125-128). We initially studied drugs belonging to the antidepressant and antimalarial classes in combination with lapatinib. The antidepressants (siramesine and desipramine) demonstrated synergy with lapatinib in triggering cell death, while the antimalarial (tafenoquine) did not (Figures 4.3 and 4.5). These results do not indicate that antimalarials are unable to induce cell death or permeabilize lysosomes, as there are several studies demonstrating their effectiveness at permeabilizing lysosomes in malignant cells. For example, the antimalarial mefloquine was shown to be preferentially cytotoxic to primary AML cells, compared with normal hematopoietic cells, both *in vitro* and in a mouse xenograft model (118). In addition, mefloquine and tafenoquine induced cytotoxicity and lysosome permeabilization in CLL cells (124). However, in the context of the present study, the antimalarials did not synergize with lapatinib to cause increased cell death, in contrast to the antidepressants and antihistamine classes.

A recent study investigating the repurposing of antihistamines as anti-cancer agents examined antihistamines (clemastine, loratadine, desloratadine, terfenadine, astemizole, and ebastine) known to target lysosomes (128). Ellegard et al. showed that the regular use of some common non-prescription antihistamines was associated with reduced all-cause mortality among patients with NSCLC. The antihistamines re-sensitized A549-MDR cells to vinorelbine, and sensitized NCI-H1299 and NCI-H661 cell lines to vinorelbine or cisplatin (128). Based on these observations, we extended our studies to include the evaluation of antihistamines in the drug combination studies. The three antihistamines that were selected (clemastine, loratadine, and desloratadine) are licensed and commercially available (129). Clemastine and loratadine are available as over-the-counter preparations; desloratadine is available by prescription. All three

antihistamines demonstrated synergism with lapatinib in inducing cell death in A549 and U87 cells (Figures 4.5).

The lysosomotropic antihistamines, antimalarials and antidepressants evaluated in our study belong to a general category of drugs known as cationic-amphiphilic drugs (CADs) (128). CADs are characterized by a hydrophobic ring structure and a hydrophilic side chain with a cationic amine group, and passively diffuse across cell membranes, including lysosomal membranes. When CADs diffuse into lysosomes, they become protonated in the acidic environment, restricting their diffusion back across the lysosomal membrane into the cytosol, a process referred to as lysosomal trapping (125, 126, 128).

CADs can inhibit a variety of lysosomal enzymes including acid sphingomyelinase (ASM), a lysosomal lipid-metabolizing enzyme that catalyzes the breakdown of sphingomyelin into ceramide and phosphatidylcholine (130). ASM has been shown to be essential for lysosomal stability and as a corollary, for cell survival (127, 131, 132). Lysosome destabilization results in lysosome membrane permeabilization and a partial or complete release of lysosomal contents (including lysosomal proteases), ultimately leading to cell death mediated by ROS (133, 134). The lysosomotropic antidepressants and antihistamines (but not the antimalarials) are functional inhibitors of ASM (or FIASMAs) (135). The observation that only the FIASMAs caused synergic cell death in combination with lapatinib suggests a central role for lysosomal ASM in the cell death induced by the drug combination.

Altered sphingolipid metabolism has previously been described in malignant cells (127, 136, 137). Sphingolipid metabolism is a complex process, which centres on the reversible metabolism of sphingomyelin to ceramide, ceramide to sphingosine, and sphingosine to sphingosine-1-phosphate. Some of these metabolites, particularly sphingosine-1-phosphate and

ceramide, can act as second messengers in signaling pathways that regulate a variety of cellular events including cell growth, differentiation, and the balance between cell survival and cell death (138). Previous studies have identified alterations in sphingosine kinase (the enzyme that converts sphingosine to sphingosine-1-phosphate) and/or ASM in a wide array of cancers, including breast, colon, gastric, renal, hepatocellular, prostate, and lung (127, 136, 137). Altered sphingomyelin metabolism potentially renders cancer cells more sensitive to ASM inhibition. Levels of sphingomyelin, and of ASM, are decreased in cancer cells; the reduced levels of ASM may be a compensatory response to the lower levels of sphingomyelin (127). When the levels of sphingomyelin are reduced, cancer cells may adapt by decreasing the levels of ASM in order to maintain sufficient sphingomyelin. This creates a potential tipping point for cancer therapeutics. It is possible that if malignant cells already have reduced levels of ASM, then lower concentrations of ASM inhibitors would be expected to destabilize and permeabilize the lysosomal membranes, resulting in the release of ROS and lysosomal iron into the cytoplasm.

Several studies have shown that malignant cells are more sensitive to treatment with CADs, and specifically to ASM inhibitors (127). Ellegard et al. recently demonstrated that CAD antihistamines induced significantly more cell death in transformed mouse embryonic fibroblasts than in the corresponding control cells (128). An extensive review of clinically relevant CADs with ASM inhibitory activity was done to determine whether they displayed cancer-specific cytotoxicity (127). It was found that the FIASMAs killed transformed fibroblasts at concentrations too low to affect the survival of control cells, and that the transformed cells were also more sensitive to long-term cytotoxicity as demonstrated by a colony formation assay (127). The FIASMAs also killed *Ras*-driven HCT116 colon carcinoma cells more effectively than *Ras*-

depleted Hkh2 colon carcinoma cells (127). In addition, the ASM inhibitors caused cytotoxicity in cell lines derived from ovarian, breast, prostate, cervix, and bone cancers (127).

The question still remains of how the combination of FIASMAs and TKIs synergize to induce cell death via ferroptosis. We theorize that the drugs are targeting multiple pathways, resulting in enhanced cell death, when they are used in combination. Inhibition of ASM is the most likely mechanism for the lysosome targeting agents in the combination, with the permeabilization of the lysosome resulting in the release of lysosomal iron into the cytoplasm where it can participate in the Fenton reaction. The TKIs may be inhibiting System X_C- and preventing the antioxidant activity of GPX4 (as has been demonstrated for sorafenib) or altering the intracellular iron levels by other processes that still require investigation.

Discovering new uses for approved drugs provides the quickest possible transition from laboratory to clinical care, and is referred to as drug repurposing or repositioning. Drug repurposing has become an important approach to identifying new effective therapies for malignant diseases. There are great advantages in evaluating FDA- or Health Canada-approved drugs for novel purposes, when compared to *de novo* novel drug development. Drugs that have received regulatory approval have known clinical safety and pharmacological profiles, existing formulations, and established maximum tolerated doses. *De novo* drug development is a process that can take longer than 10 years from idea to marketable drug, if successful; drug repurposing can take as few as 3 years (139). Thus, the application and translation of repurposed drugs into the clinic is expedited and less expensive.

This repurposing of drugs is a common strategy in numerous research fields, and has led to the effective use of drugs such as sildenafil (originally developed to treat angina) for erectile dysfunction (139), thalidomide (originally developed to treat pregnancy-associated nausea) for

multiple myeloma (140) and for inflammatory leprosy (139), and all-trans retinoic acid (originally used to treat acne) for the treatment of acute promyelocytic leukemia (141). More recent studies have shown promising anti-cancer effects with metformin (treatment for type 2 diabetes) (142) and mebendazole (a commonly used anti-helminthic drug) (143).

The present study has focused on the potential of repurposing specific antidepressants and antihistamines as anti-cancer drugs. The antidepressants and antihistamines synergized with TKIs to induce cancer cell death by a mechanism that is only partially understood. Siramesine was developed as a sigma-2 receptor antagonist and entered clinical trials as an antidepressant in 2001 (144). Desipramine is an FDA and Health Canada-approved tricyclic antidepressant that inhibits the re-uptake of the neurotransmitter norepinephrine (145). Sorafenib is an FDA and Health Canada-approved multi-kinase inhibitor originally developed for treatment of renal cell carcinoma (146). Lapatinib is an FDA and Health Canada-approved dual tyrosine kinase inhibitor for EGFR and HER2 that was developed and approved for the treatment of advanced and metastatic breast cancer (147). Clemastine, loratadine, and desloratadine are all FDA and Health Canada-approved commercially available antihistamines (129, 148-150). In order to repurpose these drugs for cancer therapy, additional investigations will be required.

5.2 CONCLUSIONS

In conclusion, the studies presented in this thesis identify that the combination of siramesine and lapatinib induce synergic cell death in lung adenocarcinoma and glioblastoma cells, as do several other similar combinations of lysosomal targeting agents and TKIs. The characteristics of this cell death are consistent with ferroptosis: reduced by ferroptosis inhibitors and enhanced by the addition of iron. The combination triggered increases in the level of

intracellular iron, and of ROS, including specifically, lipid ROS. Treatment with siramesine and lapatinib did not cause major changes in the levels of iron transport proteins, but did increase expression of the cystine/glutamate antiporter, possibly in response to its functional inhibition. Finally, these studies suggest that only lysosomal targeting agents that are ASM inhibitors are effective in combination with lapatinib, providing some additional clues about the means by which these drugs are inducing ferroptosis. Siramesine and lapatinib in combination can be added to a growing list of agents that can induce ferroptotic cell death and potentially provide a mechanism to circumvent cancer drug resistance.

CHAPTER 6: FUTURE DIRECTIONS

The next experimental steps in understanding the mechanisms involved in the synergic cell death induced by the combination of lysosomal targeting agents and TKIs would include determining whether autophagy is playing a role in the synergic cell death, investigating ASM as the potential target, and testing the effects of these drug combinations in a 3-dimensional culture model.

Previous studies in breast cancer cell lines suggested that, in addition to ferroptosis, autophagy also contributed to cell death induced by the combination of siramesine and lapatinib. To determine whether autophagy contributes to cell death in the lung adenocarcinoma and glioblastoma cells, pretreating the cells with the autophagy inhibitors 3-methyladenine (3-MA) or spautin-1 over a time course of exposure to siramesine and lapatinib would indicate whether and when autophagic cell death was occurring. I hypothesize that these inhibitors would partially protect the cells from siramesine and lapatinib-induced cell death. Knocking down the autophagy genes *Atg5* or *Becn1*, and measuring the effects of these knock-downs on cell death, would provide additional evidence for the role of autophagy in the cell death induced by the drug combination.

The results of our present studies provide evidence that only lysosomal targeting agents that inhibit ASM are effective in synergizing with lapatinib to induce cell death. This suggests that ASM inhibition plays a key role in the effect of this drug combination. To test this hypothesis, knocking down ASM using siRNA, and repeating the cell death experiments with siramesine and lapatinib will help to clarify the role of ASM in this context.

It will be necessary to develop more biologically relevant models in order to identify the best candidate drug combinations to be used in pre-clinical animal model studies. Better than the

2-dimensional culture systems used in the present studies, 3-dimensional culture systems provide *in vitro* models that more closely resemble *in vivo* environments. For example, tumour spheroid assays would be valuable to evaluate the effectiveness of the combination treatments in a model that more closely mirrors a solid tumour in a patient. Tumour spheres may also be relevant models because they are enriched in cancer stem cells, more closely modeling the *in vivo* setting. Many drugs tested in monolayer culture do not successfully progress through clinical development because of lack of clinical efficacy and/or unacceptable toxicity. Spheroid models that mimic the cell-cell interactions of a tumour provide a more accurate prediction of the effects of these drugs *in vivo*, and ideally would determine whether moving to animal studies was warranted.

In the era of drug repurposing, identifying novel uses for old drugs may yield new therapeutic options. Drug repurposing success stories and companies leveraging repurposing strategies are increasing in number; both the use of non-cancer drugs to treat cancer, and anti-cancer agents to treat non-malignant diseases. The major problems of conventional cancer chemotherapy drugs (mainly DNA damaging agents) are the toxicities that limit the dose intensity, but also significantly reduce the quality of life of patients. As many non-chemotherapeutic agents have more tolerable side effects in humans, repurposing these drugs for anti-cancer therapy will continue to be an excellent strategy for future anti-cancer drug development.

The current increase in drug repurposing raises the question about the approach: when the obvious candidates for repurposing have been exhausted, will anything be left to repurpose? Fortunately, the number of potential drugs exceeds the present screening capacity of most companies. Although the current activity may consume the most obvious candidates, it is likely

that evaluation of drugs for repurposing will continue, providing further opportunities to target the differences between malignant and non-malignant cell biology.

CHAPTER 7: REFERENCES

1. Nuttall R, Bryan S, Dale D, De P, Demers A, Ellison L, et al. Canadian Cancer Statistics 2016. Toronto, ON: Canadian Cancer Society; 2016.
2. Nuttall R, Bryan S, Dale D, De P, Demers A, Ellison L, et al. Canadian Cancer Statistics 2017. Toronto, ON: Canadian Cancer Society; 2017.
3. Xie L, Semenciw R, Mery L. Cancer incidence in Canada: trends and projections (1983-2032). Health Promot Chronic Dis Prev Can. 2015;35 Suppl 1:2-186.
4. Hanahan D, Weinberg RA. Hallmarks of cancer: the next generation. Cell. 2011;144(5):646-74.
5. Munger K. Disruption of oncogene/tumor suppressor networks during human carcinogenesis. Cancer Invest. 2002;20(1):71-81.
6. Hanahan D, Weinberg RA. The hallmarks of cancer. Cell. 2000;100(1):57-70.
7. Burton TR, Henson ES, Azad MB, Brown M, Eisenstat DD, Gibson SB. BNIP3 acts as transcriptional repressor of death receptor-5 expression and prevents TRAIL-induced cell death in gliomas. Cell Death Dis. 2013;4:e587.
8. Huse JT, Holland E, DeAngelis LM. Glioblastoma: molecular analysis and clinical implications. Annu Rev Med. 2013;64:59-70.
9. Vanan MI, Eisenstat DD. Management of high-grade gliomas in the pediatric patient: Past, present, and future. Neurooncol Pract. 2014;1(4):145-57.
10. Verhaak RG, Hoadley KA, Purdom E, Wang V, Qi Y, Wilkerson MD, et al. Integrated genomic analysis identifies clinically relevant subtypes of glioblastoma characterized by abnormalities in PDGFRA, IDH1, EGFR, and NF1. Cancer Cell. 2010;17(1):98-110.
11. Mason WP, Maestro RD, Eisenstat D, Forsyth P, Fulton D, Laperriere N, et al. Canadian recommendations for the treatment of glioblastoma multiforme. Curr Oncol. 2007;14(3):110-7.
12. Lacroix M, Abi-Said D, Fourney DR, Gokaslan ZL, Shi W, DeMonte F, et al. A multivariate analysis of 416 patients with glioblastoma multiforme: prognosis, extent of resection, and survival. J Neurosurg. 2001;95(2):190-8.
13. Sanai N, Polley MY, McDermott MW, Parsa AT, Berger MS. An extent of resection threshold for newly diagnosed glioblastomas. J Neurosurg. 2011;115(1):3-8.
14. Fan CH, Liu WL, Cao H, Wen C, Chen L, Jiang G. O6-methylguanine DNA methyltransferase as a promising target for the treatment of temozolomide-resistant gliomas. Cell Death Dis. 2013;4:e876.
15. Patel MA, Kim JE, Ruzevick J, Li G, Lim M. The future of glioblastoma therapy: synergism of standard of care and immunotherapy. Cancers (Basel). 2014;6(4):1953-85.
16. Choucair AK, Levin VA, Gutin PH, Davis RL, Silver P, Edwards MS, et al. Development of multiple lesions during radiation therapy and chemotherapy in patients with gliomas. J Neurosurg. 1986;65(5):654-8.

17. Kitange GJ, Carlson BL, Schroeder MA, Grogan PT, Lamont JD, Decker PA, et al. Induction of MGMT expression is associated with temozolomide resistance in glioblastoma xenografts. Neuro Oncol. 2009;11(3):281-91.

18. Cosse JP, Michiels C. Tumour hypoxia affects the responsiveness of cancer cells to chemotherapy and promotes cancer progression. Anticancer Agents Med Chem. 2008;8(7):790-7.

19. Rouschop KM, Wouters BG. Regulation of autophagy through multiple independent hypoxic signaling pathways. Curr Mol Med. 2009;9(4):417-24.

20. Brahimi-Horn MC, Chiche J, Pouyssegur J. Hypoxia and cancer. J Mol Med. 2007;85(12):1301-7.

21. Torre LA, Siegel RL, Ward EM, Jemal A. Global Cancer Incidence and Mortality Rates and Trends--An Update. Cancer Epidemiol Biomarkers Prev. 2016;25(1):16-27.

22. Corner J, Hopkinson J, Fitzsimmons D, Barclay S, Muers M. Is late diagnosis of lung cancer inevitable? Interview study of patients' recollections of symptoms before diagnosis. Thorax. 2005;60(4):314-9.

23. Travis WD, Garg K, Franklin WA, Wistuba, II, Sabloff B, Noguchi M, et al. Bronchioloalveolar carcinoma and lung adenocarcinoma: the clinical importance and research relevance of the 2004 World Health Organization pathologic criteria. J Thorac Oncol. 2006;1(9 Suppl):S13-9.

24. Edge SB, Compton CC. The American Joint Committee on Cancer: the 7th edition of the AJCC cancer staging manual and the future of TNM. Ann Surg Oncol. 2010;17(6):1471-4.

25. de Groot PM, Carter BW, Betancourt Cuellar SL, Erasmus JJ. Staging of lung cancer. Clin Chest Med. 2015;36(2):179-96, vii-viii.

26. Tsim S, O'Dowd CA, Milroy R, Davidson S. Staging of non-small cell lung cancer (NSCLC): a review. Respir Med. 2010;104(12):1767-74.

27. Detterbeck FC, Lewis SZ, Diekemper R, Addrizzo-Harris D, Alberts WM. Executive Summary: Diagnosis and management of lung cancer, 3rd ed: American College of Chest Physicians evidence-based clinical practice guidelines. Chest. 2013;143(5 Suppl):7S-37S.

28. Vansteenkiste J, De Ruysscher D, Eberhardt WE, Lim E, Senan S, Felip E, et al. Early and locally advanced non-small-cell lung cancer (NSCLC): ESMO Clinical Practice Guidelines for diagnosis, treatment and follow-up. Ann Oncol. 2013;24 Suppl 6:vi89-98.

29. Eberhardt WE, De Ruysscher D, Weder W, Le Pechoux C, De Leyn P, Hoffmann H, et al. 2nd ESMO Consensus Conference in Lung Cancer: locally advanced stage III non-small-cell lung cancer. Ann Oncol. 2015;26(8):1573-88.

30. Reck M, Popat S, Reinmuth N, De Ruysscher D, Kerr KM, Peters S, et al. Metastatic non-small-cell lung cancer (NSCLC): ESMO Clinical Practice Guidelines for diagnosis, treatment and follow-up. Ann Oncol. 2014;25 Suppl 3:iii27-39.

31. Ernani V, Steuer CE, Jahanzeb M. The End of Nihilism: Systemic Therapy of Advanced Non-Small Cell Lung Cancer. Annu Rev Med. 2017;68:153-68.

32. Kris MG, Johnson BE, Berry LD, Kwiatkowski DJ, Iafrate AJ, Wistuba, II, et al. Using multiplexed assays of oncogenic drivers in lung cancers to select targeted drugs. JAMA. 2014;311(19):1998-2006.

33. Kanthala S, Pallerla S, Jois S. Current and future targeted therapies for non-small-cell lung cancers with aberrant EGF receptors. Future Oncol. 2015;11(5):865-78.

34. Yu HA, Arcila ME, Rekhtman N, Sima CS, Zakowski MF, Pao W, et al. Analysis of tumor specimens at the time of acquired resistance to EGFR-TKI therapy in 155 patients with EGFR-mutant lung cancers. Clin Cancer Res. 2013;19(8):2240-7.

35. Kwak EL, Bang YJ, Camidge DR, Shaw AT, Solomon B, Maki RG, et al. Anaplastic lymphoma kinase inhibition in non-small-cell lung cancer. N Engl J Med. 2010;363(18):1693-703.

36. Shaw AT, Yeap BY, Mino-Kenudson M, Digumarthy SR, Costa DB, Heist RS, et al. Clinical features and outcome of patients with non-small-cell lung cancer who harbor EML4-ALK. J Clin Oncol. 2009;27(26):4247-53.

37. Chen Z, Fillmore CM, Hammerman PS, Kim CF, Wong KK. Non-small-cell lung cancers: a heterogeneous set of diseases. Nat Rev Cancer. 2014;14(8):535-46.

38. Torti SV, Torti FM. Iron and cancer: more ore to be mined. Nat Rev Cancer. 2013;13(5):342-55.

39. Wu XN, Su D, Wang L, Yu FL. Roles of the hepcidin-ferroportin axis and iron in cancer. Eur J Cancer Prev. 2014;23(2):122-33.

40. Wang J, Pantopoulos K. Regulation of cellular iron metabolism. Biochem J. 2011;434(3):365-81.

41. Silva B, Faustino P. An overview of molecular basis of iron metabolism regulation and the associated pathologies. Biochim Biophys Acta. 2015;1852(7):1347-59.

42. Wallace DF. The regulation of iron absorption and homeostasis. Clin Biochem Rev. 2016;37(2):51-62.

43. Hentze MW, Muckenthaler MU, Galy B, Camaschella C. Two to tango: regulation of Mammalian iron metabolism. Cell. 2010;142(1):24-38.

44. Gozzelino R, Arosio P. Iron homeostasis in health and disease. Int J Mol Sci. 2016;17(1).

45. Ponka P, Beaumont C, Richardson DR. Function and regulation of transferrin and ferritin. Semin Hematol. 1998;35(1):35-54.

46. Ohgami RS, Campagna DR, Greer EL, Antiochos B, McDonald A, Chen J, et al. Identification of a ferrireductase required for efficient transferrin-dependent iron uptake in erythroid cells. Nat Genet. 2005;37(11):1264-9.

47. Gunshin H, Mackenzie B, Berger UV, Gunshin Y, Romero MF, Boron WF, et al. Cloning and characterization of a mammalian proton-coupled metal-ion transporter. Nature. 1997;388(6641):482-8.

48. Herbison CE, Thorstensen K, Chua AC, Graham RM, Leedman P, Olynyk JK, et al. The role of transferrin receptor 1 and 2 in transferrin-bound iron uptake in human hepatoma cells. Am J Physiol Cell Physiol. 2009;297(6):C1567-75.

49. Arosio P, Ingrassia R, Cavadini P. Ferritins: a family of molecules for iron storage, antioxidation and more. Biochim Biophys Acta. 2009;1790(7):589-99.

50. Shi H, Bencze KZ, Stemmler TL, Philpott CC. A cytosolic iron chaperone that delivers iron to ferritin. Science. 2008;320(5880):1207-10.

51. Kakhlon O, Cabantchik ZI. The labile iron pool: characterization, measurement, and participation in cellular processes. Free Radic Biol Med. 2002;33(8):1037-46.

52. Nemeth E, Ganz T. The role of hepcidin in iron metabolism. Acta Haematol. 2009;122(2-3):78-86.

53. Torti SV, Torti FM. Ironing out cancer. Cancer Res. 2011;71(5):1511-4.

54. Hubert N, Hentze MW. Previously uncharacterized isoforms of divalent metal transporter (DMT)-1: implications for regulation and cellular function. Proc Natl Acad Sci USA. 2002;99(19):12345-50.

55. Rouault TA. The role of iron regulatory proteins in mammalian iron homeostasis and disease. Nat Chem Biol. 2006;2(8):406-14.

56. Beghe C, Wilson A, Ershler WB. Prevalence and outcomes of anemia in geriatrics: a systematic review of the literature. Am J Med. 2004;116 Suppl 7A:3S-10S.

57. Beard JL. Iron biology in immune function, muscle metabolism and neuronal functioning. J Nutr. 2001;131(2S-2):568S-79S; discussion 80S.

58. Weiss G, Goodnough LT. Anemia of chronic disease. N Engl J Med. 2005;352(10):1011-23.

59. Nemeth E, Rivera S, Gabayan V, Keller C, Taudorf S, Pedersen BK, et al. IL-6 mediates hypoferremia of inflammation by inducing the synthesis of the iron regulatory hormone hepcidin. J Clin Invest. 2004;113(9):1271-6.

60. Pietrangelo A. Hereditary hemochromatosis: pathogenesis, diagnosis, and treatment. Gastroenterology. 2010;139(2):393-408, e1-2.

61. Cullen LM, Anderson GJ, Ramm GA, Jazwinska EC, Powell LW. Genetics of hemochromatosis. Annu Rev Med. 1999;50:87-98.

62. Toyokuni S. Role of iron in carcinogenesis: cancer as a ferrotoxic disease. Cancer Sci. 2009;100(1):9-16.

63. Spangler B, Morgan CW, Fontaine SD, Vander Wal MN, Chang CJ, Wells JA, et al. A reactivity-based probe of the intracellular labile ferrous iron pool. Nat Chem Biol. 2016;12(9):680-5.

64. Basuli D, Tesfay L, Deng Z, Paul B, Yamamoto Y, Ning G, et al. Iron addiction: a novel therapeutic target in ovarian cancer. Oncogene. 2017;36(29):4089-99.

65. Hotchkiss RS, Strasser A, McDunn JE, Swanson PE. Cell death. N Engl J Med. 2009;361(16):1570-83.

66. Galluzzi L, Maiuri MC, Vitale I, Zischka H, Castedo M, Zitvogel L, et al. Cell death modalities: classification and pathophysiological implications. Cell Death Differ. 2007;14(7):1237-43.

67. Aki T, Funakoshi T, Uemura K. Regulated necrosis and its implications in toxicology. Toxicology. 2015;333:118-26.

68. Vanden Berghe T, Linkermann A, Jouan-Lanhouet S, Walczak H, Vandenabeele P. Regulated necrosis: the expanding network of non-apoptotic cell death pathways. Nat Rev Mol Cell Biol. 2014;15(2):135-47.

69. Feltham R, Vince JE, Lawlor KE. Caspase-8: not so silently deadly. Clin Transl Immunology. 2017;6(1):e124.

70. Oberst A. Death in the fast lane: what's next for necroptosis? FEBS J. 2016;283(14):2616-25.

71. Elmore S. Apoptosis: a review of programmed cell death. Toxicol Pathol. 2007;35(4):495-516.

72. Bratton SB, Salvesen GS. Regulation of the Apaf-1-caspase-9 apoptosome. J Cell Sci. 2010;123(Pt 19):3209-14.

73. Chen Y, Azad MB, Gibson SB. Methods for detecting autophagy and determining autophagy-induced cell death. Can J Physiol Pharmacol. 2010;88(3):285-95.

74. Maiuri MC, Zalckvar E, Kimchi A, Kroemer G. Self-eating and self-killing: crosstalk between autophagy and apoptosis. Nat Rev Mol Cell Biol. 2007;8(9):741-52.

75. Dixon SJ, Lemberg KM, Lamprecht MR, Skouta R, Zaitsev EM, Gleason CE, et al. Ferroptosis: an iron-dependent form of nonapoptotic cell death. Cell. 2012;149(5):1060-72.

76. Yang WS, Stockwell BR. Ferroptosis: Death by lipid peroxidation. Trends Cell Biol. 2016;26(3):165-76.

77. Dolma S, Lessnick SL, Hahn WC, Stockwell BR. Identification of genotype-selective antitumor agents using synthetic lethal chemical screening in engineered human tumor cells. Cancer Cell. 2003;3(3):285-96.

78. Yang WS, Stockwell BR. Synthetic lethal screening identifies compounds activating iron-dependent, nonapoptotic cell death in oncogenic-RAS-harboring cancer cells. Chem Biol. 2008;15(3):234-45.

79. Cao JY, Dixon SJ. Mechanisms of ferroptosis. Cell Mol Life Sci. 2016;73(11-12):2195-209.

80. Yang WS, SriRamaratnam R, Welsch ME, Shimada K, Skouta R, Viswanathan VS, et al. Regulation of ferroptotic cancer cell death by GPX4. Cell. 2014;156(1-2):317-31.

81. Zilka O, Shah R, Li B, Friedmann Angeli JP, Griesser M, Conrad M, et al. On the mechanism of cytoprotection by Ferrostatin-1 and Liproxstatin-1 and the role of lipid peroxidation in ferroptotic cell death. ACS Cent Sci. 2017;3(3):232-43.

82. Yagoda N, von Rechenberg M, Zaganjor E, Bauer AJ, Yang WS, Fridman DJ, et al. RAS-RAF-MEK-dependent oxidative cell death involving voltage-dependent anion channels. Nature. 2007;447(7146):864-8.

83. Dixon SJ, Patel DN, Welsch M, Skouta R, Lee ED, Hayano M, et al. Pharmacological inhibition of cystine-glutamate exchange induces endoplasmic reticulum stress and ferroptosis. eLife. 2014;3:e02523.

84. Sato H, Tamba M, Ishii T, Bannai S. Cloning and expression of a plasma membrane cystine/glutamate exchange transporter composed of two distinct proteins. J Biol Chem. 1999;274(17):11455-8.

85. Bridges RJ, Natale NR, Patel SA. System xc(-) cystine/glutamate antiporter: an update on molecular pharmacology and roles within the CNS. Br J Pharmacol. 2012;165(1):20-34.

86. Gout PW, Buckley AR, Simms CR, Bruchovsky N. Sulfasalazine, a potent suppressor of lymphoma growth by inhibition of the x(c)- cystine transporter: a new action for an old drug. Leukemia. 2001;15(10):1633-40.

87. Lachaier E, Louandre C, Godin C, Saidak Z, Baert M, Diouf M, et al. Sorafenib induces ferroptosis in human cancer cell lines originating from different solid tumors. Anticancer Res. 2014;34(11):6417-22.

88. Louandre C, Ezzoukhry Z, Godin C, Barbare JC, Maziere JC, Chauffert B, et al. Iron-dependent cell death of hepatocellular carcinoma cells exposed to sorafenib. Int J Cancer. 2013;133(7):1732-42.

89. Panka DJ, Wang W, Atkins MB, Mier JW. The Raf inhibitor BAY 43-9006 (Sorafenib) induces caspase-independent apoptosis in melanoma cells. Cancer Res. 2006;66(3):1611-9.

90. Coriat R, Nicco C, Chereau C, Mir O, Alexandre J, Ropert S, et al. Sorafenib-induced hepatocellular carcinoma cell death depends on reactive oxygen species production in vitro and in vivo. Mol Cancer Ther. 2012;11(10):2284-93.

91. Liu L, Cao Y, Chen C, Zhang X, McNabola A, Wilkie D, et al. Sorafenib blocks the RAF/MEK/ERK pathway, inhibits tumor angiogenesis, and induces tumor cell apoptosis in hepatocellular carcinoma model PLC/PRF/5. Cancer Res. 2006;66(24):11851-8.

92. Xie Y, Hou W, Song X, Yu Y, Huang J, Sun X, et al. Ferroptosis: process and function. Cell Death Differ. 2016;23(3):369-79.

93. Ursini F, Maiorino M, Gregolin C. The selenoenzyme phospholipid hydroperoxide glutathione peroxidase. Biochim Biophys Acta. 1985;839(1):62-70.

94. Weiwer M, Bittker JA, Lewis TA, Shimada K, Yang WS, MacPherson L, et al. Development of small-molecule probes that selectively kill cells induced to express mutant RAS. Bioorg Med Chem Lett. 2012;22(4):1822-6.

95. Yu H, Guo P, Xie X, Wang Y, Chen G. Ferroptosis, a new form of cell death, and its relationships with tumourous diseases. J Cell Mol Med. 2017;21(4):648-57.

96. Schott C, Graab U, Cuvelier N, Hahn H, Fulda S. Oncogenic RAS mutants confer resistance of RMS13 rhabdomyosarcoma cells to oxidative stress-induced ferroptotic cell death. Front Oncol. 2015;5:131.

97. Jiang L, Kon N, Li T, Wang SJ, Su T, Hibshoosh H, et al. Ferroptosis as a p53-mediated activity during tumour suppression. Nature. 2015;520(7545):57-62.

98. Gao M, Monian P, Quadri N, Ramasamy R, Jiang X. Glutaminolysis and transferrin regulate ferroptosis. Mol Cell. 2015;59(2):298-308.

99. Yant LJ, Ran Q, Rao L, Van Remmen H, Shibatani T, Belter JG, et al. The selenoprotein GPX4 is essential for mouse development and protects from radiation and oxidative damage insults. Free Radic Biol Med. 2003;34(4):496-502.

100. Chen L, Hambright WS, Na R, Ran Q. Ablation of the ferroptosis inhibitor glutathione peroxidase 4 in neurons results in rapid motor neuron degeneration and paralysis. J Biol Chem. 2015;290(47):28097-106.

101. Friedmann Angeli JP, Schneider M, Proneth B, Tyurina YY, Tyurin VA, Hammond VJ, et al. Inactivation of the ferroptosis regulator Gpx4 triggers acute renal failure in mice. Nat Cell Biol. 2014;16(12):1180-91.

102. Matsushita M, Freigang S, Schneider C, Conrad M, Bornkamm GW, Kopf M. T cell lipid peroxidation induces ferroptosis and prevents immunity to infection. J Exp Med. 2015;212(4):555-68.

103. Schnabel D, Salas-Vidal E, Narvaez V, Sanchez-Carbente Mdel R, Hernandez-Garcia D, Cuervo R, et al. Expression and regulation of antioxidant enzymes in the developing limb support a function of ROS in interdigital cell death. Dev Biol. 2006;291(2):291-9.

104. Skouta R, Dixon SJ, Wang J, Dunn DE, Orman M, Shimada K, et al. Ferrostatins inhibit oxidative lipid damage and cell death in diverse disease models. J Am Chem Soc. 2014;136(12):4551-6.

105. Angeli JPF, Shah R, Pratt DA, Conrad M. Ferroptosis inhibition: mechanisms and opportunities. Trends Pharmacol Sci. 2017;38(5):489-98.

106. Chen L, Li X, Liu L, Yu B, Xue Y, Liu Y. Erastin sensitizes glioblastoma cells to temozolomide by restraining xCT and cystathionine-gamma-lyase function. Oncol Rep. 2015;33(3):1465-74.

107. Yamaguchi H, Hsu JL, Chen CT, Wang YN, Hsu MC, Chang SS, et al. Caspase-independent cell death is involved in the negative effect of EGF receptor inhibitors on cisplatin in non-small cell lung cancer cells. Clin Cancer Res. 2013;19(4):845-54.

108. Ma S, Henson ES, Chen Y, Gibson SB. Ferroptosis is induced following siramesine and lapatinib treatment of breast cancer cells. Cell Death Dis. 2016;7:e2307.

109. Green DR, Victor B. The pantheon of the fallen: why are there so many forms of cell death? Trends Cell Biol. 2012;22(11):555-6.

110. Chou TC, Talalay P. Quantitative analysis of dose-effect relationships: the combined effects of multiple drugs or enzyme inhibitors. Adv Enzyme Regul. 1984;22:27-55.

111. Chou TC. Theoretical basis, experimental design, and computerized simulation of synergism and antagonism in drug combination studies. Pharmacol Rev. 2006;58(3):621-81.

112. Chou TC. Drug combination studies and their synergy quantification using the Chou-Talalay method. Cancer Res. 2010;70(2):440-6.

113. Geary N. Understanding synergy. Am J Physiol Endocrinol Metab. 2013;304(3):E237-53.

114. Holohan C, Van Schaeybroeck S, Longley DB, Johnston PG. Cancer drug resistance: an evolving paradigm. Nat Rev Cancer. 2013;13(10):714-26.

115. Housman G, Byler S, Heerboth S, Lapinska K, Longacre M, Snyder N, et al. Drug resistance in cancer: an overview. Cancers (Basel). 2014;6(3):1769-92.

116. Gao M, Monian P, Pan Q, Zhang W, Xiang J, Jiang X. Ferroptosis is an autophagic cell death process. Cell Res. 2016;26(9):1021-32.

117. Ma S, Dielschneider RF, Henson ES, Xian W, Chen Y, Gibson SB. Ferroptosis and autophagy induced cell death occur independently after siramesine and lapatinib treatment in breast cancer cells PloS One. 2017 (Submitted).

118. Sukhai MA, Prabha S, Hurren R, Rutledge AC, Lee AY, Sriskanthadevan S, et al. Lysosomal disruption preferentially targets acute myeloid leukemia cells and progenitors. J Clin Invest. 2013;123(1):315-28.

119. Perera RM, Stoykova S, Nicolay BN, Ross KN, Fitamant J, Boukhali M, et al. Transcriptional control of autophagy-lysosome function drives pancreatic cancer metabolism. Nature. 2015;524(7565):361-5.

120. Menashe I, Figueroa JD, Garcia-Closas M, Chatterjee N, Malats N, Picornell A, et al. Large-scale pathway-based analysis of bladder cancer genome-wide association data from five studies of European background. PloS One. 2012;7(1):e29396.

121. Ploper D, Taelman VF, Robert L, Perez BS, Titz B, Chen HW, et al. MITF drives endolysosomal biogenesis and potentiates Wnt signaling in melanoma cells. Proc Natl Acad Sci USA. 2015;112(5):E420-9.

122. Glunde K, Guggino SE, Solaiyappan M, Pathak AP, Ichikawa Y, Bhujwalla ZM. Extracellular acidification alters lysosomal trafficking in human breast cancer cells. Neoplasia. 2003;5(6):533-45.

123. Ono K, Kim SO, Han J. Susceptibility of lysosomes to rupture is a determinant for plasma membrane disruption in tumor necrosis factor alpha-induced cell death. Mol Cell Biol. 2003;23(2):665-76.

124. Dielschneider RF, Eisenstat H, Mi S, Curtis JM, Xiao W, Johnston JB, et al. Lysosomotropic agents selectively target chronic lymphocytic leukemia cells due to altered sphingolipid metabolism. Leukemia. 2016;30(6):1290-300.

125. Halliwell WH. Cationic amphiphilic drug-induced phospholipidosis. Toxicol Pathol. 1997;25(1):53-60.

126. Kazmi F, Hensley T, Pope C, Funk RS, Loewen GJ, Buckley DB, et al. Lysosomal sequestration (trapping) of lipophilic amine (cationic amphiphilic) drugs in immortalized human hepatocytes (Fa2N-4 cells). Drug Metab Dispos. 2013;41(4):897-905.

127. Petersen NH, Olsen OD, Groth-Pedersen L, Ellegaard AM, Bilgin M, Redmer S, et al. Transformation-associated changes in sphingolipid metabolism sensitize cells to

lysosomal cell death induced by inhibitors of acid sphingomyelinase. Cancer Cell. 2013;24(3):379-93.

128. Ellegaard AM, Dehlendorff C, Vind AC, Anand A, Cederkvist L, Petersen NH, et al. Repurposing cationic amphiphilic antihistamines for cancer treatment. EBioMedicine. 2016;9:130-9.

129. Simons FE, Simons KJ. Histamine and H1-antihistamines: celebrating a century of progress. J Allergy Clin Immunol. 2011;128(6):1139-50 e4.

130. Smith EL, Schuchman EH. The unexpected role of acid sphingomyelinase in cell death and the pathophysiology of common diseases. FASEB J. 2008;22(10):3419-31.

131. Kirkegaard T, Roth AG, Petersen NH, Mahalka AK, Olsen OD, Moilanen I, et al. Hsp70 stabilizes lysosomes and reverts Niemann-Pick disease-associated lysosomal pathology. Nature. 2010;463(7280):549-53.

132. Piao S, Amaravadi RK. Targeting the lysosome in cancer. Ann NY Acad Sci. 2016;1371(1):45-54.

133. Aits S, Jaattela M. Lysosomal cell death at a glance. J Cell Sci. 2013;126(Pt 9):1905-12.

134. Boya P, Kroemer G. Lysosomal membrane permeabilization in cell death. Oncogene. 2008;27(50):6434-51.

135. Kornhuber J, Tripal P, Reichel M, Muhle C, Rhein C, Muehlbacher M, et al. Functional inhibitors of acid sphingomyelinase (FIASMAs): a novel pharmacological group of drugs with broad clinical applications. Cell Physiol Biochem. 2010;26(1):9-20.

136. Ryland LK, Fox TE, Liu X, Loughran TP, Kester M. Dysregulation of sphingolipid metabolism in cancer. Cancer Biol Ther. 2011;11(2):138-49.

137. Don AS, Lim XY, Couttas TA. Re-configuration of sphingolipid metabolism by oncogenic transformation. Biomolecules. 2014;4(1):315-53.

138. Pralhada Rao R, Vaidyanathan N, Rengasamy M, Mammen Oommen A, Somaiya N, Jagannath MR. Sphingolipid metabolic pathway: an overview of major roles played in human diseases. J Lipids. 2013;2013:178910.

139. Ashburn TT, Thor KB. Drug repositioning: identifying and developing new uses for existing drugs. Nat Rev Drug Discov. 2004;3(8):673-83.

140. Palumbo A, Facon T, Sonneveld P, Blade J, Offidani M, Gay F, et al. Thalidomide for treatment of multiple myeloma: 10 years later. Blood. 2008;111(8):3968-77.

141. Degos L, Wang ZY. All trans retinoic acid in acute promyelocytic leukemia. Oncogene. 2001;20(49):7140-5.

142. Kasznicki J, Sliwinska A, Drzewoski J. Metformin in cancer prevention and therapy. Ann Transl Med. 2014;2(6):57.

143. Pantziarka P, Bouche G, Meheus L, Sukhatme V, Sukhatme VP. Repurposing drugs in oncology (ReDO)-mebendazole as an anti-cancer agent. Ecancermedicalscience. 2014;8:443.

144. Heading C. Siramesine H Lundbeck. Curr Opin Investig Drugs. 2001;2(2):266-70.

145. Arieff AJ. Desipramine and nortriptyline in mental depression. Am J Psychiatry. 1966;122(11):1291-2.

146. Escudier B, Eisen T, Stadler WM, Szczylik C, Oudard S, Siebels M, et al. Sorafenib in advanced clear-cell renal-cell carcinoma. N Engl J Med. 2007;356(2):125-34.

147. Untch M, Luck HJ. Lapatinib - member of a new generation of ErbB-targeting drugs. Breast Care (Basel). 2010;5(s1):8-12.

148. Clemastine. Health Canada [cited 2017. Available from: http://webprod.hc-sc.gc.ca/nhpid-bdipsn/ingredReq.do?id=11729&lang=eng].

149. Loratadine. Health Canada [cited 2017. Available from: http://webprod.hc-sc.gc.ca/nhpid-bdipsn/ingredReq.do?id=4753&lang=eng].

150. Desloratadine. Health Canada [cited 2017. Available from: https://pdf.hres.ca/dpd_pm/00022801.PDF].

APPENDIX A: LIST OF SOLUTIONS

Cell Culture

Media

DMEM Media	500 mL
FBS (5%)	25 mL
Pen Strep (1%)	5 mL
Total Volume	530 mL

Cell Staining

Phosphate Buffered Saline (PBS)

NaCl	240.0 g
KCl	6.0 g
$Na_2HPO_4 – 7H_2O$	80.4 g
KH_2PO_4	7.2 g
ddH_2O	2.4 L
Adjust pH to 7.4	
ddH_2O	Bring volume up to 3.0 L
Total Volume	3.0 L

Western Blot

1% NP40 Buffer (Stock Solution)

Tris base (20 mM)	400.0 µL
NaCl (150 mM)	1.5 mL
Glycerol (10%)	1.0 mL
Ethylenediaminetetraacetic acid (EDTA; 2 mM)	40.0 µL
NP40 (1%)	100.0 µL
ddH_2O	Bring volume up to 10.0 mL
Protease Inhibitor Tablet	1 Tablet per 10.0 mL
Total Volume	10.0 mL

Lysis Buffer

1% NP40 Buffer	1.0 mL
PMSF	10.0 µL
Sodium Orthovanadate	20.0 µL
Phosphatase Inhibitor Cocktail 2	1.0 µL
Phosphatase Inhibitor Cocktail 3	1.0 µL
Total Volume	1.32 mL

6X Loading Buffer

Tris base (20 mM)	400.0 µL
SDS (2%)	200.0 µL
Glycerol (5%)	500.0 µL
β-mercaptoethanol (1%)	100.0 µL
Bromophenol blue (0.05%)	5.0 µL
ddH_2O	Bring volume up to 10.0 mL
Total Volume	10.0 mL

10X Running Buffer (Stock Solution)

Tris Base	30.3 g
Glycine	141.2 g
SDS	10.0 g
ddH_2O	Bring volume up to 1.0 L
Total Volume	1.0 L

1X Running Buffer

10X Running Buffer (Stock)	100.0 mL
ddH_2O	900.0 mL
Total Volume	1.0 L

Transfer Buffer

Tris Base	3.03 g
Glycine	14.4 g
Methanol	200.0 mL
ddH_2O	800.0 mL
Total Volume	1.0 L

PBS-Tween20 (PBST)

PBS	100.0 mL
Tween-20	1.0 mL
Total Volume	101.0 L

5% Milk (w/v)

Milk Powder	5.0 g
PBST	100.0 mL
Total Volume	100.0 mL

Brightfield Microscopy

3.7% Formaldehyde

Formaldehyde (37%)	1.0 mL
ddH_2O	9.0 mL
Total Volume	10.0 mL